

UNIVERSITA' DEGLI STUDI DI CATANIA

---

Dottorato di Ricerca in Ingegneria Fisica  
XXIV ciclo



Investigation on the Microwave-based techniques  
to improve the performances of the Electron  
Cyclotron Resonance Ion Sources

PhD Thesis

Author:

**Fabio Maimone**

Tutor:

Prof. **Francesco Musumeci**

Supervisors:

GSI: Dr. **Klaus Tinschert,**

**Peter Spädtke**

INFN-LNS: Ing. **Luigi Celona**

PhD Coordinator:

Prof. **Gaetano Giaquinta**

---

ANNO ACCADEMICO 2010-2011

*A mio Padre,  
con cui avrei tanto voluto  
condividere questo traguardo.*

# Contents

<b>Introduction</b>	<b>iv</b>
<b>1 Elements of plasma physics applied to the ECR ion sources</b>	<b>1</b>
1.1 Definition of plasma and basic parameters . . . . .	1
1.1.1 The particle density . . . . .	2
1.1.2 The particle temperature . . . . .	2
1.1.3 The plasma sheath and the charge neutrality . . . . .	3
1.1.4 The plasma oscillations . . . . .	4
1.2 Collisions of charged particles in plasmas . . . . .	4
1.3 Ionization . . . . .	5
1.3.1 Ionization by electron impact . . . . .	5
1.3.2 Multiple ionization . . . . .	6
1.4 Magnetic confinement of plasmas . . . . .	8
1.4.1 Particle motion in a magnetized plasma . . . . .	8
1.4.2 Magnetic confinement . . . . .	10
1.4.3 Magnetic pressure . . . . .	11
1.5 Wave propagation in plasmas . . . . .	12
1.5.1 Electromagnetic waves in homogeneous non magnetized plasmas . . . . .	13
1.5.2 Electromagnetic waves in magnetized plasmas . . . . .	15
1.5.3 Electromagnetic waves with wave vector perpendicular to the magnetic field direction . . . . .	18
1.5.4 Electromagnetic waves with wave vector parallel to the magnetic field direction . . . . .	19
1.6 Electron heating at the ECR . . . . .	20
<b>2 The technology of the ion sources</b>	<b>22</b>
2.1 Definition of ion source . . . . .	22
2.2 Ion beam parameters, formation and transport . . . . .	24

2.3	Ion sources for the production of beams of multiply charged ions . . . . .	27
2.4	The ECR ion sources . . . . .	30
2.4.1	Working principle and empirical scaling laws . . . . .	30
2.4.2	General description . . . . .	31
2.4.3	History and state of the art of the ECRISs . . . . .	34
2.4.4	The metal ion production with the ECRIS . . . . .	38
2.5	Diagnostic tools of the ion beam properties . . . . .	40
2.5.1	The Faraday Cup and the Beam Transformer . . . . .	41
2.5.2	Viewing Targets for the measurement of the ion beam shape . . . . .	43
2.5.3	Tools for the emittance's measurement . . . . .	44
2.5.4	Plasma diagnostic tools: the Langmuir Probe . . . . .	45
<b>3</b>	<b>The electromagnetic field inside the ECRIS and the microwave coupling to the ECR plasmas</b>	<b>47</b>
3.1	The ECRIS plasma chamber as a resonant cavity . . . . .	47
3.1.1	Resonant modes inside a cylindrical plasma chamber . . . . .	48
3.1.2	Resonant modes and resonant frequencies perturbations . . . . .	52
3.1.3	Waveguide apertures inside the plasma chamber . . . . .	53
3.1.4	Electromagnetic field in the ECR resonance surface . . . . .	54
3.2	Effect of the electromagnetic field on the particle motion . . . . .	56
3.3	The electromagnetic field inside the CAPRICE ECRIS . . . . .	59
3.4	Plasma filled resonant cavity . . . . .	63
3.5	Microwave coupling to the plasma filled chamber . . . . .	65
3.6	Microwave coupling to the CAPRICE ECRIS plasma . . . . .	71
3.7	Plunger tuning on the CAPRICE ECRIS . . . . .	76
<b>4</b>	<b>The frequency tuning and the double frequency heating</b>	<b>81</b>
4.1	Application of the frequency tuning on the ECRIS . . . . .	81
4.1.1	Experimental evidences and observations on the performance variation . . . . .	82
4.2	Operation of the CAPRICE ECRIS with applying the frequency tuning . . . . .	85
4.2.1	The CAPRICE ECR ion source description . . . . .	87
4.2.2	The experimental set-up . . . . .	87
4.2.3	The effect of the frequency tuning on the ion extracted current . . . . .	89
4.2.4	Enhancement of the current of highly charged ions . . . . .	94
4.2.5	The effect on the beam shape . . . . .	97

---

4.2.6	Application of the frequency tuning for the production of metal ions . . . . .	100
4.3	The double frequency heating . . . . .	104
4.4	Operation of the CAPRICE ECRIS with the double frequency heating . . . . .	105
4.4.1	Effect of the double frequency heating on the current of highly charged ions . . . . .	111
4.5	Comparative analysis of the frequency tuning and of the plunger tuning . . . . .	115
	<b>Conclusions and future perspectives</b>	<b>118</b>
	<b>Acknowledgements</b>	<b>122</b>
	<b>Bibliography</b>	<b>124</b>

# Introduction

Intense ion beams are used at the accelerator facilities for nuclear physics experiments, for tumor treatments and for other applications. Since the energy of the accelerated ions is proportional to the charge over mass ratio, highly charged ions are requested for all the high energy experiments or applications. For this purpose the Electron Cyclotron Resonance Ion Sources (ECRISs) are suitable devices to fulfil these requirements because they proved to be able to produce intense beams of high charge state ions in a reliable and continuous way.

In an ECR ion source a magnetically confined plasma is fed by electromagnetic waves at high power and with frequencies higher than a few GHz. Several ECRISs are installed in many laboratories all over the world and better performing ones are continuously under development. An enhancement of performances in terms of more intense beams of higher charge state ions has been obtained with ECR ion sources operating at higher microwave frequencies than 18 GHz with improved magnetic confinement. In fact the increase of the microwave frequency, under proper conditions, leads to higher plasma densities which are mandatory to reach the desired performances.

In the last years, together with the trend to increase the microwave frequency, new techniques have been evaluated in order to improve the performances of the existing ECRIS or of those under development. The variation of the microwave frequency is a promising aspect for suchlike improvement. Several experiments confirming this assumption have been carried out in the last years and interesting interpretations of the results of this "so called" *frequency tuning effect* have been proposed. Another technique successfully used to enhance the ion beam current and the production of highly charged ions is called *double frequency heating* and consists in the multiple injection of two electromagnetic waves at different frequencies into the ion source. These techniques are based on the different electromagnetic field patterns which can be excited inside an ECRIS and on the improvement

of the microwave coupling between the electromagnetic waves and the confined plasma. However, even if these techniques provided interesting results, a better understanding of the effect of the microwave coupling between waves and cavity filled with plasma is mandatory.

For this reason a research work has been carried out with the aim to validate the theoretical assumptions concerning the standing waves presence inside the plasma chamber of the ECRIS and, by investigating the microwave coupling to the ECR plasma, to analyze in detail these new techniques to improve the performances of the ECRISs. The experimental investigations have been carried out with the CAPRICE ECRIS installed at GSI Helmholtzzentrum für Schwerionenforschung GmbH, and the achieved results, which turned out to be important both for the scientific relevance and for the development of new ECR ion sources, are here described.

The organization of the reported research work is described in the following. Since the ion production inside an ECRIS passes through the creation of a plasma, the ion source physics is mostly related to the plasma physics. Then the main aspects concerning the plasma physics which can be applied to the ECR ion sources are introduced in the first chapter.

A plasma source is different than an ion source or better than an ion beam source. Then, in the second chapter the concept of ion source is introduced and, by focusing on the ECR ion sources, the main ion sources for the ion beam production are described. A description of the most important properties of the ion beams and the main tools to measure the ion beam parameters are also included within this chapter.

The electromagnetic field within the plasma chamber of the ECRIS and the properties of the electromagnetic waves feeding the plasma affect the plasma properties and the ion beam production. The third chapter presents the detailed analysis carried out about the electromagnetic field inside the ECRIS and about the microwave coupling to the ECR plasmas. By applying the theory of the resonant cavities, the electromagnetic field patterns (modes) have been calculated inside the plasma chamber of several ion sources and the plasma properties have been analyzed for different excited electromagnetic field patterns. Several experiments to relate the extracted ion beam properties to the electromagnetic field excited inside the ECRIS have been carried out and the interesting results are analyzed within this chapter.

These investigations are mandatory to explain the enhancement of performances when techniques, like the frequency tuning, based on the variation of the microwave coupling to the ECR plasma, are applied. In the fourth chapter the experimental analysis of the efficient applicability of the fre-

quency tuning and of the double frequency heating for the production of intense beams of highly charged ions is described. In the conclusive section the results of this research work are summarized and new perspectives and future investigations on these techniques are proposed.



# Chapter 1

## Elements of plasma physics applied to the ECR ion sources

The ions production inside an ion source passes through the extraction of the ionic content from a magnetized plasma created from a neutral gas where accelerated electrons strike with the atoms or with the ions. For this reason the ion sources physics is mostly related to the plasma physics and within this chapter the main aspects concerning the plasma physics applied to the ECR Ion Sources are discussed.

### 1.1 Definition of plasma and basic parameters

The physics of the ion sources is strongly related to the plasma physics since the plasma is the medium where the ions are created and extracted. In order to understand the working principle of the ion sources an introductive definition of plasma and of its main features is here reported. A plasma is a state of matter where the particles which constitutes this medium are in general ions, electrons and neutrals atoms. This feature distinguishes the gas, where the individual particles are the molecules of the gas, from the plasmas. A gas in thermal equilibrium presents an amount of ionization in according to the Saha equation:[1]

$$\frac{n_i}{n_n} = 2.4 \times 10^{21} \frac{T^{3/2}}{n_i} e^{-U_i/KT} \quad (1.1)$$

Where  $n_i$  and  $n_n$  are the density of ionized atoms and of neutral atoms, respectively,  $T$  is the temperature in  $K^\circ$ ,  $K$  is the Boltzmann's constant and  $U_i$  is the ionization energy (to remove the most outer electrons from an atom). At room temperature the ratio between the ionized and the neutral atoms is quite low and increases with the high increase of the temperature and the gas evolves in a plasma state; for this reason in nature this state of matter is present where environments with adequately high temperatures exist like the sun, the stars or the ionosphere. However, a laboratory plasma can be created by providing energy to the plasma electrons which, by hitting the neutral atoms, enhance the ionized atoms density. Several techniques are used to create a laboratory plasma like, for instance, by making use of an electric discharge, by the interaction with electromagnetic waves or else by laser ablation. In the specific case of the Electron Cyclotron Resonance ion sources a plasma is created by the absorption by the electrons of an electromagnetic wave with a frequency, the *electron cyclotron frequency*, in the range of the microwaves. The basic parameters featuring a plasma are the particle (electrons and ions) densities (expressed in particles divided by cubic meter or by cubic centimeters) and the particle energy or temperature (measured in eV).

### 1.1.1 The particle density

In the general case a plasma contains electrons with charge  $q_i = e = -1$  and density  $n_e$ , single or multiple charged ions with charge  $q_i = +1, +2, \dots$  and density  $n_i$  and also neutral particle with density  $n_n$ . A percentage of ionization of a plasma is defined by the following ratio:

$$\frac{n_i}{n_e + n_n} \quad (1.2)$$

A *fully ionized* plasma does not presents any neutral particles. A plasma is precisely described by the electron density together with the distribution of the ion charge states, and for an ECR plasma the electron density is in the order of  $10^{12} \text{ cm}^{-3}$ . As it will be described in the section 1.5 this parameter is very important for the waves propagation in plasmas.

### 1.1.2 The particle temperature

It is conventionally accepted the assumption of the concept of temperature in order to define the energy of the charged particles constituting the plasma. For this reason is usual to define the plasma temperature in units of electron Volts, eV ( $1\text{eV} = 11600 \text{ }^\circ\text{K}$ ). It is possible to convert the temperature

in energy by multiplying it for the  $K$  constant. The plasma particles can assume several temperatures. Ions and electrons can have different temperatures  $T_i$  and  $T_e$ . For the ECR plasmas for instance the ion temperature is in the order to the eV while the electron temperature can rise up to several hundreds of keV. In the case of a magnetized plasma, due to the induced anisotropy, also the temperatures of each particle can be different, according to the direction of motion with respect to the direction of the  $\vec{B}$ :  $T_{i||}$ ,  $T_{i\perp}$ ,  $T_{e||}$  and  $T_{e\perp}$  for a motion parallel or perpendicular to the magnetic field direction, respectively.

### 1.1.3 The plasma sheath and the charge neutrality

A fundamental characteristic of a plasma is the property to shield the electric fields which are applied to it. A boundary layer, called *plasma sheath*, is formed at the interface between the plasma and its boundary or in the surrounding of a charged object (i.e. a probe, or an electrode) which is perturbing the plasma neutral condition. Within this layer the plasma particles, mostly the electrons due to the higher mobility, assume a distribution able to neutralize the electric field applied. An estimation of this layer is given by the following expression:

$$\lambda_D = \sqrt{\frac{\epsilon_0 K T_e}{n_e e^2}} \quad (1.3)$$

Where  $\epsilon_0$  is the electric permittivity in vacuum. The parameter  $\lambda_D$ , called *Debye length* and expressed in *cm*, allows to estimate the distance over which local charge distributions are neutralized. The charged particles contained in a plasma exhibit an electric field and, if they are in motion, a magnetic field which create an interaction with the other particles. A charge neutrality, over a dimension in the order of the Debye length is a basic property of a plasma and any variation of this condition leads to an electric field which limits the charging. This condition is expressed by the expression [2]:

$$\sum q_i n_i = n_e \quad (1.4)$$

A criterion to call a ionized gas a plasma is that it is enough dense that the Debye length is much smaller than the dimension  $L$  of the plasma. In other words a plasma is able to neutralize applied electric field or charge accumulations in a small region of it without affecting the plasma total electric field or potential. The Debye shielding concept is valid only if there

are enough particles within the plasma sheath. It is possible to calculate the number of particles  $N_D$  contained inside the so called Debye sphere:

$$N_D = n_e \frac{4}{3} \pi \lambda_D^3 \quad (1.5)$$

Then the second conditions characterizing a plasma is that  $N_D \gg 1$ .

#### 1.1.4 The plasma oscillations

Several modes of oscillations are presents inside a plasma. If  $\omega$  is the typical plasma oscillation and  $\tau$  is the mean time between collisions with neutral atoms the third condition to call a ionized gas as a plasma is that  $\omega\tau \gg 1$ . The main plasma oscillations are related to the electron plasma frequency and the ion plasma frequency:

$$\omega_{pe}^2 = \frac{e^2 n_e}{\epsilon_0 m_e} \quad (1.6)$$

$$\omega_{pi}^2 = \frac{q_i^2 e^2 n_i}{\epsilon_0 m_i} \quad (1.7)$$

Where  $q_i$  is the ion charge state,  $m_e$  and  $m_i$  are the electron and ion mass respectively. The frequencies of oscillations are often in the order of the GHz for the electrons and of the MHz for the ions.

## 1.2 Collisions of charged particles in plasmas

In the previous section it was introduced the concept of collisions in the plasmas. Here this concept will be explained. Often it is used the quantity *collision's frequency* in order to analyze the various collisions in a plasma. For this reason it is important to introduce the mean free path  $\lambda_m$  for a given process with cross section  $\sigma$ :

$$\lambda_m = \frac{1}{n\sigma} \quad (1.8)$$

Where  $n$  indicates the appropriate particle density. The time between two consecutive collisions is then the collision time:

$$\tau = \frac{\lambda_m}{v} = \frac{1}{n\sigma\langle v \rangle} \quad (1.9)$$

Where  $\langle v \rangle$  is the mean particle velocity (since in general the plasma particles follow some energy distribution function and often it can be assumed a Maxwellian distribution). The collision frequency is then:

$$\frac{1}{\tau} = n\sigma\langle v \rangle \quad (1.10)$$

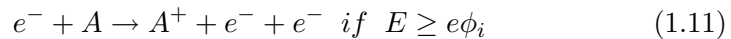
The main collisions involving the different particles inside a plasma can be classified in two main groups: multiple collisions and binary collisions. The first group includes the particles' deflections due to the interactions with other particles and to the second class belong the interactions between two particles determining phenomena like the ionization of neutral atoms or the recombination between electrons and ions.

## 1.3 Ionization

The ionization process is one the main aspect for the creation of a plasma. The ways in which an ionization mechanism occurs include the electron impact ionization, the photoionization, the field ionization, the surface ionizations, etc. Here the ionization by electron impact is discussed since it is the main process which determines the plasma start-up inside an ECRIS.

### 1.3.1 Ionization by electron impact

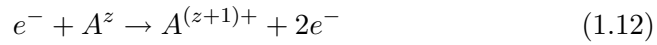
The ionization of neutral atoms by electron impact occurs when an electron, in a low pressure gas and accelerated by an applied electric field, collides with a neutral atom. The ionization process takes place when the energy of the electron exceed the energy to remove the most external electron bound to a neutral atom. This energy is called ionization potential and we can resume this mechanism in the following reaction:



Where an electron  $e^-$ , having energy  $E$  higher than the product between the charge and the ionization potential  $\phi_i$ , by colliding with neutral atom  $A$ , removes an electron and leaves a positive ion  $A^+$ . With the process called *step by step ionization* the ionization proceeds through the removal of a single electron per time from the atomic shells.

### 1.3.2 Multiple ionization

When only an electron is removed by a neutral atom, the ion which remains after the reaction is *singly ionized* and the ion charge state is  $q_i = +1$ . In order to fulfill the increasing demand of energy provided by the accelerator facilities the ion sources and, in particular, the ECR Ion Sources are requested to produce beams of multiply charged ions. When more than an electron is removed by a neutral atom or by an ion, the ion is called *multiply charged* ion and the charge state is  $q_i = +2, +3 + 4, \dots$ . In such a case the reaction is resumed in the following:



With  $z \geq 1$ . In order to produce ions of charge  $q_i = n+$  the electron must have got an energy equal or higher than the  $n^{\text{th}}$  ionization potential. In the figure 1.1 the ionization potential (better the ionization energy) for all charge states of all elements up to 100 as atomic number is shown.

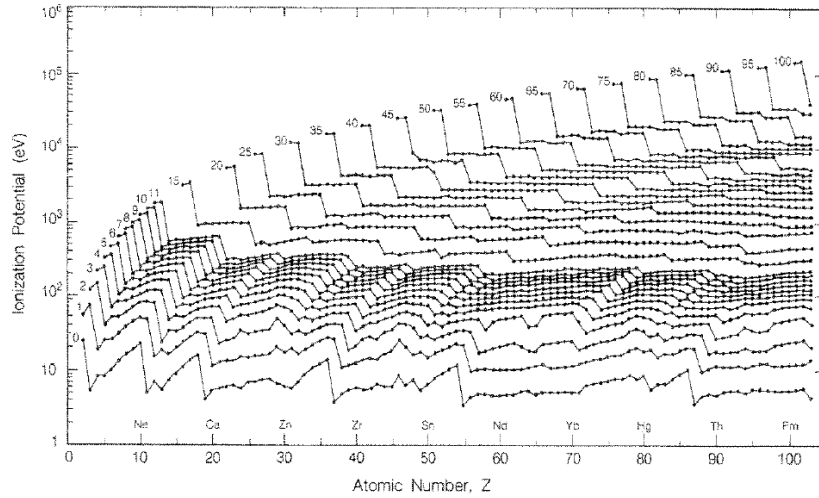


Figure 1.1: *Ionization potentials for multiply charged ions of the elements up to 100 as atomic number.*[3]

In order to "use" the electrons in a more efficient way, it is possible to force them to proceed over a longer distance than the mean free path. For instance they can be reflected forward and backwards many times in a potential well created by negatively biased electrodes, along the axial

magnetic field lines (this is the typical mechanism to create a plasma in a (PIG) Penning Ion Source). Or else it is possible to confine ions and electrons in a magnetic mirror configuration like in the ECR Ion Sources. Here comes the importance of the analysis of magnetized plasmas which will be treated in the following section. Since it comes out that an enhancement of ionization occurs in confined plasmas, together with the electron energy an other important parameter for the multiple charged ion production is the *ion confinement time*  $\tau_i$ . In fact if  $\tau_i$  is too short in the plasma region where the step by step ionization process takes places, the desired high charge states ions are not produced even if the electron energy is enough high. This assumption can be expressed by the following condition:[4]

$$\tau_i \geq \frac{1}{n_e \langle \sigma_{k,k+1} v_e \rangle} \quad (1.13)$$

Where  $\sigma_{k,k+1}$  is the cross section for ionization from the charge state  $k$  to a charge state  $k+1$ ,  $v_e$  is the electron velocity and the average is taken over the distribution of electron velocities. This means that the ion confinement time has to be longer than the time of the ion's transition from the charge state  $k$  to a charge state  $k+1$  for an electron impact. The product of the cross section and the electron velocity is a function of the electron energy ( $T_e$ ). It is possible to write the equation (1.13) as [5]:

$$n_e \tau_i \geq \frac{5 \cdot 10^4 (T_{opt}^{3/2})}{\sum_{i=1}^N q_i} \quad (1.14)$$

The condition expressed in the (1.14) is fundamental for the ECRIS since it establish the plasma optimum parameters for the production of high charge states ions. Usually  $T_{opt}$  is at least 3 – 4 times the ionization energy of the desired charge state ion. The product  $n_e \tau_i$  is called *quality factor* for an ion source and it is interesting to relate the quality factor and the required energy with the desired charge state ion. This can be done by analyzing the Golovanisky plot in figure 1.2. Here the ions in the circles are *completely stripped* (ion with no longer electrons) and in brackets the *not-completely stripped* ions, requiring the same quality factor and energy of the ones in the circles, are reported. In this diagram the combinations of electron temperature, electron density and ion confinement time to produce completely stripped ions are shown.

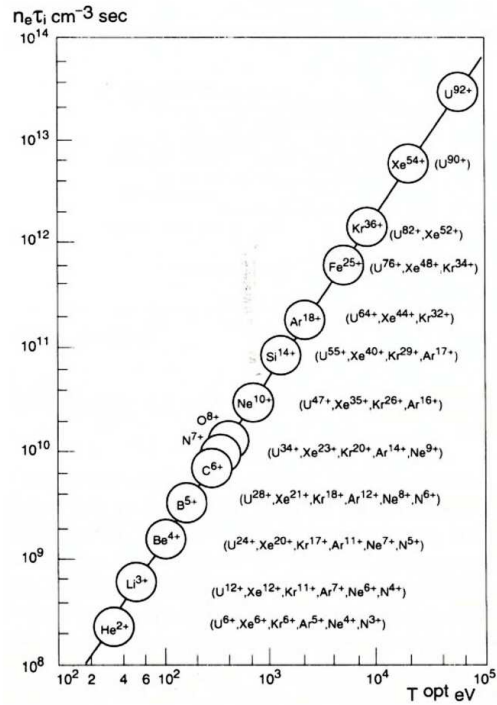


Figure 1.2: Golovanivsky's diagram of the quality factor criteria for the production of highly charged ions.[6]

## 1.4 Magnetic confinement of plasmas

In the previous section the importance of imposing a magnetic field to confine the plasma particles has been introduced. This imposition determines a change of the plasma dielectric properties: it will turn in an electrically anisotropic medium. Ions and electrons, since are particle in motion, experience an interaction with the magnetic field where the plasma is confined. Within this section this interaction will be discussed.

### 1.4.1 Particle motion in a magnetized plasma

Let's consider a particle with charge  $q$  and mass  $m$  moving with velocity  $\vec{v}$  in presence of a stationary and uniform magnetic field  $\vec{B}$ . This particle experiences a force  $\vec{F}$ , called Lorentz's force given by:



$$\vec{F} = m \frac{d\vec{v}}{dt} = q\vec{v} \times \vec{B} \quad (1.15)$$

By solving this equation of motion in a  $\widehat{xyz}$  coordinate systems (and assuming that  $\vec{B} = B\widehat{z}$ ) it is possible to demonstrate that the motion of a charged particle in a magnetic field is the composition of an uniform and rectilinear motion along the direction of  $\vec{B}$  and of a circular and uniform motion along the perpendicular direction. In fact, it is possible to develop the previous equation in:

$$\frac{d^2v_x}{dx^2} = -\omega_c^2 v_x \quad (1.16)$$

$$\frac{d^2v_y}{dy^2} = -\omega_c^2 v_y \quad (1.17)$$

This is the equation of an harmonic oscillator with frequency  $\omega_c$  which is called ***cyclotron frequency*** or ***gyro-frequency***:

$$\omega_c = \frac{|q|B}{m} \quad (1.18)$$

The solution of this motion equation is

$$(x - x_c) = \frac{v_{o\perp}}{\omega_c} \sin(\omega_c t + \phi) \quad (1.19)$$

$$(y - y_c) = \frac{v_{o\perp}}{\omega_c} \cos(\omega_c t + \phi) \quad (1.20)$$

Then the charged particle describes a circumference trajectory in the direction perpendicular to the direction of  $\vec{B}$  with a radius, called Larmor radius equal to:

$$R = \frac{v_{o\perp}}{\omega_c} = \frac{mv_{o\perp}}{|q|B} \quad (1.21)$$

The center of this circumference, also called guiding center is

$$(x_c = x_o - \frac{v_{o\perp}}{\omega_c} \sin \phi), \quad (y_c = y_o - \frac{v_{o\perp}}{\omega_c} \cos \phi) \quad (1.22)$$

Where

$$\tan \phi = \frac{v_{oy}}{v_{ox}}, \quad v_{o\perp}^2 = v_{ox}^2 + v_{oy}^2 \quad (1.23)$$

and  $v_{ox}$ ,  $v_{oy}$ ,  $x_{ox}$ ,  $y_{oy}$  depend on the initial conditions. Then, since the motion along the direction of  $\vec{B}$  is rectilinear and uniform (the velocity component ( $v_{||}$  has no interaction with the magnetic field, since  $v_{||} \times \vec{B} = v_z \times B\hat{z} = 0$ ), the trajectory described by the charged particle during the motion is a cylindrical helical. The presence of the plasma collisions oscillating with pulsation  $\omega_{eff}$  introduces a force  $-m\omega_{eff}\vec{v}$  in the motion equation. In this case the solution of this equation is a spiral motion along the magnetic field line with a radius decreasing with the time according to the equation:

$$R(t) = \frac{v_{o\perp}}{\sqrt{\omega_{eff}^2 + \omega_c^2}} e^{-i\omega_{eff}t} \quad (1.24)$$

The order of magnitude of the plasma collisions is in the order of the MHz. The magnetized plasma are created in the ECRISs with the ECR absorption of the electromagnetic waves at the ECR frequency which is in the order of the GHz. Then the particles motion, the electron velocity and then the kinetic energy, and the orbit radius are not affected by the collisions in a period of the electromagnetic waves. For this reason such a kind of plasma can be considered as collisionless for the electromagnetic wave absorption.

### 1.4.2 Magnetic confinement

The previous section introduced the concept of plasma confinement in the direction perpendicular of the magnetic field direction through the fact that the electrons and the ions are tied in their motion to the field lines. The plasma loss along the field can be reduced if the magnetic field strength is increased at the end of the confinement region also called "magnetic mirror". In order to better confine the plasma particle in a magnetic mirror the following conditions must be fulfilled:

- a magnetic field gradient directed along the direction of the field must exist
- the vector  $\vec{B}$  must have a radial component
- the velocity vector of the charged particles must form a particular angle with the field lines

The charged particle, moving in a non-uniform magnetic field experiences a force

$$\vec{F}_{||} = -\mu\vec{\nabla}_{||}\vec{B} \quad (1.25)$$

Where  $\mu$ , called magnetic moment of the particle, does not vary with the time and is given by:

$$\mu = \frac{1}{2} \frac{mv_{\perp}^2}{B} \quad (1.26)$$

Where  $B$  is the amplitude of the magnetic field. The demonstration of this invariance can be found in [1] and according to this assumption, since the particle moves along a region where the  $\vec{B}$  increases, the velocity along the perpendicular direction has to increase as well. Then since the magnetic field does not apply any work on the particle the particle energy:

$$E = E_{\parallel} + E_{\perp} = \frac{1}{2}mv_{\parallel}^2 + \frac{1}{2}mv_{\perp}^2 \quad (1.27)$$

has to remain constant. Then as the velocity along the perpendicular direction increases, the velocity along the parallel direction to  $\vec{B}$  decreases. If the magnetic field is strong enough the parallel velocity is decreased until it is zero and the particle is then reflected backwards. These assumption are given in conditions of absence of collisions or electric fields. It is then possible to trap charged particles in a configuration of two mirrors fields with enough high magnetic magnitude. In fact, according to the third condition above reported there is an angle  $\theta_{min}$ :

$$\theta_{min} = \arcsin \left( \sqrt{\frac{B_o}{B_m}} \right) = \arcsin \left( \sqrt{\frac{1}{R_m}} \right) \quad (1.28)$$

which defines the so called *loss cone*. In fact, if the magnetic field has a value  $B_o$  at the middle point and  $B_m$  is the maximum value and the particle has got a velocity vector with an angle  $\theta$  with the magnetic field line lower than  $\theta_{min}$  it is in this loss cone and it is lost from the confinement field.  $R_m$  is called *mirror ratio*.

### 1.4.3 Magnetic pressure

In order to define some conditions to maintain a stable confinement let's define the magnetic pressure and the  $\beta$  parameter. The region of space occupied by a magnetic field has got an energy density due to the magnetic field. The pressure exerted by the magnetic field in the direction transverse to the field is given by:

$$P_{mag} = \frac{B^2}{2\mu_0} \quad (1.29)$$

Where  $\mu$  is the magnetic permeability. The pressure exerted by a gas is given by:

$$P_{gas} = nkT \quad (1.30)$$

For a plasma it is possible to define a pressure which is the sum of the contribution of the electrons and of the ions and in the case of the plasma confined in a mirror field the perpendicular component of the energy is relevant. Then the plasma pressure perpendicularly to the magnetic field is:

$$P_{plasma} = n_e k T_{e\perp} + n_i k T_{i\perp} \quad (1.31)$$

At the equilibrium the sum of the pressures in the internal region of the plasma must be the same of the pressure in the external region. This condition is satisfied if:

$$\frac{B_{int}^2}{2\mu} + n_e k T_{e\perp} + n_i k T_{i\perp} = \frac{B_{ext}^2}{2\mu} \quad (1.32)$$

The ratio between the plasma pressure and the pressure exerted by the confinement field is a parameter providing information about the confinement stability and it is called  $\beta$  parameter:

$$\beta = \frac{P_{plasma}}{P_{mag}} = \frac{2\mu(n_e k T_{e\perp} + n_i k T_{i\perp})}{B_{ext}^2} \quad (1.33)$$

The  $\beta$  parameter is then an useful parameter to describe a magnetic confinement system for a plasma. In fact if  $\beta \ll 1$  the magnetic pressure is higher than the plasma pressure and is the possible to magnetically confine the plasma.[4]

## 1.5 Wave propagation in plasmas

There are two main types of waves propagating in a plasma: self-generated waves and electromagnetic waves sent to the plasma from the outer. The propagation of both of them is regulated by the proper features of the plasma. The self generation of waves in a plasma is very important, as described in the following, for the determination of the electromagnetic field propagation. In section 1.1 the plasma frequency has been introduced as a consequence of the motion of the electrons from this position at the equilibrium. Due to the mass of the ions, they can be assumed as fixed. For

both of the plasma oscillations indicated in the (1.6) and (1.7), the propagation constant  $k$  is not present. Then there is no wave propagation due to the plasma oscillations since the group velocity ( $v_g = d\omega/dk$ ) is zero. However the plasma oscillation can be called a plasma wave since the oscillating electrons moving into adjacent layers of plasma can carry information about the features of the oscillating fields from the region of origin. The new expression describing the plasma frequency is [1]:

$$\omega_{LM}^2 = \omega_p^2 + \frac{3}{2}k^2v_{th}^2 \quad (1.34)$$

which is called Langmuir frequency and  $v_{th} = 2KT_e/m_e$  is the electron velocity. Now the plasma frequency is depending on the wave constant and the group velocity is finite.

There are also waves due to the ions called Ion Waves. In a collisionless plasma the ions can transmit vibrations to each other because of their charge and acoustic waves can occur through the intermediary of an electric field. The ion movement can then originate wave similar to the acoustic waves. Further details about the ion waves can be found in [1].

### 1.5.1 Electromagnetic waves in homogeneous non magnetized plasmas

An electromagnetic wave while is propagating in a plasma, interacts with all the plasma particles: electrons, ions, and neutral particles. However, the interaction with the neutral particles is lower, compared to the interaction with the charged particles, and it can be neglected. Furthermore, since the ions have a higher mass than the mass of the electrons the velocity transferred to the ions is quite low with respect to the one transferred to the electrons. Then, when an electromagnetic wave is propagating in a highly ionized plasma, the plasma electrons strongly affect the wave transmission. The effect of the ions is sensitive at lower frequencies while the ECR plasma are heated at several GHz of frequency for the electromagnetic wave igniting the plasma. By assuming the electric and magnetic field associated to the wave as monochromatic, with pulsation  $\omega$ ,  $\vec{E} = \vec{E}_0e^{-i\omega t}$  and  $\vec{H} = \vec{H}_0e^{-i\omega t}$ , from the solution of the Maxwell equations defined in a dielectric medium with losses with a negative electric susceptibility it is possible to calculate the plasma constitutive parameters like the plasma conductivity  $\sigma$  and the electric permittivity  $\epsilon$ : [7]

$$\sigma = \frac{\epsilon_0 \omega_{eff} \omega_p^2}{\omega^2 + \omega_{eff}^2} \quad (1.35)$$

$$\epsilon = \epsilon_0 \left( 1 - \frac{\omega_p^2}{\omega^2 + \omega_{eff}^2} \right) \quad (1.36)$$

where  $\omega_{eff}$  is the collisions frequency and  $\omega_p$  is the plasma pulsation defined in the (1.6). The propagation of a transverse electromagnetic wave in this medium can be calculated by indicating the modulus of the wave vector ( $\mu = \mu_0$ ):

$$k^2 = \omega^2 \mu_0 \epsilon + i \omega \mu_0 \sigma \quad (1.37)$$

And since the plasma behaves as a conductive medium with conductivity  $\sigma$  the wave vector can be expressed as:

$$k = \beta + i\alpha \quad (1.38)$$

where the propagation factor  $\beta$  and the attenuation factor  $\alpha$  are:

$$\beta = \omega \sqrt{\frac{\mu\epsilon}{2} \left[ 1 + \sqrt{1 + \frac{\sigma^2}{\epsilon^2 \omega^2}} \right]} \quad (1.39)$$

$$\alpha = \omega \sqrt{\frac{\mu\epsilon}{2} \left[ \sqrt{1 + \frac{\sigma^2}{\epsilon^2 \omega^2}} - 1 \right]} \quad (1.40)$$

In the case of a collisionless plasma ( $\omega_{eff} = 0$  and  $\sigma = 0$ ) the plasma electric permittivity  $\epsilon$  becomes:

$$\epsilon = \epsilon_0 \left( 1 - \frac{\omega_p^2}{\omega^2} \right) \quad (1.41)$$

and then  $\alpha = 0$  and:

$$\beta = \frac{\omega}{c} \sqrt{1 - \left( \frac{\omega_p^2}{\omega^2} \right)} \quad (1.42)$$

It turns out that, in order to have a wave propagation, the frequency of the electromagnetic wave must be higher than the plasma frequency. If  $\omega < \omega_p$  the wave is called evanescent and does not transport any energy. The frequency where  $\omega = \omega_p$  is called *cut-off frequency*, the magnetic field is zero and the electric field must obey on the equation  $\vec{\nabla} \times \vec{E}(t) = 0$ .

Then a transverse wave cannot exist at the cut-off, however a longitudinal wave called *plasma wave* or *electrostatic wave* can exist. In the case of a plasma with low loss rate (when  $\sigma/\epsilon\omega \ll 1$ ) the equations (1.39) and (1.40) become:

$$\beta = \frac{\omega}{c} \sqrt{1 - \frac{\omega_p^2}{\omega^2 + \omega_{eff}^2}} \quad (1.43)$$

$$\alpha = \frac{\frac{1}{2}\omega_{eff}\omega_p^2}{c(\omega^2 + \omega_{eff}^2) \sqrt{1 - \frac{\omega_p^2}{\omega^2 + \omega_{eff}^2}}} \quad (1.44)$$

It is then possible to develop the formula of the plasma frequency at the cut-off by defining the cut-off density:

$$n_{cut-off} = \frac{m\epsilon}{c^2} \omega_p^2 \quad (1.45)$$

In order to permit the wave propagation in an homogeneous non magnetized plasma the density cannot exceed the cut-off density.

### 1.5.2 Electromagnetic waves in magnetized plasmas

If a magneto-static field,  $\vec{B}_0$ , is applied to a plasma, it becomes electrically anisotropic for the electromagnetic waves. This means that the dielectric constant  $\epsilon$  becomes a tensorial quantity  $\vec{\epsilon}$ . It is possible to calculate the elements of this tensor by making use of the single particle theory. The charged particle motion (it is taken into account an electron, with charge  $q_e$  and mass  $m_e$ , but it is possible to repeat the calculation for an ion) is then calculated in a medium where it is subjected to: an electric force, an impulsive force due to the collisions and the Lorentz force due to the applied magneto-static field:

$$m_e \frac{d\vec{v}}{dt} = q_e \vec{E} - m_e \vec{v} \omega_{eff} + q_e \vec{v} \times \vec{B}_0 \quad (1.46)$$

It is possible to assume the magnetic field as oriented along the  $\hat{z}$  direction of a  $\widehat{xyz}$  coordinate system then  $\vec{B}_0 = B_0 \hat{z}$  and then the equation (1.46) becomes:

$$\frac{d\vec{v}}{dt} + \vec{v} \omega_{eff} = \frac{q_e \vec{E}}{m_e} + \omega_g \vec{v} \times \hat{z} \quad (1.47)$$

Where  $\omega_g$  has the dimension of a pulsation, is called **electron cyclotron frequency** and is equal to:

$$\omega_g = \frac{q_e B_0}{m_e} \quad (1.48)$$

Since the electric field is harmonic ( $\vec{E} = \vec{E}_0 e^{-i\omega t}$ ) then the solution for the velocity is harmonic as well ( $\vec{v} = \vec{v}_0 e^{-i\omega t}$ ) and replaced in the equation (1.47), the motion equation becomes:

$$(-i\omega + \omega_{eff})\vec{v} + \omega_g \hat{z} \times \vec{v} = \frac{q_e \vec{E}}{m_e} \quad (1.49)$$

The solutions for the velocities along the orthogonal axis can be used to calculate the current density vector  $\vec{J} = n_e q_e \vec{v}$  to confirm the electrical anisotropy of the magnetized plasmas. In fact it is possible to demonstrate [7] that the current density vector is no longer parallel to the electric field vector. From the Maxwell equation:

$$\vec{\nabla} \times \vec{H} = \vec{J} - i\omega \epsilon_0 \vec{E} = -i\omega \vec{\epsilon}' \cdot \vec{E} = -i\omega \vec{D} \quad (1.50)$$

it is possible to calculate the tensorial electric permittivity. In fact it is clear that the vector  $\vec{D} = \vec{J} / -i\omega + \epsilon_0 \vec{E}$  is no longer parallel to the electric field vector (condition of electrical anisotropy). A matrix representing the tensorial electric permittivity describing the electric properties of a magnetized plasmas is obtained:

$$\vec{\epsilon}' = \begin{pmatrix} \epsilon'_{xx} & \epsilon'_{xy} & 0 \\ \epsilon'_{yx} & \epsilon'_{yy} & 0 \\ 0 & 0 & \epsilon'_{zz} \end{pmatrix}$$

The terms of this matrix are:

$$\epsilon'_{xx} = \epsilon'_{yy} = \epsilon_0 \left( 1 - \frac{\omega_p^2 (\omega + i\omega_{eff})}{\omega [(\omega + i\omega_{eff})^2 - \omega_g]} \right) \quad (1.51)$$

$$\epsilon'_{xy} = -\epsilon'_{yx} = -i\epsilon_0 \frac{\omega_p^2 \omega_g}{\omega [(\omega + i\omega_{eff})^2 - \omega_g]} \quad (1.52)$$

$$\epsilon'_{zz} = \epsilon_0 \left( 1 - \frac{\omega_p^2}{\omega (\omega + i\omega_{eff})} \right) \quad (1.53)$$

It is also possible to consider the interaction of the electric field and of the magnetic field with the ions, but since the mass of the ions is three order



of magnitude heavier than the one of the electrons, if the frequency of the electromagnetic wave is enough high, the ion motion is almost not affected by the wave field in comparison with the motion of the electron.

Let's analyze the propagation of a plane wave (electromagnetic field which vectors depend only on one coordinate and on the time) in a homogeneous magnetized plasma (with  $\vec{B}_0 = B_0 \hat{z}$ ). The electric and magnetic field of a monochromatic plane wave are:

$$\vec{E}(\vec{r}) = \vec{E}_0 e^{i\vec{k}\cdot\vec{r}} e^{-i\omega t}, \quad \vec{H}(\vec{r}) = \vec{H}_0 e^{i\vec{k}\cdot\vec{r}} e^{-i\omega t} \quad (1.54)$$

Where  $\vec{E}_0$  and  $\vec{H}_0$  are constant vectors,  $\vec{r}$  is the position vector and  $\vec{k}$  is the wave vector:

$$\vec{k} = \hat{n} \frac{\omega}{v} \quad (1.55)$$

Where  $\hat{n}$  is the unitary vector in the propagation direction thus forming an angle  $\theta$  with the direction of the magnetic field and  $v$  is the phase velocity (velocity of propagation of a phase) of the wave. In order to analyze the wave propagation, the wave vector describing the wave propagation and the vector  $\vec{E}_0$  describing the wave polarization must be calculated starting from the Maxwell equations. It is then possible to obtain the Appleton formula:

$$\frac{v^2}{c^2} = \left[ 1 - \frac{X}{1 + iZ - \frac{1}{2} \frac{(Y \sin \theta)^2}{1+iZ-X} \mp \sqrt{\frac{1}{4} \frac{(Y \sin \theta)^4}{(1+iZ-X)^2} + (Y \cos \theta)^2}} \right]^{-1} \quad (1.56)$$

where  $X = (\omega_p/\omega)^2$ ,  $Y = -(\omega_g/\omega)$  and  $Z = (\omega_{eff}/\omega)$ . for the propagation constants (see equation (1.55)) they are:

$$k'_\theta = \frac{\omega}{c} \left[ 1 - \frac{X}{1 + iZ - \frac{1}{2} \frac{(Y \sin \theta)^2}{1+iZ-X} + \sqrt{\frac{1}{4} \frac{(Y \sin \theta)^4}{(1+iZ-X)^2} + (Y \cos \theta)^2}} \right]^{\frac{1}{2}} \quad (1.57)$$

$$k''_\theta = \frac{\omega}{c} \left[ 1 - \frac{X}{1 + iZ - \frac{1}{2} \frac{(Y \sin \theta)^2}{1+iZ-X} - \sqrt{\frac{1}{4} \frac{(Y \sin \theta)^4}{(1+iZ-X)^2} + (Y \cos \theta)^2}} \right]^{\frac{1}{2}} \quad (1.58)$$

The found result concerning the propagation vector reveals that there are two electromagnetic waves traveling in an arbitrary direction  $\theta$  with different propagation constants  $k'_\theta$  and  $k''_\theta$  called *ordinary wave* (since is the

same of the propagation constant in an isotropous plasma) and *extraordinary wave*, respectively. A more detailed explanation of the behavior of an electromagnetic wave propagating in a plasma can be found by calculating the refraction index associated to a plasma ( $n = c/v$ ). This quantity is a function of the angle  $\theta$  and of the pulsation of the electromagnetic wave  $\omega$ . This reveals the presence of resonances for defined values of the angle  $\theta$  like  $0^\circ$  or  $90^\circ$  for defined values of the ratio  $\omega/\omega_p$ . It is interesting to better develop the equations for the situations of wave propagation perpendicular to the magnetic field direction and wave propagation parallel to the magnetic field direction.

### 1.5.3 Electromagnetic waves with wave vector perpendicular to the magnetic field direction

When the wave propagation direction is perpendicular to the direction of the magnetic field the angle  $\theta = \pi/2$  and the propagation constants become:

$$k'_{\frac{\pi}{2}} = \frac{\omega}{c} \sqrt{1 - \frac{\omega_p^2}{\omega(\omega + i\omega_{eff})}} \quad (1.59)$$

$$k''_{\frac{\pi}{2}} = \frac{\omega}{c} \sqrt{1 - \frac{\omega_p^2 \left(1 + i\frac{\omega_{eff}}{\omega} - \frac{\omega_p^2}{\omega^2}\right)}{(\omega + i\omega_{eff}) \left(\omega + i\omega_{eff} - \frac{\omega_p^2}{\omega}\right) - \omega_g^2}} \quad (1.60)$$

The waves propagating along a perpendicular direction to the magnetic field are called *O waves* or *X waves* depending on the direction of the orientation of the electric field associated to the wave with respect to the magnetostatic field direction. The O waves have an electric field with a parallel direction to the direction of  $\vec{B}_0$  while the electric field of the X waves have is perpendicular to the direction of  $\vec{B}_0$ . It is possible to calculate the refraction index related to the two waves:

$$n_{Owaves}^2 = \frac{c^2}{v^2} = \frac{c^2 (k'_{\frac{\pi}{2}})^2}{\omega^2} = 1 - \frac{\omega_p^2}{\omega^2} \quad (1.61)$$

$$n_{Xwaves}^2 = \frac{c^2}{v^2} = \frac{c^2 (k''_{\frac{\pi}{2}})^2}{\omega^2} = 1 - \frac{\omega_p^2}{\omega^2} \frac{\omega^2 - \omega_p^2}{\omega^2 - \omega_p^2 - \omega_g^2} \quad (1.62)$$

It is evident that the O waves have no resonances while the X waves resonate at the pulsation  $\omega_h$  defined as *upper hybrid resonance* defined as:

$$\omega_h = \sqrt{\omega_p^2 + \omega_g^2} \quad (1.63)$$

#### 1.5.4 Electromagnetic waves with wave vector parallel to the magnetic field direction

When the propagation direction is parallel to the direction of the magnetic field the angle  $\theta = 0^\circ$  and the propagation constants become:

$$k'_0 = \frac{\omega}{c} \sqrt{1 - \frac{\omega_p^2}{\omega(\omega + i\omega_{eff} - \omega_g)}} \quad (1.64)$$

$$k''_0 = \frac{\omega}{c} \sqrt{1 - \frac{\omega_p^2}{\omega(\omega + i\omega_{eff} + \omega_g)}} \quad (1.65)$$

The two waves propagating in a perpendicular direction to the magnetic field are named *R waves* and *L waves* according to their polarization (R is corresponding to the right hand polarization and L is referred to the left hand polarized waves). As for the propagation along the perpendicular direction to the direction of  $\vec{B}_0$ , it is possible to calculate the refraction index for the parallel propagation:

$$n_{Rwaves}^2 = \frac{c^2}{v^2} = \frac{c^2(k'_0)^2}{\omega^2} = 1 - \frac{\frac{\omega_p^2}{\omega^2}}{1 - \frac{\omega_g}{\omega}} \quad (1.66)$$

$$n_{Lwaves}^2 = \frac{c^2}{v^2} = \frac{c^2(k''_0)^2}{\omega^2} = 1 - \frac{\frac{\omega_p^2}{\omega^2}}{1 + \frac{\omega_g}{\omega}} \quad (1.67)$$

It is then possible to point out that the refraction index related to the R waves becomes infinitive when the angular frequency is equal to the electron cyclotron frequency defined in the paragraph 1.4.1 and this implies that the R wave is in resonance with the cyclotron motion of the electrons. This resonance is called **Electron Cyclotron Resonance** and is of primary importance for the ECRISs. No resonance of the refraction index occurs when a L wave propagates in a magnetized plasma. It is possible to summarize the different cases of wave propagation in the table 1.1:

Table 1.1: Wave types propagating in a magnetized plasma and related refraction indexes.

vector orientation	refraction index	wave type
$\vec{k} \perp \vec{B}_o, \vec{E} \parallel \vec{B}_o$	$1 - \frac{\omega_p^2}{\omega^2}$	O Wave
$\vec{k} \perp \vec{B}_o, \vec{E} \perp \vec{B}_o$	$1 - \frac{\omega_p^2}{\omega^2} \frac{\omega^2 - \omega_p^2}{\omega^2 - \omega_p^2 - \omega_g^2}$	X Wave
$\vec{k} \parallel \vec{B}_o$	$1 - \frac{\omega_p^2}{1 - \frac{\omega_g^2}{\omega^2}}$	R Wave
$\vec{k} \parallel \vec{B}_o$	$1 - \frac{\omega_p^2}{1 + \frac{\omega_g^2}{\omega^2}}$	L Wave

## 1.6 Electron heating at the ECR

It is important to describe the effect on the electron motion in a magnetized plasma when an electromagnetic wave is propagating in a parallel direction to the magnetic field. The injection of such an electromagnetic wave is the most common way to produce a laboratory plasma and it is also used as a working principle for the normal operation of an ECR Ion Source. For this purpose it is interesting to analyze the propagation of left or right hand circularly polarized waves and their effect on the electron motion. The wave polarization is a wave property which describes the spatial orientation of the wave field vectors. If the electric field, during the wave propagation, describes a circumference, the wave is called circularly polarized. A left hand (electric field rotating counterclockwise in the direction of travel) circularly polarized wave has an electric field:

$$\vec{E}'' = (\hat{x} + i\hat{y})Ae^{ik_0''z} \quad (1.68)$$

where A is a constant related to the field amplitude. By inserting the  $k_0''$  from the (1.65) in the (1.68) and inserting the electric field components in the solution of the differential equation (1.49), the components of the velocity (in the plane  $z = 0$ ) of an electron become:

$$|v_x|^2 = |v_y|^2 = \frac{q_e^2}{m_e^2} A^2 \frac{1}{(\omega_g + \omega)^2 + \omega_{eff}^2} \quad (1.69)$$

$$|v_z|^2 = 0 \quad (1.70)$$

Then the electron velocity does not experience any resonance. In the case of a right hand (electric field rotating clockwise in the direction of travel) circularly polarized wave the electric field vector associated to this wave is:

$$\vec{E}' = (\hat{x} - i\hat{y})Be^{ik'_0z} \quad (1.71)$$

where B is a constant related to the field amplitude. In this case by inserting the  $k'_0$  from the (1.64) in the (1.71) and inserting the electric field components in the solution of the differential equation (1.49), the components of the velocity (in the plane  $z = 0$ ) of an electron become:

$$|v_x|^2 = |v_y|^2 = \frac{q_e^2}{m_e^2} B^2 \frac{1}{(\omega_g - \omega)^2 + \omega_{eff}^2} \quad (1.72)$$

$$|v_z|^2 = 0 \quad (1.73)$$

By analyzing the function:

$$F(\omega) = \frac{1}{(\omega_g - \omega)^2 + \omega_{eff}^2} \quad (1.74)$$

It turns infinite when the pulsation  $\omega = \omega_g$ . This determines an increase of the electron velocity and then of the electron kinetic energy. It is worth to observe that independently of the conventional way to describe the coordinate system and the motion of the electrons, a resonance occurs when the direction of rotation of the plane of polarization is the same of the direction of the gyration of the electrons around the lines of the magnetic field. The wave then loses its energy while it accelerates the electrons and it is absorbed by the (electrons of the) magnetized plasma.

## Chapter 2

# The technology of the ion sources

Within this chapter a brief introduction of the main ion sources, focused on the ECR type, is presented. Since the ion sources are mainly used for the production of ion beams, the most important parameters and the main tools for measuring the main properties of an ion beam are here reported.

### 2.1 Definition of ion source

In the first chapter the definition of plasma and of its main parameters has been introduced. A plasma source, however, is different than an ion source or better than an ion beam source. Most of the ion sources are plasma-based in the sense that the plasma is used to produce the ions which are formed in an energetic ion beam. The ionic content from the plasma is extracted by applying a positive high voltage to a (plasma) electrode where at least a hole is present. In the next sections more details will be discussed about the properties of the extraction system in order to improve the ion beam properties. Then the main features of an ion source are a magnetized plasma source, an extractor and the obtained ion beam. It is possible to represent an ideal ion source like shown in figure 2.1. Here the energy  $E_i$  associated to the extracted positive ion beam is given by:

$$E_i = zQ(V_{pl} - V_{ch}) = zQV_{ext} \quad (2.1)$$

It is assumed that the vacuum chamber where the ion beam is drifting is

at  $V_{ch} = 0$  potential and that the plasma chamber is at a potential imposed by a power supply at  $V_{ext}$  potential. The quantity  $z = +1, +2, ..$  is the charge state (or ionization state) of the extracted ion and  $Q$  is the charge of the ion.

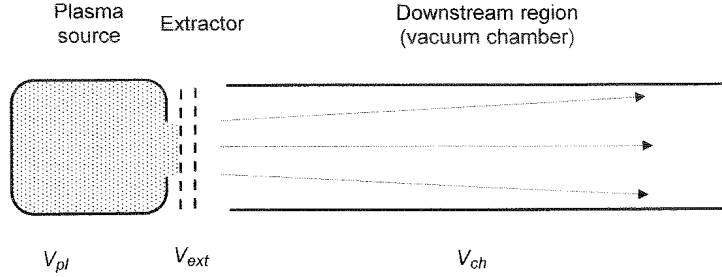


Figure 2.1: *Elementary ion source scheme: first extractor grid incorporated into the plasma chamber structure; the downstream region is the vacuum chamber at ground potential and a high voltage power supply provides the extraction voltage for the plasma chamber and the extractor grid.*[4]

The  $V_{pl}$  is the plasma potential defined as the potential of the plasma with respect to the wall of the chamber that contains it. Since this potential is in the order of a few Volts, this voltage can be neglected with respect to the extraction potential.

The way how the plasma is created usually assigns the name to the ion source: in an ECR ion source the plasma is created by applying an electromagnetic wave at high power and with frequency of several GHz to a magnetically confined plasma; if the microwave frequency is in the order of a few GHz (usually 2.45 GHz) and the magnetic field is flat for the whole dimension of the plasma chamber the source is called Microwave (Discharge) Ion Source (the absence of a double mirror magnetic system makes this kind of ion sources suitable for providing several mA of singly charged ions); in the Laser Ion Sources the plasma is created with the interaction of a high energy Laser with a plasma obtained by ablation of a solid material; the EBIS (Electron Beams Ion Sources) make use of a focused electron beams to ionize the neutral atoms. A more detailed description of the main ion sources used for the production of high charge state ion beams will be reported in section 2.3.

## 2.2 Ion beam parameters, formation and transport

The ion beam formation is mostly dependant on the plasma parameters, i.e. the magnetic system, the microwave power, the extraction voltage. The extraction system is also very important for the beam formation and for the beam properties. In the most simple case an extractor is constituted by a plasma electrode positively charged with high voltage (for the production of positive ion beams) which is in contact with the plasma and a second electrode at a fixed voltage, usually at ground potential. The accelerating electric field is between these two electrodes. An example of this structure is shown in figure 2.2. Single hole electrodes or multi-aperture design are used. Some ion sources make use of multiple electrodes systems [4] negatively biased in order to prevent that the back-streaming electrons formed in the extraction region can be accelerated backwards to the source direction.

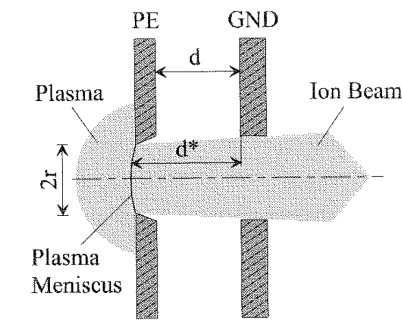


Figure 2.2: Diode extraction system and beam formation. PE is the plasma electrode GND is the ground electrode.

In some cases the ground electrode can be moved in order to vary the ion beam properties. An ion beam can be gaseous or metallic, if it is formed from a plasma obtained by the ionization of a gaseous material or by the vapor of a metallic material, respectively. In section 2.4.4 the main techniques to produce a metal ion beam will be described. An ion beam can be also singly charged or multiply charged or else, as mostly occurs, a mixture of charge states which can be separated by a magnetic dipole. The ion beam formed by an ion source can be described with many different parameters: the beam energy, the ion current, the beam shape and the beam divergence calculated with the so called beam emittance and brightness. For increasing the **beam**



**energy**, defined as the energy per ion in the beam, according to the (2.1) it is possible to increase the extraction voltage or to choose the proper ion source which is able to efficiently produce high charge state ions.

The **beam current** is the total current carried by the beam. In the most simple case of an extractor made by two electrodes (a plasma electrode at positive potential and a ground electrode at ground potential) separated by a distance  $d$ , the extracted current density is defined by the Child-Langmuir law [8],[9]:

$$j = \frac{4}{9} \epsilon_0 \sqrt{\frac{2zQ}{m_i}} \frac{1}{d^2} U^{3/2} \quad (2.2)$$

Where  $U$  is the voltage drop between the two electrodes. This extraction system is described in figure 2.2. Here the distance  $d^*$  indicates the distance between the emission surface of the ions at the plasma boundary, called plasma meniscus [10], and the ground electrode. The ions with mass  $m_i$  and charge  $zQ$  will experience an accelerating force due to the electric field which amplitude is  $|\vec{E}| = U/d$ . If the plasma electrode is a single aperture electrode with radius  $r$ , a cylindrical symmetric beam (if the diverging forces are neglected) is formed with current:

$$I = \frac{4}{9} \pi \epsilon_0 \sqrt{\frac{2zQ}{m_i}} \frac{r^2}{d^2} U^{3/2} \quad (2.3)$$

In most of the cases the beam extracted by an ion source has to be transported into accelerators to achieve the required energy by the main projects making use of accelerator facilities. Then beam lines connecting the ion source with the accelerators are assembled. Along a beam line the beam is filtered according to the mass over charge ratio, is focused, steered and analyzed. It is then important to reduce the losses along the beam and then, for an efficient beam transport, the beam quality represents an important parameter. The **beam quality** is measured by the *emittance* which is roughly the product between the beam diameter and the transverse momentum spread. In accelerators physics it is common to define the emittance with an ellipse. Following Liouville's theorem [11] (the six dimensional volume stays constant if only conservative forces are applied) the phase space of a particle beam can be described by a so called phase space ellipse, see Fig. 2.3. The beam emittance stays constant in the six dimensional space  $(x, y, z, v_x, v_y, v_z)$ . If there is no coupling between the different planes, this assumption is true for the two dimensional subspaces as well. The area of the ellipse stays constant if only conservative forces act on the ion beam. If

the area occupied by particles in phase space is known at any location of the beam line, the emittance is known.

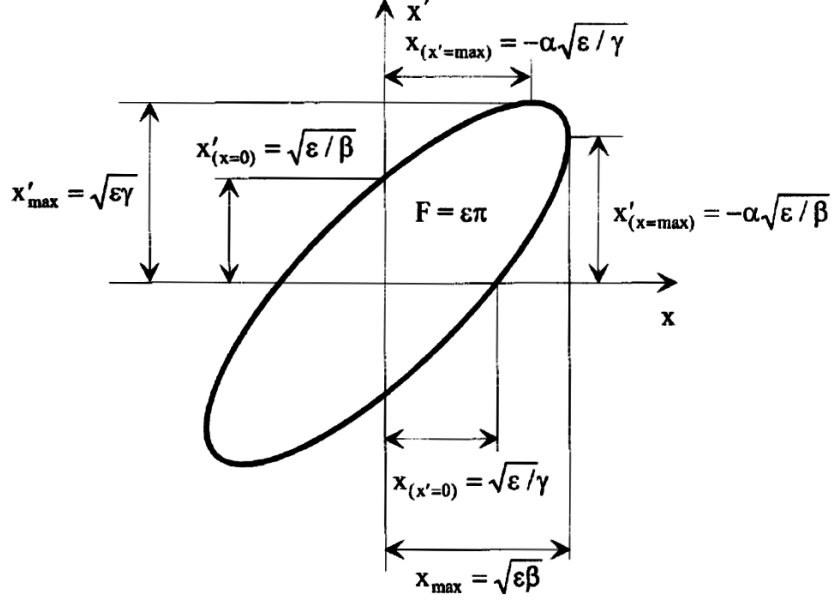


Figure 2.3: *The emittance ellipse and important abbreviations.*

The area enclosed by the phase space ellipse divided by  $\pi$  is the beam emittance  $\epsilon$  and can be described as:

$$\epsilon = \gamma x^2 + 2\alpha x x' + \beta x'^2 \quad (2.4)$$

$$1 = \beta\gamma - \alpha^2 \quad (2.5)$$

$\alpha$ ,  $\beta$  and  $\gamma$ , called Twiss parameters, determine the shape and orientation of the ellipse. During the transport of the beam it passes through linear elements i.e. drift sections, solenoids, quadrupoles, or dipoles. These elements modify the Twiss parameters, but keeps the area of the ellipse, the emittance, constant. Therefore it is possible to calculate the emittance by the knowledge of the beam size in, at least, three different positions along the beam line and the transport properties of the beam line. This provides a system of linear equations which can be solved according to the three positions method described in section 2.5.3.

An other parameter featuring the beam quality is the *beam brightness* which measures the the current per unit solid angle and it is defined by:

$$B = \frac{I}{\epsilon_x \epsilon_y} \quad (2.6)$$

Here the current  $I$  is expressed in amperes and, with the brightness parameter, it is normalized by the emittances of the two-dimensional sub-spaces.

### 2.3 Ion sources for the production of beams of multiply charged ions

The ion sources can provide beams of single or multi charged positively ions according to the purpose they are designed for. The industrial applications making use of an ion source include, for instance, the ion implantation, the surfaces treatments, the thin-film deposition. However, the increasing demand of the ion sources is carried out by the laboratories or the facilities where at least a particle accelerator is present. A particle accelerator facility provides high energy beams for nuclear physics experiments, for medical applications, for instance for the cancer therapy, or for else the nuclear trashes transmutation etc. In order to fulfill the accelerators request a spreading request of higher current of highly charge state ion beams has to be fulfilled. For this reason the main requirements of an ion source, to be used as an accelerator injector, are:

- high current beams;
- beams of highly charged ions;
- low emittance beams;
- possibility to produce metal ion beams;
- high reliability and low cost and maintenance;

An intense ion beam is requested from the experiments where a low cross section reaction measurement must be carried out. In fact if the provided current is reasonably high the aquisition/measurement time can be reduced. If the transmission through the beam line or at the accelerator output is not optimized, an high extracted current can compensate the ion beam losses. For this reason, and in order to match the so called accelerator *acceptance*

(maximum beam area, in the space phase, an accelerator can accept as a beam input), a low emittance beam is also a requirement. Since the ion beam energy is  $q\Delta V$  in the case of a linear accelerator and it is proportional to the square of the charge in the case of a circular accelerator, like a cyclotron, then it is clear that the achievable beam energy can be enhanced if the accelerated beam is made of highly charged ions. Concerning the high charge state ions production, in the section 1.3.2 the requirements that an ion source must achieve are described. They are summarized in the concept of quality factor which is the product of the electron density and of the confinement time. Then a suitable source for this purpose has to be conceived to produce a well confined plasma featured by a high electron density (and energy according to the diagram shown in figure 1.2). The demand of ions obtained from not gaseous elements like Uranium, Titanium, Chromium, Calcium [12] restricts the suitable ion sources on the ones able, with low effort, to produce metal ion beams with high efficiency and long lifetime. Some interesting techniques used by the main ion sources for the production of these beams are listed in section 2.4.4.

Several types of ion sources fulfilling the above listed requirements exist. One of the most used categories of ion sources for the production of high current ion beams is represented by the so called **filament driven ion sources**. Within this category it is possible to include all the devices where the plasma is generated by electron-impact of high energy electrons emitted by a cathode and travelling towards the anode (100 - 1000  $\Delta V$ ) dissipating their energy in the plasma generation. In order to enhance the high charge states ion production the charged particles are magnetically confined by a transverse magnetic field (0.1 T - 1 T). However some disadvantages of these ion sources include the short lifetime of the filament and of the main components, the low quality of the extracted beam and a not so high charge state ion production.

A similar kind of ion source, which makes use of an electron beam focused by a high magnetic flux density is the **Electron Beam Ion Source (EBIS)** [13],[14]. Figure 2.4 describes the working principle of an EBIS: the dense and strongly focused electron beam forms, by its space charge, a radial well for the ions, closed on the longitudinal direction by potentials applied to cylindrical electrodes.

The neutral atoms are ionized by electron impact inside the electron beam and the obtained ions are trapped and subjected to stepwise ionization until they are extracted in a pulsed regime. The higher confinement magnetic field makes these kind of sources suitable for the production of high

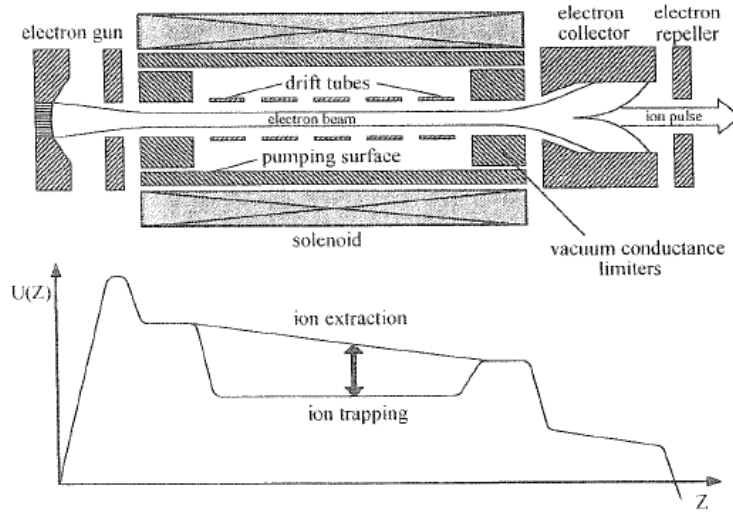


Figure 2.4: Working principle of an EBIS.[2]

charge state ions in not so intense beams. This is mainly due to the higher confinement times which lower the extractable ion current (since  $I \propto n_e/\tau_i$ ). The possibility of provide pulsed beams is largely covered by the **Laser Ion Sources (LIS)**. Inside a LIS a plasma is produced with the power of a focused laser ablating a target made of the solid material which ions are requested. An interaction of the high energy laser and of the electrons of the so called *plasma plume* generated during the ablation process accelerates the electrons and the ionization process takes place. A successive ionization proceed for the electron-ion collisions. Higher is the power density of the laser and higher is the electron energy. The plasma expands along a direction where an extraction plane is placed. Intensive pulsed beams of any kind of solid material can be produced with a LIS but, even if highly charge state ions can be produced, it has to be mentioned that the short pulse length and the low repetition rate restrict the operation of the LIS as a beam supplier for the main accelerator facilities.

Besides the presented types also others ion sources exist, like, for instance, the Vacuum Arc Ion Sources or the RF Ion Sources or else the Microwave Ion Sources, but they are mainly used to produce single or low charged ion beams.

The main ion sources for the highly charge state ions production have been

shortly described (more details about the reported ion sources can be found in [2] and [4]) and it turns out that in order to fulfill all the above present requirements an other kind of ion source must be used: the ECR Ion Source. In the next section they are described and it is explained the reason why they are so largely used for providing higher charge state ion beams for the accelerator facilities.

## 2.4 The ECR ion sources

The Electron Cyclotron Ion Sources are nowadays one of the most used ion sources for producing high charge state ion beams for the particle accelerators facilities. A long life-time, low maintenance/repair works, high stability in producing intense CW or pulsed beams of highly charged ions (of gaseous and metallic elements), make these ion sources a very powerful beam injector. Due to the increasing demand of higher charge states they are continuously under development and new and more performing ECRISs are running in several laboratories. This request of higher performances made also increase the cost of such devices, in particular for the ones making use of (or planned for working with) a superconductive magnetic system. Some disadvantages include the long conditioning times, the power consumption and the not easy production of metallic ion beams. Within this section the working principles and a detailed description of the main parts of the ECRISs will be introduced together with a review of the developed ion sources from the first ones up to the state of the arts.

### 2.4.1 Working principle and empirical scaling laws

The working principles of the ECR Ion Sources are based on the electron heating and on the particle confinement. When a gas is injected into the plasma chamber of an ECRIS the limited number of free electrons moves in spiral trajectories around the confinement magnetic field lines as described in section 1.4.1. Under the effect of the electromagnetic wave, with a frequency  $f$ , they are accelerated by the wave field. An absorption of the wave energy occurs when the electrons cross the surface where is fulfilled the condition:

$$B_{ECR} = 2\pi \frac{m_e}{e} f \quad (2.7)$$

The energized electrons by striking with the neutral atoms are able to ionize them and a plasma ignition occurs. A continuous process, sustained by the particles confinement in a double mirror magnetic field, ensures to

reach high values of electron density and confinement times. This makes possible to obtain the high charge state ions to be extracted by placing the plasma chamber at a high voltage. On the basis of the results obtained with the MINIMAFIOS ECR ion source in 1985 R. Geller formulated the so-called **scaling laws** regulating the performances of the ECRISs [5]:

$$I \sim \frac{\omega_{RF}^2}{M} \quad (2.8)$$

$$q_{opt} \sim \log \omega_{RF}^3 \quad (2.9)$$

These empirical scaling laws relate the operative frequency of the ECRISs and the extractable current  $I$  and the charge state  $q_{opt}$  (giving the maximum ion current) of the ions with mass  $M$ . These results predicted also that the development of the ECRIS must be accompanied by an increase of the operative frequency in order to achieve higher intensities of higher charge state ions. However next experiments brought to the formulation of the so called **high-B mode** principle [15]. According to this experimental principle, the increase of the magnetic confinement generates an enhancement of the electron density and of electron temperature which consequently improves the ECRIS performances. Then together with the increase of the microwave frequency, the confinement field must be increased as well. This principle can be resumed in the following condition

$$\frac{B}{B_{ECR}} \geq 2 \quad (2.10)$$

Where the  $B/B_{ECR}$  is called *mirror ratio* of the ECRIS. It will be shown in the next section how the above introduced laws have accompanied the development of the ECRISs through the years.

### 2.4.2 General description

The main components of an ECR ion source are:

- a vacuum chamber which is a metallic cylinder where the gas is injected, with apertures for the income of the microwaves or for the insertion of devices useful for the normal operation of the source. The plasma chamber is insulated from the magnetic coils and positively charged for the ion extraction. Usually the plasma chamber is water cooled or in the case of superconductive sources the cooling is operated by the coolant bath where the magnetic system and the plasma chamber are immersed;

- a magnetic system which provides a longitudinal and radial confinement of the charged particles;
- the gas injection system;
- the microwave injection system mainly composed by a high power microwave generator providing the feeding electromagnetic wave through a waveguide line connected to the ion source;
- an extraction system which includes at least a plasma electrode biased at the same voltage of the plasma chamber and a grounded electrode.;
- ancillary components like the ion source supports, the water and the gas pipes, the electrical cables, the pumping systems, etc.;

In the next chapter the plasma chamber and the microwave injection system will be largely discussed. The magnetic trap is composed by two solenoid coils (or permanent magnets) producing a longitudinal double mirror magnetic configuration and a multipole producing a radial magnetic field constraining the particle to be entrapped in the plasma chamber center both axially and radially. Iron yokes are used to reduce the power consumption of the coils and the stray field around the source (detrimental in the extraction region for the ion beam emittance increase). According to the (2.10) it is clear that for ECRIS operating at frequencies higher than 18 GHz ( $B_{ECR} \sim 0.64T$ ) the room temperature coils cannot produce the necessary magnetic flux density to get an optimal confinement. Then, as described in the next section, the new ECRIS are equipped with superconductive coils. Different multipole structure can be used to produce a radial magnetic field as shown in figure 2.5.

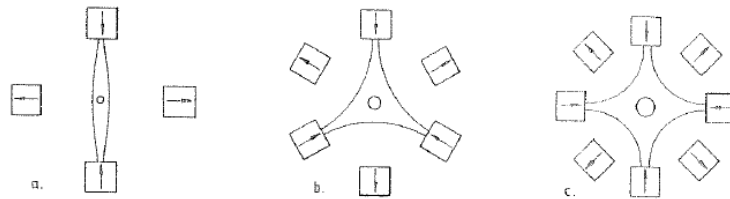


Figure 2.5: *Different multipoles for the radial magnetic confinement: a) quadrupole; b) sextupole; c) octupole.*



Higher is the number of multipoles and larger is the loss area of the chamber end points and lower is the flux density achievable far away from the poles position. For these reasons the most used geometry is the sextupole. In figure 2.6 the magnetic field structure for an ECRIS (a CAPRICE-type) is shown. In the left image the magnetic field ( $B_{ECR}$ ) for the operation at 14.5 GHz is indicated. At the two points (a closed egg shaped surface in the 3D plot) where the condition  $B = B_{ECR}$  occurs, an absorption of the electromagnetic energy by the electrons takes places.

Concerning the gas injection system, it is composed by a remotely controlled valve for the precise control of the gas pressure (in order to maintain low the neutral atoms rate in the plasma). Most of the ECRIS make use of a gas inlet where two kind of gases are provided in a mixture. This technique, called *gas mixing*, is operated by adding a lighter gas (Helium or Oxygen) to the plasma which produces an ion cooling. The explanation of the benefits of this effect is connected to the cooling of the highest charged ions by the lowest charged mixing ions thus increasing the confinement time of the higher charged ions [5].

When a beam of metallic ions is requested, the gas inlet is exchanged with the components necessary for the metal evaporation. The different techniques for this purpose are described afterwards.

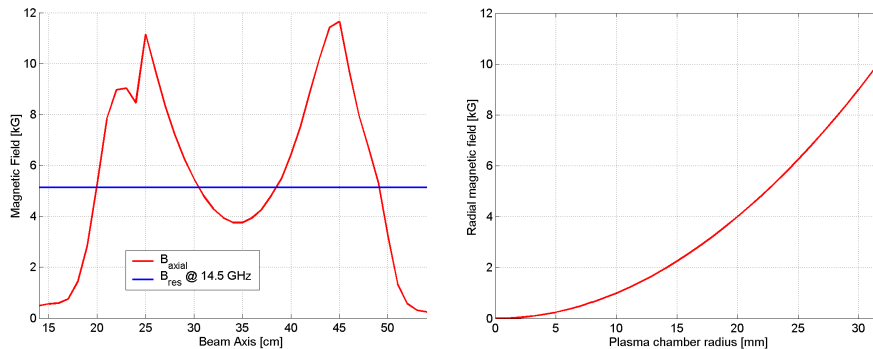


Figure 2.6: Axial magnetic field profile (left) and radial magnetic field profile (without considering the effect of the solenoids) produced by a sextupole (right).

The extraction of the ions from the plasma is obtained by applying a positive potential (several kV) to the source. Some considerations about the beam formation have been already introduced in section 2.2. As shown in figure 2.7, in addition to the plasma electrode and to the grounded puller,

sometimes intermediate electrodes negatively biased are present in the extraction column in order to prevent that the back-streaming electrons can be accelerated back to the extraction region. The effect of the electrons, escaping along the field lines from the magnetic trap and leaving a trace on the plasma electrode, is clear in this picture. Some typical values of the settings of the extraction voltage and of the screening voltage, for the CAPRICE ion source, are also shown.

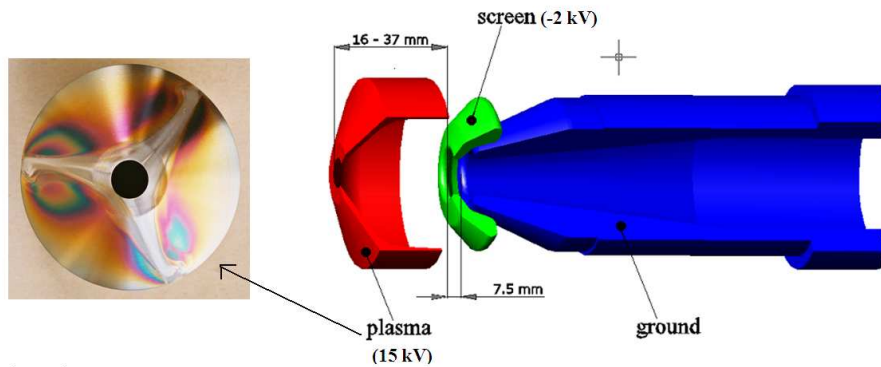


Figure 2.7: Main components of the extraction system of a CAPRICE-type ECRIS: in red is indicated the plasma electrode, in green the screening electrode and in blue the grounded puller electrode.

### 2.4.3 History and state of the art of the ECRISs

The born of the ECRISs date time the late 1960s when R. Geller applied his experience with mirror machines for fusion plasma studies to assembly the first ECRIS for the production of high charge state ions and making use of mirror solenoid coils. This ECRIS called MAFIOS [16] was not well performing for the production of high charge states and in 1975 he proposed an improved version called SuperMAFIOS [17], which was equipped with a hexapolar magnetic field (for the radial confinement) together with the mirror magnetic system. This ion source was able to produce high charge states due to the longer ion lifetime. The main problem of such an ECRIS was the power consumption (around 3 MW) by the room temperature coils. The idea to make use of permanent magnets for the sextupole radial confinement field was used by Geller to assembly the MICROMAFIOS ECRIS [18] which was then further modified, developed and renamed as MINIMAFIOS

[19]. This source, which drawing is shown in figure 2.8 has been built by Geller's team for several laboratories.

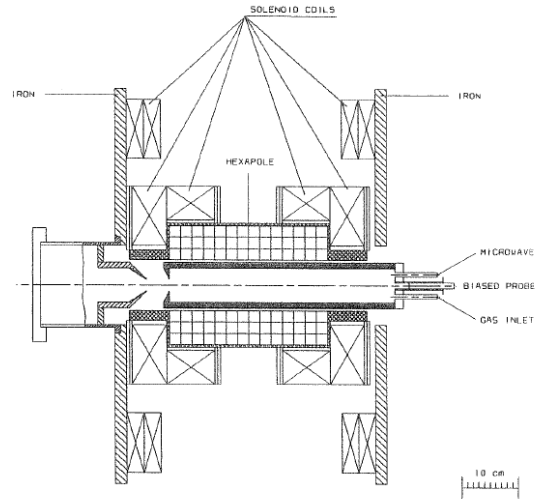


Figure 2.8: *Cross section of the MINIMAFIOS ion source.*

A further improvement of this source was performed in 1984 when a stronger magnetic field and higher microwave frequency were used for the construction of the MINIMAFIOS-16 GHz [20] with the fulfilled aim to get more intense beams of higher charge states. This second generation of ECRIS was followed by other ion sources with higher operative frequency and stronger magnetic flux density. It is the example of the Advanced ECR (AEER) [21] and the Advanced ECR-Upgrade (AEER-U) [22] ion sources dated 1990 and 1996, respectively, and installed at LBNL and in other laboratories [23],[24]. A cross section of the AEER-U ion source is shown in figure 2.9. In this figure the two resonance surfaces at 10 GHz and at 14 GHz are also indicated. It has to be mentioned that this ion source can operate with the double frequency technique which will be described in the fourth chapter.

The ECR-4 [25] and the CAPRICE ion sources (Compact ion source A Plusieurs Resonances Ionisantes Cyclotron Electroniques) were developed in Ganil and in Grenoble in the same years. A complete description of the CAPRICE-Type ion source will be reported in the fourth chapter. Other sources like RTECR installed at MSU [26], or ion sources making use of fully permanent magnets like NeoMAFIOS [27] or Nanogan [28] or else the

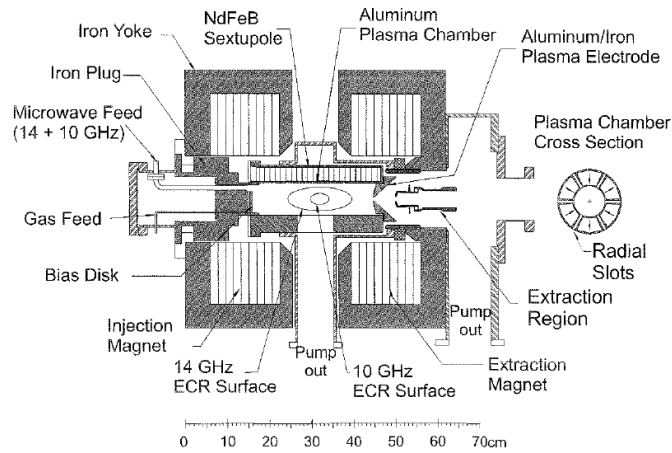


Figure 2.9: Cross section of the AECR-U ion source.

Low cost ECRIS [29] installed at Giessen have been developed. The main parameters of the ion sources, here briefly introduced, are listed in the table 2.1.

The increasing demand of more intense beams of higher charge states required a development of better performing ECRISs operating at higher microwave frequency and equipped with magnetic systems based on the superconductive technology. Ion sources like SERSE (Superconducting Electron cyclotron resonance ion source) installed at INFN-LNS, [30], [31], [32] or SC-ECRIS installed at RIKEN laboratory in Japan [33], or else the SUSI (Superconducting Source for Ions) superconducting ion source [34] at NSCL, USA, have been assembled. In the beginning of 2005 the high temperature superconducting electron cyclotron resonance ion source (HTS-ECRIS) called PKDELIS [35] was installed at IUAC, India and the SECRAL ECRIS has been installed in Lanzhou, China. The SECRAL ECRIS, has a special design of the magnetic structure, as shown in figure 2.10, with the sextupole surrounding the solenoid coils.[36] This structure has the advantages of the lower magnetic flux density required by the solenoid coils to achieve a good axial confinement and a lower stray field effect of the sextupole on the extracted beam [37].

These ion sources are using 18 GHz microwave generators and for most of them it is also planned to work at higher frequency. It is the example of the SUSI and SECRAL Ion source now operating at 24 GHz. Very in-

Table 2.1: Table reporting the main features and performances of the main ECRISs.[2]

		MiniMAF.	Caprice	MSU-RTECR	LBL-AECR	ECR-4	NeoMAFIOS	Nanogan	Low cost
RF frequency	(GHz)	10-18	10-14.5	6.4	14.5	14.5	8-10	10-14.5	5
Microwave Power	(kW)	1-5	1	0.5	1.5	≤2	≤0.6	≤0.1	≤1
Axial field	(T)	1.5	1.2	0.38	1	1.1	0.56	0.75	0.5
Hexapole field	(T)	0.7	0.8-1.2	0.34	0.8	1	0.42	0.7	0.5
Magnet supply	(kW)	150	1.2	80	90	45	-	-	30
Gas flow	(scm)	0.1	0.1	0.1	0.1	0.1	0.1	0.1	0.1
Extraction	(mm)Ø	8-12	6-10	8	8-10	6-10	6-8	5	6
Extr. volt.	(kV)	0-2.5	0-25	5-20	10	30	0-15	0-15	0-15
Plasma chamber	(cm)Ø	6.6	6.6	14	7.5	6.6	6.5	2.6	7
Chamber length	(cm)	36	16	82	30	16	18	16	25
N <sup>6+</sup>	(µA)	110	150	13	41	-	2.8	-	-
O <sup>7+</sup>	(µA)	180	50	5	131	-	0.3	0.3	2
Ne <sup>8+</sup>	(µA)	-	7	1	7.5	-	-	-	-
Ar <sup>8+</sup>	(µA)	280	550	40	210	500	90	65	40
Kr <sup>17+</sup>	(µA)	-	42	5	48	50	1	1	-
Xe <sup>20+</sup>	(µA)	50	42	6	27	41	5	3	-
Al <sup>3+</sup>	(µA)	-	-	-	-	-	28	-	-
Ta <sup>16+</sup>	(µA)	-	-	-	-	-	15	-	-
Ca <sup>11+</sup>	(µA)	-	18	-	47	-	-	-	-
Au <sup>86+</sup>	(µA)	-	13	-	-	-	-	-	-
Pb <sup>25+</sup>	(µA)	-	25	-	-	30	-	-	-
Bi <sup>25+</sup>	(µA)	50	20	-	10	-	-	-	-
U <sup>28+</sup>	(µA)	6	6	2.8	-	5	-	-	-
Max. charge state	N	7	7	7	7	-	6	-	6
Max. charge state	Ne	10	9	10	9	-	6	-	-
Max. charge state	Ar	18	18	17	16	16	12	12	12
Max. charge state	Kr	26	23	24	28	20	20	18	-
Max. charge state	Xe	32	29	31	31	29	23	22	-
Max. charge state	Ta	30	29	-	-	31	22	-	-
Max. charge state	U	35	31	36	-	28	-	-	-

interesting for this development were the results of the experiments carried out in 2001 at LNS when a 28 GHz gyrotron generator was coupled to the SERSE source [38]. A "third generation" of ECRISs is making use of 28 GHz gyrotron system like the VENUS ECRIS at LBNL [39] or the European MS-ECRIS (Multipurpose fully Superconducting ECRIS), designed to work at 28 GHz [40] and described in figure 2.11. Here a comparison between the expected performances of MS-ECRIS and the ones fulfilled by SERSE is also reported. Even if most of new ECRISs are facing some problems connected to the stronger magnetic fields, like the VENUS ion source [41] and the MS-ECRIS ion source [42], it is clear that the development of more performing ECRISs is still ongoing.

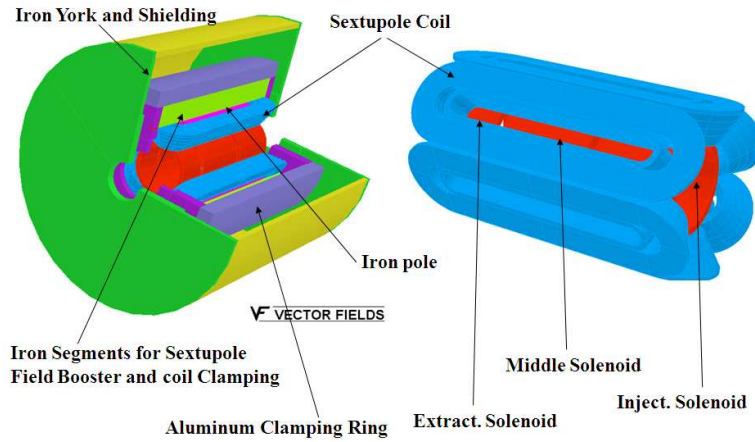


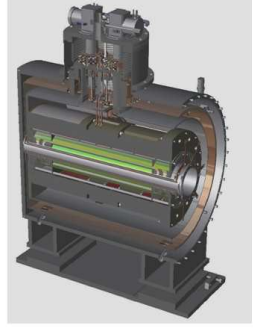
Figure 2.10: *Magnetic structure of the SECRAL ion source.* [36]

#### 2.4.4 The metal ion production with the ECRIS

In order to fulfill the request of beams of ions obtained from metallic elements the ECRISs are demanded to produce efficiently such ion beams. The most important techniques to obtain an ion beam from a metallic material include:

- insertion of ovens for the material evaporation;
- direct insertion of solid materials into the plasma;
- sputtering;
- use of gaseous or volatile chemical compounds (MIVOC);

An oven for the metal vapor production can be introduced in an ECRIS radially or axially through a housing where a pushing rod can be moved inside the ion source. The use of a water flow keeps low the temperature in the whole structure. In figure 2.12 the two kinds of ovens used at GSI for the metal ion production are shown. The principle of the STO (*Standard Temperature Oven*) is a tungsten wire wound on a ceramic body (heater) where a voltage is applied (of a few ten of Volts). Normally all of the ceramic parts are made from Alumina. The material to be evaporated is filled directly into the heater and a vapor pressure between  $10^{-3}$  and  $10^{-2}$  mbar is needed for an effective evaporation. If a possible chemical reaction between the material to be evaporated and the ceramic might occur, an additional crucible, which fits into the opening of the heater, can be used.



	<i>SERSE</i>	<i>MS-ECRIS</i>
$f$	18 GHz	28 GHz
$B_{radial}$	1.55 T	2.7 T
$B_{inj}$	2.7 T	4.5 T
$B_{ext}$	1.6 T	3.2 T
$\phi_{chamber}$	130 mm	180 mm
$L_{chamber}$	550 mm	640 mm
$\phi_{cryostat}$	1000 mm	1100 mm
$L_{cryostat}$	1310 mm	1347 mm
$V_{extr}$	20-25 kV	40 to 60 kV
$LHe$	~4l/h	0
$O^{8+}$	~7 $\mu A$	~ 20 to 50 $\mu A$
$Ar^{12+}$	15 $\mu A$	100 $\mu A$
$Au^{45}$	~1 pA	~0.1 $\mu A$
$Xe^{20+}$	10 $\mu A$	50 $\mu A$
$Pb^{27+}$	----	40 $\mu A$

Figure 2.11: *MS-ECRIS* and magnetic system (left). On the right a table describes the *ECRIS*'s main features. A comparison with the *SERSE* ion source is also indicated.

The STO oven works in the range of  $500^{\circ}C$ - $1600^{\circ}C$ . In some special cases, for example when evaporating a material at very high operating (melting) temperature, a big amount of condensed material can be deposited at the front of the ceramic body. When the STO cannot be refilled, a new oven must be used. The HTO (*High Temperature Oven*) is requested for materials with a melting point higher than  $1600^{\circ}C$ . The main problem to design an oven for higher temperatures (up to  $2000^{\circ}C$  was the goal to evaporate uranium oxide for production of uranium ions beams) was connected to the small dimensions inside the CAPRICE-type ECRIS. It was intended to use the same outer and inner diameter for the HTO compared to the STO. The only suitable material for the heating wire is a special tungsten alloy. Another problem was the material for the crucible retainer (violet). This part extends over a length of 55 mm and it is made of a tungsten alloy containing 2% of  $La_2O_3$ . In the CAPRICE-Type ECR source, installed at GSI, titanium at  $1750^{\circ}C$  and vanadium at  $1850^{\circ}C$  can be vaporized with the HTO. [43]

The *direct insertion* technique is carried out by using a solid rod positioned close to the plasma where the high energetic electrons can be heated to a temperature sufficient to evaporate the material from the sample. The the vapor is ionized there and the stability in the operation and in the ionization is obtained by moving axially the rod.[44] The *sputtering* method makes use of the plasma ions for the insertion of neutral metal atoms to be ionized.

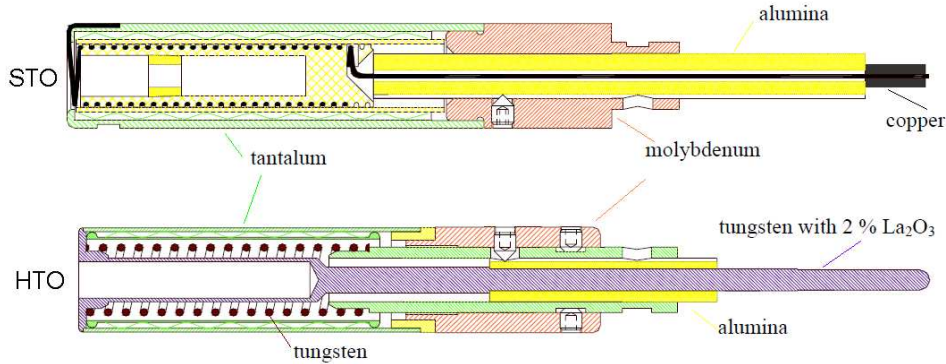


Figure 2.12: Ovens used at GSI for the metal ion production: Standard Temperature Oven (Top) and High Temperature Oven (Bottom)

In fact with this technique a negatively biased sample material is mounted radially at the periphery of the plasma and it is sputtered by the plasma ions. Some difficulties, in applying this technique, in tuning the source parameters, due to the not-separation between the plasma creation from the evaporation process, must be mentioned.[45],[46] *Gaseous compounds* of the metallic material and lighter elements can be injected into the source or else *volatile compounds* can be injected through a so called MIVOC chamber into the source.[47] However the application of the techniques making use of these compounds is limited for the contamination of the plasma chamber walls and for the short duration of the source stability and performances.

## 2.5 Diagnostic tools of the ion beam properties

In section 2.2 the most important beam parameters have been introduced. It is necessary to carry out a precise measurement of them in order to estimate the transmission along the beam line connecting the ion sources to the accelerators. Within this section some tools used in the main accelerator facilities for the measurement of the beam current, of the beam profile (intensity distribution in the transverse direction over the beam cross section) and of the beam emittance, are reported. The main devices for the ion beam intensity measurements are the Faraday Cups or the Beam current Transformers, nevertheless calorimetric measurements [48] can be also carried out



to indirectly measure the ion beam current. Concerning the beam profile measurements, viewing screens, profile grids, beam profile monitors based on the residual gas ionization, wire scanners, or combinations of slits-Faraday Cup are used. Since in the chapter four the results of measurements with viewing targets are reported, in this section a short introduction on these diagnostic tools is reported. Since the formation and the transport of the beam are strongly dependant on the beam optical properties, the concept and the measurement of the beam emittance are of primary importance, specially if beam imperfections, aberrations, due to the space charge, take place. In [2] the main emittance measurements methods are described, while here a brief introduction of them is reported. Since most of the beam properties can be related to the ion source properties in terms of plasma parameters and conditions, in this section a short description of one of the main used plasma diagnostic tool, the Langmuir probe, it has been included.

### 2.5.1 The Faraday Cup and the Beam Transformer

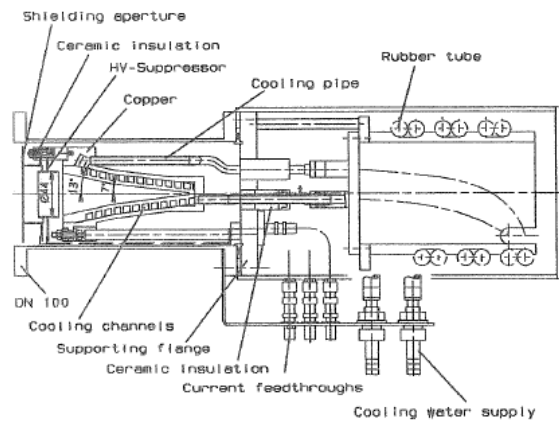


Figure 2.13: Scheme of a Faraday Cup designed to measure currents of ion beams with powers levels up to 25 kW.

In order to have an accurate measurement of the beam current there is the possibility to use destructive methods like the Faraday cup or non-destructive measurement devices like the beam transformers. A Faraday cup collects the ions of the measured ion beam in an electrically insulated cup and the charge is measured by means of a calibrated resistor. Some effects must be included in the design of a Faraday Cup, in the measurement of

the ion current and on the lifetime of the device; these effects include the emission of secondary electrons, the generation of particles from the ionization of the residual, the leak current generation due to the deterioration of the material due, for instance, to the high power beams. For most of the reasons above reported, the main Faraday Cups are water cooled. The use of a repulsion biased electrode in front of the cup can reduce the income of secondary electrons perturbing the measurements. The state of the art of Faraday Cups are also provided with a water-cooled system in order to also measure the current of high power beams. A scheme of a Faraday cup is shown in figure 2.13. Usually the Faraday Cups are mounted on feedthroughs support in order to be placed on the beam axis to measure the beam current. The possibility to take the cup out of the beam line can, for instance, allow the insertion of other device for the measurement of the beam profile or of the emittance but a simultaneous measurement of intensity and beam profile/emittance cannot be preformed.

The advantage of a current transformer is to provide a non destructive current measurement independent on the beam position and size. In fact it measures the current induced in a secondary circuit by the beams passing through the device. The working principle of a current transformer is shown in figure 2.14.

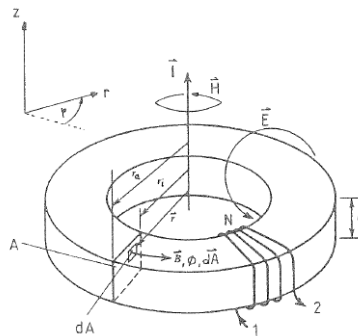


Figure 2.14: Working principle of a beam transformer.

The physical model of this current transformer takes into account a beam which current creates a magnetic field  $\vec{B}$  which can be guided by a toroidal guide with high magnetic permeability  $\mu_r$  inducing a current, proportional to the beam current, on a secondary circuit obtained by winding  $N$  times a wire around the toroid. The transformer inductance is

$$L = \frac{N^2 \mu_o \mu_r h}{2\pi} \ln \frac{r_a}{r_i} \quad (2.11)$$

Where  $h$ ,  $r_i$  and  $r_a$  are the core height, inner radius and outer radius, respectively.[2]

### 2.5.2 Viewing Targets for the measurement of the ion beam shape

A promising technique to measure the beam inhomogeneities and aberrations is the use of viewing screens, coated with scintillating materials, where the hitting beam is recorded by a video camera. This real-time method does not require any controlling electronic device rather that a feedthrough remotely controlled to be inserted and taken out from the beam line (see left figure 2.15). Some disadvantages of this technique include the fact that it is

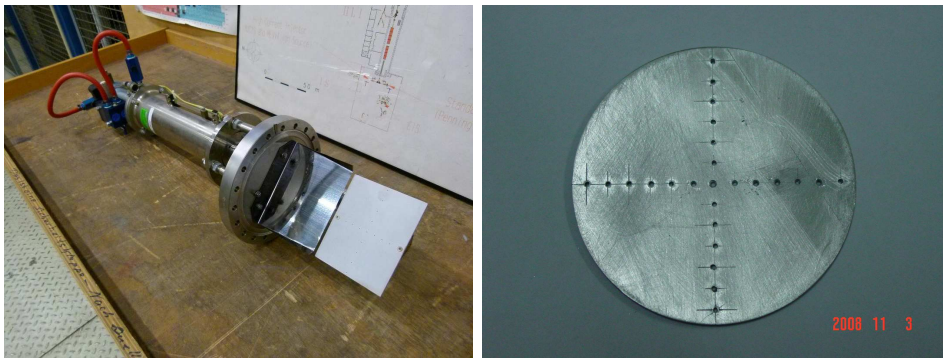


Figure 2.15: Viewing target mounted on a feedthrough and (left) aluminum plate for viewing target production before coating (right).

a destructive technique together and the lack of information concerning the beam intensity. In the last years, at Kiel University a device able to monitor the beam shape and to measure the current intensity has been developed.[49] In order to measure the ion beam quality and its shape for different modes of operation of the ion source, viewing targets have been used to achieve an online recording of the ion beam shape. By changing the ion source parameters separately the influence on the beam behavior could be observed and analyzed. This method has been used for different ion sources like SUSI [50], SUPERNANOGAN [51], CAPRICE [52], SECRAL [53], showing similar behavior for these ion sources. Several scintillating materials can be used

for the target coating: barium fluoride ( $BaF_2$ ) can be used as scintillator because it is suitable for intense beams and it showed a reasonable lifetime; a potassium bromide ( $KBr$ ) coated target has been used due to its higher sensitivity, but at the expense of shorter lifetime. A viewing target made from 1.5 mm thick aluminum plates of 70 mm diameter, with drilled holes as visible marks is visible in right figure 2.15. The distance between the marks on the used targets is 5 mm horizontally and vertically.[53]

### 2.5.3 Tools for the emittance's measurement

As for the techniques to measure the intensity and the beam profile, for the emittance measurements they exist non destructive methods based on the transport matrix formalism and making use of three different settings of a quadrupole in front of a profile measuring device (*gradient variation method*) or by measuring the beam profile at three different beam longitudinal positions (*three positions method*). In both cases the knowledge of the Twiss parameters derived from the profile measurements allows, by solving a linear equations system, to calculate the emittance [53]. The main destructive methods of carry out an emittance measurement make use of one or more slits or holes devices followed by current or profile measurement devices.[2] A promising emittance measurement device is the Pepper Pot: it consists of an array of small holes placed in front of a viewing screen. The  $x - y$  coordinates (transverse plane) are determined by the holes and the beam divergence can be determined by the spacing of the beamlets visualized on the viewing screen. The advantage in using such a device is the possibility of measure the emittance along the vertical direction and along the horizontal direction, if the device is provided with a moving system along the  $x$ -axis. A picture of such a device and of a  $^{40}Ar^{8+}$  beam extracted by an ECRIS are shown in (the right) figure 2.16.

In (the left) figure 2.16 the pepper plate (indicated in (1)) mounted on the moving slit is shown. It separates the ion beam in beamlets hitting a multichannel plate with a Phosphor screen (2) which image is mirrored (3) to a CCD camera (4). By observing the right image of the figure 2.16 it is possible to confirm that when used for the ECRIS emittance measurements, such a device can provide more information with respect to a slit device. In fact the diagnostic tools integrating over one space coordinate like wire harps for profile measurements or slit-slit devices, respectively slit-grid devices to measure the emittance might be applicable for beam transport investigations in a quadrupole channel, but they are not very meaningful for investigations regarding the ECRIS symmetry.[55]

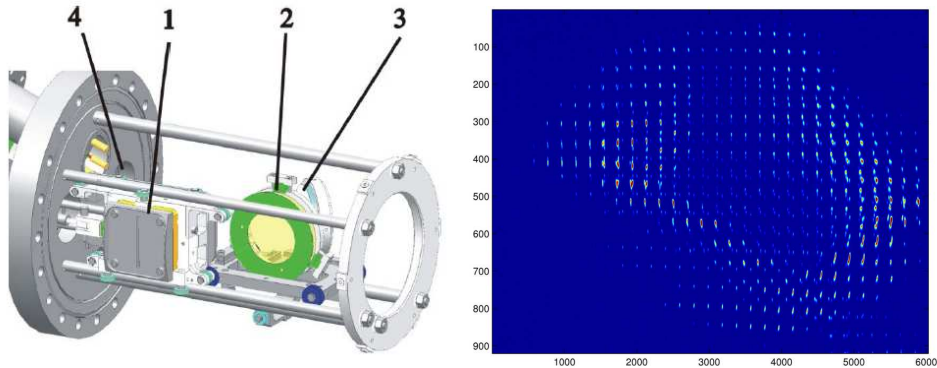


Figure 2.16: *Layout of a 4-D pepper-pot emittance meter [54] (left) and beam spots behind a pepper plate (right). Both axis are scaled in pixel.*

#### 2.5.4 Plasma diagnostic tools: the Langmuir Probe

A plasma diagnostic device which has been used to perform interesting measurements of the plasma parameters described in the first chapter is the Langmuir probe. This device is constituted by a biased electrode mounted in a feedthrough system inserted into the plasma.[57] By measuring the  $V - I$  characteristic of the Debye sheath it is possible to calculate: the electron temperature and density, the plasma potential, the ion density and temperature, or the electron energy distribution function (EEDF). The typical  $V - I$  slope which describes the evolution of the current versus the applied voltage (by assuming that the probe current does not disturb the plasma equilibrium since the probe diameter is less than the electron mean free path) is shown in figure 2.17.

The probe  $V - I$  characteristic shown in figure 2.17 can be divided into three regions:

- (a) for  $V < V_f$  (called floating potential, for which the current collected is zero) the probe current is mainly positive ion current.
- (b) for  $V_f < V < V_p$  (the plasma potential), the current is mostly due to electron diffusion to the probe. It is expected to vary exponentially with the probe voltage.
- (c) for  $V > V_p$  the current is space charge limited electron current, and for a cylindrical probe in an ideal plasma the square of the current is expected to vary linearly with the probe voltage.

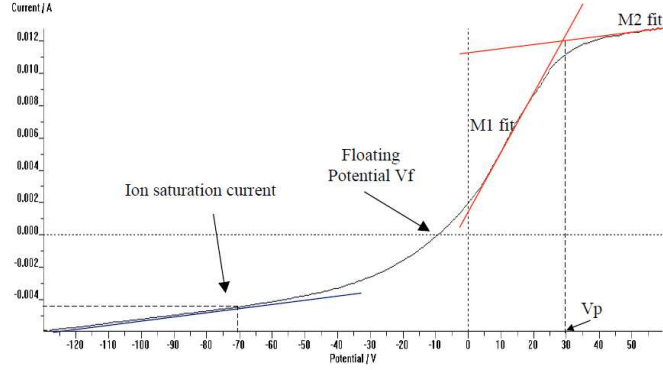


Figure 2.17: Voltage-Current characteristic of a Langmuir probe.

By assuming that the plasma electron component is following a Maxwell-Boltzmann distribution, the current  $I_e$  measured by the probe when a voltage  $V$  is applied (among a few hundreds of Volts from negative values to positive values), according to the Langmuir theory is given by [58]:

$$I_e = n_e e A_p \frac{kT_e}{2\pi m_e} e^{\frac{e(V-V_p)}{kT_e}} \quad (2.12)$$

where  $n_e$  is the electron density and  $A_p$  the probe area. The plasma potential  $V_p$  can be determined by plotting the logarithmic of the probe current versus the applied voltage; it corresponds to the interception of the fits to the electron saturating and accelerating regions. Since the electron temperature  $T_e$  is inversely proportional to the  $V - I$  slope where  $V < V_p$ , it is possible to calculate  $T_e$  from the Langmuir theory. Once known the electron temperature, the electron density can be calculated according to equation (2.12). [58]

## Chapter 3

# The electromagnetic field inside the ECRIS and the microwave coupling to the ECR plasmas

The microwave coupling between the electromagnetic wave and the plasma determines the efficient transfer of the energy from the microwaves to the plasma electrons inside the ECRIS. The plasma chamber, on the other hand, is a resonant cavity for the electromagnetic waves and, when the magnetized plasma is created, the electrical permittivity of the medium filling the chamber is not longer homogeneous and not longer electrically isotropous. We carried out a detailed investigation to demonstrate that the performances of the ECR ion sources depend on the electromagnetic field excited inside the plasma chamber and on the coupling mechanism used for providing the microwaves to the plasma.

### 3.1 The ECRIS plasma chamber as a resonant cavity

In order to characterize the electromagnetic field which is present inside the plasma chamber of the ECR ion sources and where the particles motion occurs it is fundamental to make the following assumption: the plasma chamber is a resonating cavity for the electromagnetic wave feeding the plasma. The coupling between the electromagnetic wave and the plasma

filled chamber and the electromagnetic field patterns which can be excited inside the resonating cavity are of primary importance for the characterization and for the properties of the plasma. Furthermore the characterization of the plasma chamber in terms of excitable electromagnetic field allows to make some assumptions about the charged particles motion and energy as described in the following sections.

### 3.1.1 Resonant modes inside a cylindrical plasma chamber

A plasma chamber can be represented, in a first order approximation, by a cylinder with a radius  $a$  and length  $l$  filled by a medium with a certain electric permittivity  $\epsilon$  and a certain magnetic permeability  $\mu$ . Then a discrete number of electromagnetic field patterns can exist inside the plasma chamber: the so called *resonant modes*. They can be defined by the equations defined in a cylindrical coordinates system  $(\rho, \phi, z)$ : [59]

$$E_\rho = -\frac{x_{n\nu}}{a} \frac{r}{l} \frac{\pi}{h^2} C_n J'_n \left( \frac{x_{n\nu} \rho}{a} \right) \cos n\phi \sin \left( \frac{r\pi z}{l} \right) \quad (3.1)$$

$$E_\phi = \frac{n}{\rho} \frac{r}{l} \frac{\pi}{h^2} C_n J_n \left( \frac{x_{n\nu} \rho}{a} \right) \sin n\phi \sin \left( \frac{r\pi z}{l} \right) \quad (3.2)$$

$$E_z = C_n J_n \left( \frac{x_{n\nu} \rho}{a} \right) \cos n\phi \cos \left( \frac{r\pi z}{l} \right) \quad (3.3)$$

$$H_\rho = -i \frac{\epsilon\omega}{h^2} \frac{n}{\rho} C_n J_n \left( \frac{x_{n\nu} \rho}{a} \right) \sin n\phi \cos \left( \frac{r\pi z}{l} \right) \quad (3.4)$$

$$H_\phi = -i \frac{\epsilon\omega}{h^2} \frac{x_{n\nu}}{a} C_n J'_n \left( \frac{x_{n\nu} \rho}{a} \right) \cos n\phi \cos \left( \frac{r\pi z}{l} \right) \quad (3.5)$$

$$H_z = 0 \quad (3.6)$$

These are the equations describing the TM (Transverse Magnetic with the magnetic field components only on the transverse plane) modes. The TE (Transverse Electric with the electric field components only on the transverse plane) modes can be calculated with the following equations:



$$E_\rho = \frac{\mu\omega}{h^2} \frac{n}{\rho} C_n J_n \left( \frac{x'_{n\nu}\rho}{a} \right) \sin n\phi \sin \left( \frac{r\pi z}{l} \right) \quad (3.7)$$

$$E_\phi = \frac{\mu\omega}{h^2} \frac{x'_{n\nu}}{a} C_n J'_n \left( \frac{x'_{n\nu}\rho}{a} \right) \cos n\phi \sin \left( \frac{r\pi z}{l} \right) \quad (3.8)$$

$$E_z = 0 \quad (3.9)$$

$$H_\rho = -i \frac{x'_{n\nu}}{a} \frac{r}{l} \frac{\pi}{h^2} C_n J'_n \left( \frac{x'_{n\nu}\rho}{a} \right) \cos n\phi \cos \left( \frac{r\pi z}{l} \right) \quad (3.10)$$

$$H_\phi = i \frac{n}{\rho} \frac{r}{l} \frac{\pi}{h^2} C_n J_n \left( \frac{x'_{n\nu}\rho}{a} \right) \sin n\phi \cos \left( \frac{r\pi z}{l} \right) \quad (3.11)$$

$$H_z = -i C_n J_n \left( \frac{x'_{n\nu}\rho}{a} \right) \cos n\phi \sin \left( \frac{r\pi z}{l} \right) \quad (3.12)$$

Where the time dependance  $e^{i\omega t}$  is omitted and  $J_n$ ,  $J'_n$  are respectively the Bessel functions and the derivative of the Bessel functions of  $n$  order and  $x_{n\nu}$  and  $x'_{n\nu}$  are their related  $\nu$  roots. A discrete set of frequencies  $\omega/2\pi$  can exist inside the resonance cavity [59] and they are defined by:

$$\omega = \frac{1}{\epsilon\mu} \sqrt{\frac{r^2\pi^2}{l^2} + h^2} \quad (3.13)$$

where the value  $h$  is:

$$h = \frac{x'_{n\nu}}{a} \quad TE \text{ modes} \quad (3.14)$$

$$= \frac{x_{n\nu}}{a} \quad TM \text{ modes} \quad (3.15)$$

The electromagnetic field equations along the  $\rho$ ,  $\phi$  e  $z$  coordinates depend on the mode parameters  $n$ ,  $\nu$ ,  $\rho$  and on the amplitude  $C_n$ , i.e. the maximum amplitude associated to the wave's fields. Then the resonant modes  $TE_{n,\nu,\rho}$  and  $TM_{n,\nu,\rho}$  existing inside the plasma chamber are identified by the mode parameters and they depend on the amplitude which is related to the amplitude associated to the field strength of the wave. This last condition is strongly related to the coupling method as described in the following sections. For instance the resonant modes related to 10 resonance frequencies close to the operating frequency of 14.5 GHz for a cylinder filled with a medium with  $\epsilon_r = 1$  and  $\mu_r = 1$  of 179 mm length with a diameter of 64 mm which, in a rough approximation, are the dimensions of the plasma chamber of the CAPRICE ECRIS installed at GSI are indicated in the table 1:

Table 3.1: CAPRICE plasma chamber; 10 modes close to  $14.5 \text{ GHz} \pm 50 \text{ MHz}$ .

Mode	Frequency [GHz]
$TM_{3,1,13}$	14.457219770
$TE_{4,2,5}$	14.459947050
$TE_{8,1,2}$	14.481914796
$TE_{6,1,11}$	14.492060061
$TE_{5,1,13}$	14.492060061
$TE_{1,1,17}$	14.498241812
$TE_{0,2,12}$	14.505304176
$TM_{1,2,12}$	14.505304176
$TM_{0,3,8}$	14.538578617
$TM_{3,2,0}$	14.554128269

According to the equations (3.1)-(3.12) it is possible to calculate the electromagnetic field pattern for each of the 10 modes above reported. As an example the electromagnetic field pattern for the mode  $TE_{1,1,17}$ , which is the closest one to 14.5 GHz (operating frequency of the CAPRICE ECRIS) is shown in figure 3.1.

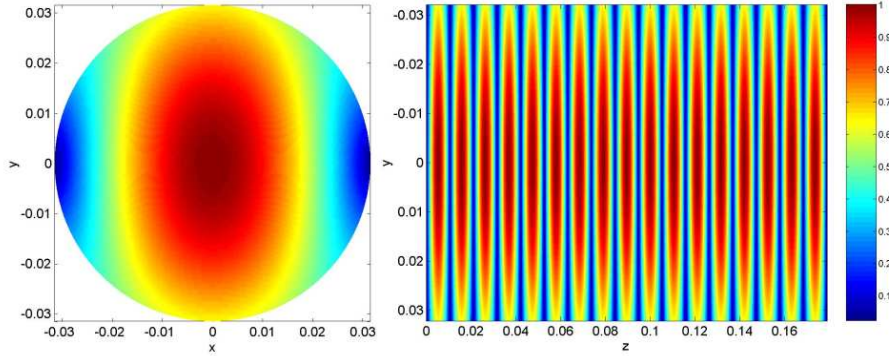


Figure 3.1: Normalized electric field amplitude for the resonant mode  $TE_{1,1,17}$  in the  $xy$  plane at the  $z$  point where it is maximum (left) and on the  $yz$  plane at  $x = 0$  (right).

One important observation concerns the modes calculation applied to the ECRIS. Since the plasma chamber dimensions, with respect to the excitation wavelength, are relatively large, the resonant modes number for higher frequencies becomes higher and this leads to many difficulties in the deter-

mination of the excited electromagnetic field. This is shown in the results of the analysis we carried out at INFN-LNS. In figure 3.2 the resonant modes distribution for the SERSE plasma chamber is shown in the 0 – 18 GHz frequency range (upper figure) and close to 14 GHz (lower figure) which is one of the SERSE operating frequency.[60]

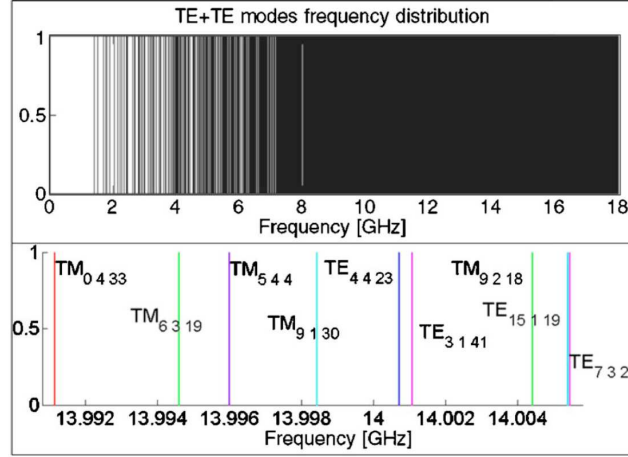


Figure 3.2: Frequency distribution of the resonant modes in the lossless cylindrical cavity representing the SERSE plasma chamber (length 450 mm, diameter 130 mm and filled with a medium with  $\epsilon_r = 1$  and  $\mu_r = 1$ ).

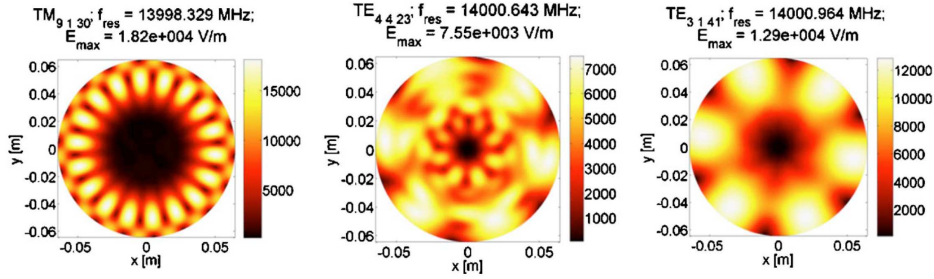


Figure 3.3: Modulus of the electric field in the plane  $xy$  at  $z = 233$  mm when the lossless cylindrical cavity representing the SERSE plasma chamber is excited at three resonant frequencies close to 14 GHz.

Furthermore the presence of holes, any geometry perturbations and also the material conductivity constituting the chamber determine a mode overlapping and makes difficult the precise calculation of the excited ones. The

$Q$  (*quality factor*) parameter of a resonating cavity, indicated in equation (3.16), is the ratio between the stored energy inside the resonator and the energy loss, in a period time and gives an indication concerning the losses of a resonating cavity.

$$\frac{1}{Q} = \frac{1}{Q_{int}} + \frac{1}{Q_{ext}} \quad (3.16)$$

Where  $Q_{int}$  depends on the proper losses (for instance due to the low conductivity wall or to the dielectric material filling the cavity) and  $Q_{ext}$  depends on the losses for energy radiated to the outer of the cavity for the presence of holes. For instance the presence of the excitation waveguide represents a source of energy losses for the plasma chamber. The position of the waveguide, its dimensions, and the microwave frequency are fundamental parameters for the determination of the electromagnetic field within the chamber.[60]

In figure 3.3 three electromagnetic field distributions for the SERSE plasma chamber are shown when the lossy cavity is excited at three resonant frequencies and with 1 W of normalized input power. The patterns and the maximum electric field vary completely when the feeding frequency varies of a few MHz. We carried out some experimental measurements on this ECRIS in order to evaluate the influence of the waveguides position and orientation. The results are shown in section 3.1.3.

### 3.1.2 Resonant modes and resonant frequencies perturbations

The approximation of the plasma chamber as a cylinder has been also used for the simulation of the motion of charged particles inside an ECRIS.[61] However the resonant modes calculation is sensitive to any small variation of the geometry and the results of the simulation can be affected by this variation. In fact, by considering a real plasma chamber, the shape of the injection flange and of the extraction flange is not plane, i.e. due to the plasma electrode. The introduction of any perturbing geometries, like a biased disc or any other probe, or of an oven for metal ion production, can affect the electromagnetic field distribution inside the chamber. We performed a series of measurements with a network analyzer in a plasma reactor operating at 2.45 GHz, according to the principles of the Microwave Discharge Ion Sources (MDIS).[2] We carried out the detailed characterization of the scattering parameter  $S_{11}$  in vacuum and the penetration of the Langmuir probe (7 mm diameter alumina cylinder) inside the plasma

reactor chamber (at  $z = 17.2$  cm inside the cavity with a slope of  $14^\circ$  with respect to the plasma chamber axis) significantly affects the reflection coefficient measured at the coaxial connector as shown in Figure 3.4. A detailed description of the experimental set-up is reported in section 3.5.[62]

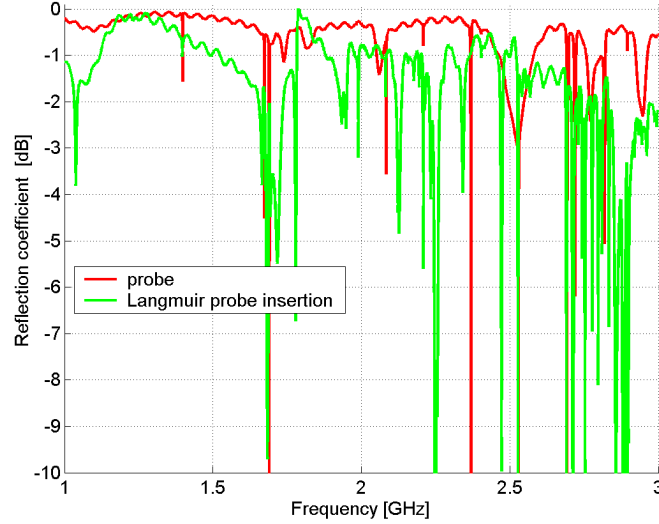


Figure 3.4: *Effect of the Langmuir probe insertion inside the plasma reactor chamber on the measured reflection coefficient.*

### 3.1.3 Waveguide apertures inside the plasma chamber

The position and the dimensions of the waveguide and the microwave frequency are fundamental parameters for the electromagnetic field patterns which can be excited inside the plasma chamber. In 2006 we carried out an analytical characterization of the resonant modes of the SERSE plasma chamber together with an experimental analysis of the microwave coupling.[63] Figure 3.5 shows a scheme of the SERSE ion source with a detailed view of the injection and extraction flanges.

In the injection flange the gas inputs, the hole for the biased disk (used to increase the amount of electrons in the plasma), and the microwaves ports (WR62 waveguide apertures) named WG1 and WG2 are present. This flange is also drilled with holes for pumping; the diameter of the holes is below  $\lambda/4$  (wavelength related to the 18 GHz microwave frequency) in order to minimize the microwave leaks and the plasma formation outside the chamber.

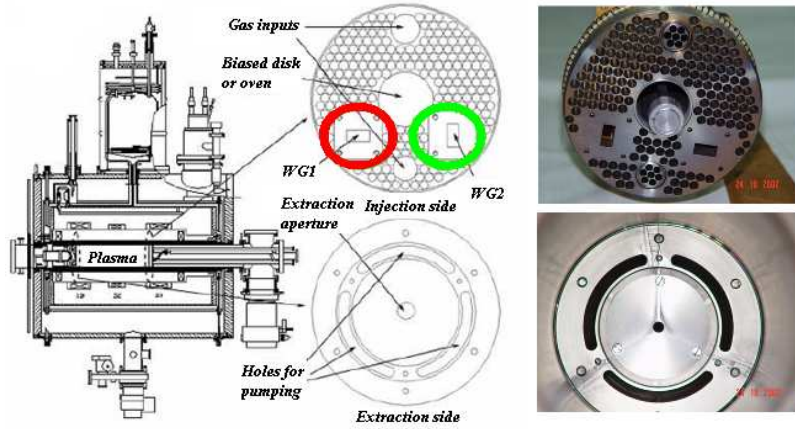


Figure 3.5: Scheme of the SERSE ion source and injection and extraction flanges.

Similar holes are also present in the extraction side, with the aperture for the ion beam extraction.

We measured the microwave coupling between the resonant cavity and the two WR62 waveguides by connecting a Network Analyzer to the waveguide ports. Figure 3.6 shows the results of the Scattering parameters measured at the two waveguide ports where the  $S_{11}$  parameter indicates the reflection coefficient at the WG1 port and the  $S_{22}$  at the waveguide WG2. The parameter  $S_{12}$  represents the signal measured at port 1 coming from the port 2. By analyzing these parameters it is possible to characterize the modes that exist inside the plasma chamber. In fact the frequencies for which we have the minimum values of the  $S_{11}$  or  $S_{22}$  and at the same time the maxima values of the  $S_{12}$  parameter occur, they represent modes excited by the microwaves from the waveguides WG1 and WG2 respectively.[64]

### 3.1.4 Electromagnetic field in the ECR resonance surface

A fundamental aspect of the operation of an ECRIS is the magnetic confinement. In fact, in order to produce high charge state ion beams, as described in sections 1.3.2 and 2.4.2, the ions must be confined in a potential well where the electrons crossing the so called ECR surface and gaining enough energy from the microwaves, can ionize them by the several impacts in such a region. A suitable magnetic field system for this purpose is composed by two solenoid coils and a sextupole generating a magnetic field according to

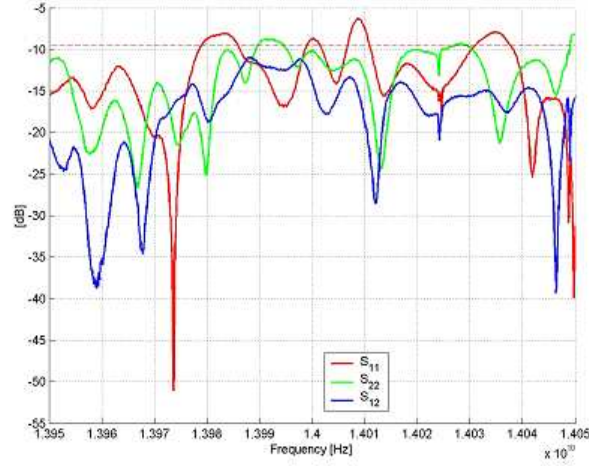


Figure 3.6: Measured scattering parameters at the two waveguide inputs of the SERSE ECRIS plasma chamber from 13.95 GHz to 14.05 GHz.

these equations:

$$B_x = -B_1xz + 2Sxy \quad (3.17)$$

$$B_y = -B_1yz + S(x^2 - y^2) \quad (3.18)$$

$$B_z = B_0 + B_1z^2 \quad (3.19)$$

It is possible to use these equations to calculate the magnetic field profile inside the SERSE plasma chamber.[65] The maximum value of the magnetic field along the plasma chamber of SERSE ECRIS is 2.7 T at the injection and the maximum value of radial field is 1.55 T. Then the constants  $B_0$ ,  $B_1$  and  $S$  to be included in the (3.17) to describe this magnetic field profile become:

$$B_0 = -0.4 [T] \quad B_1 = 25.55 [T/m^2] \quad S = 310 [T/m^2] \quad (3.20)$$

A three dimensions plot of the magnetic field for two position along the plasma chamber axis is shown in figure 3.7.

It is possible to determine the closed surface fulfilling the condition  $\omega_{RF} = \omega_g = q_e B_{ECR}/m_e$  and to calculate the electromagnetic field pattern for two modes within this surface. As an example the  $TE_{9,1,30}$  and  $TE_{1,1,42}$  resonant modes are calculated in the resonance surface and the results are

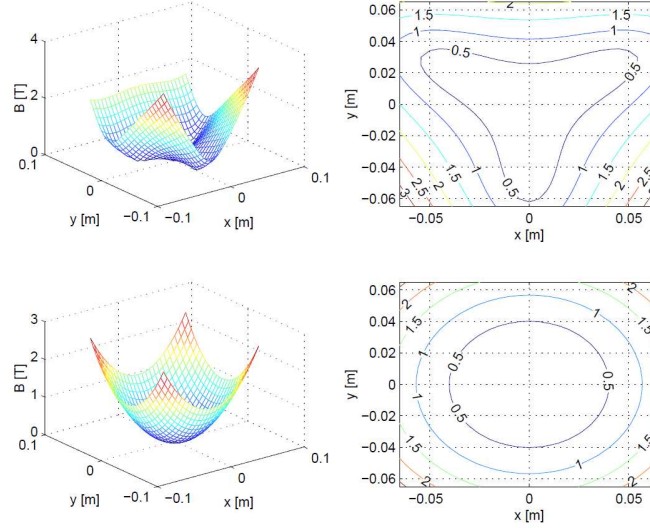


Figure 3.7: *Trend of the magnetic field of the SERSE ECRIS on the transversal plane with respect to the plasma chamber axis at the injection side  $z = -225$  mm (top), and at the middle point  $z = 0$  (bottom).*

shown in figure 3.8.[60] Since the maximum electric field amplitude and the number of maxima are dependant on the excited mode, this can significantly affect the Electron Energy Distribution Function (EEDF). In this case just a frequency of 50 MHz of difference separates the two resonances and this can explain the difference in performances obtained with the application of techniques like the *frequency tuning* described in the next chapter.

### 3.2 Effect of the electromagnetic field on the particle motion

In the previous section we calculated the electromagnetic field in the ECR surface and we pointed out that the maximum electric field amplitude and the number of maxima along the surface varies according to the excited mode. Here the choice of the excited mode is related to the properties of the charged particles in movement inside the plasma chamber. The motion equation of a particle with charge  $q$  and mass  $m_0$  moving with a velocity  $\vec{v}$  in a region where are imposed a confinement not uniform magneto-static field  $\vec{B}_s$  and an electromagnetic field  $\vec{E}_{em}, \vec{H}_{em}$  is:



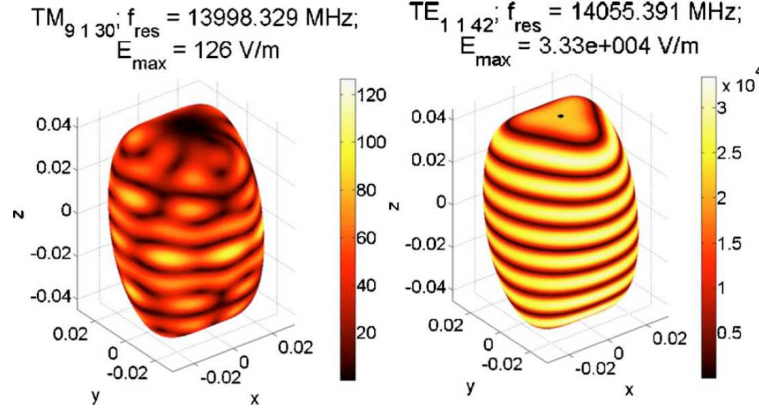


Figure 3.8: Electric field amplitude on the ECR surface of the SERSE ECRIS plasma chamber when the feeding frequency is one of the two resonance frequencies:  $TE_{9,1,30}$  (left) and  $TE_{1,1,42}$  (right).

$$m_0 \frac{d}{dt} \gamma(v) \vec{v} = q \vec{v} \times \vec{B}_s + q \vec{E}_{em} + q \vec{v} \times \mu \vec{B}_{em} \quad (3.21)$$

Where  $\mu$  is the magnetic permeability ( $\vec{B}_{em} = \mu \vec{H}_{em}$ ),  $\gamma(v)$  is the relativistic factor, function of the particle (in the considered case an electron) velocity  $|\vec{v}|$ . By including in the differential equation (3.21) the equations (3.1)-(3.12) describing the excited mode and the (3.17) describing the magneto-static profile, the solution provides the trajectory of the electrons and the energy gained from the ECR process for different electromagnetic field patterns. This calculation was applied for the SERSE plasma chamber when it is fed with the  $TE_{4,4,23}$  mode with a power of 2000 W. Figure 3.9 shows the electron energy for a simulation time of 50 ns. The red rectangles indicate the times when the electron crosses the ECR surface and it is clear that the energy gained by the electrons from the electromagnetic wave occurs in these regions.[60] According to the choice of the mode, the energy gain changes. In fact the simulations of the electron motion under the imposition of 8 different modes close to 14 GHz reveal how the choice of the microwave frequency and then of the excited mode is very important for the ion source performances. Table 3.2 confirms this assumption. Here we considered a huge number of single electrons (with an initial velocity taken from a Maxwellian distribution of velocities and with a 500 eV initial energy) simulations. The choice of the electromagnetic field and then the fine

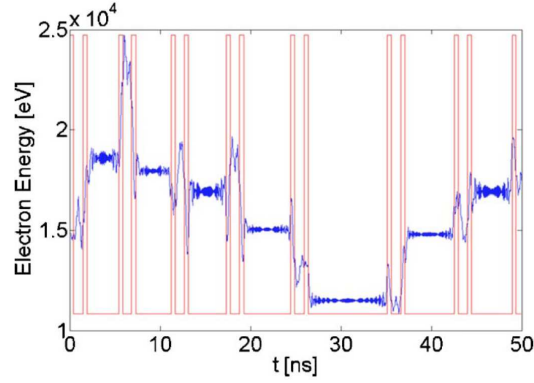


Figure 3.9: *Electron energy during the simulation time when the SERSE plasma chamber is fed with the  $TE_{4,4,23}$  mode.*

tuning of the microwave frequency can enhance the electron energy transfer thus increasing the Electron Energy Distribution Function (EEDF) [66] and the number of confined electrons. We further observed that the microwave field provides a stabilizing effect on the electron confinement.[67] The introduction of the plasma inside the model has to be taken into account of for the correct interpretation of the experimental results.

Table 3.2: *Electron energy, energy gain and percentage of confined electrons for different electromagnetic field patterns.*

Mode	Frequency [GHz]	Energy [keV]	Energy gain	Confined electrons [%]
$TE_{3,1,13}$	13.952354	13.110	24.97	95
$TE_{4,2,5}$	13.958445	11.892	22.65	93
$TE_{8,1,2}$	13.965417	2.601	4.95	93
$TM_{6,1,11}$	13.995897	0.531	1.01	88
$TM_{5,1,13}$	13.998329	0.562	1.07	87
$TE_{1,1,17}$	14.000643	3.932	7.49	95
$TE_{0,2,12}$	14.000964	3.245	6.18	92
$TE_{1,2,12}$	14.055391	17.793	33.89	95

### 3.3 The electromagnetic field inside the CAPRICE ECRIS

The CAPRICE-type ECRIS is characterized by an injection system including a copper cube, with a movable plunger system for the impedance matching, which acts as a waveguide to coaxial transformer. The inner coaxial pipe is used to house the oven or the gas injection system. The plasma electrode is conic with a 10 mm diameter hole for the ion extraction. It appears clear how the assumption of the ideal cylinder shape of the plasma chamber, carried out in section 3.1 is not longer realistic for the calculation of the electromagnetic field pattern inside this ECRIS. The analytical solution cannot be found for such a complex geometry. For this reason we used the software CST Microwave Studio [68] to simulate the electromagnetic field excited inside the plasma chamber of the CAPRICE ECRIS and the result is shown in figure 3.10.

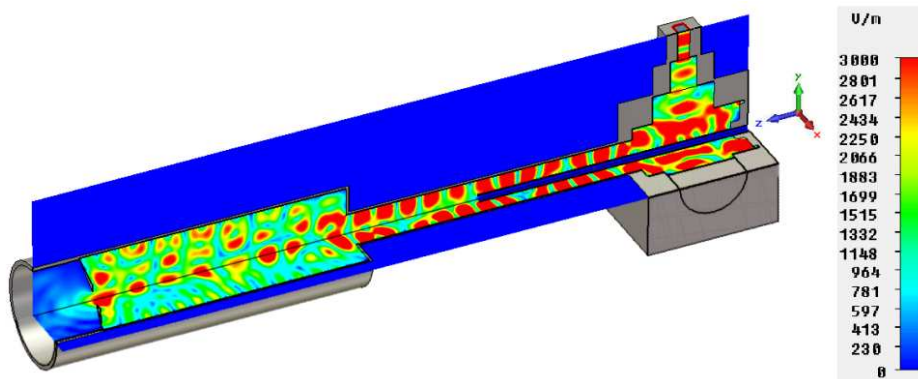


Figure 3.10: CAPRICE ECRIS Electric field amplitude at 14.5 GHz.

We took into account the geometry of the cavity including the copper cube and the plasma electrode. In this figure the electric field amplitude at 14.5 GHz is shown for the  $yz$  and  $zx$  planes relatively to the upper right part of the structure. A WR62 waveguide aperture provides an excitation signal at 14.5 GHz and 1 W power. Along the coaxial adapter the wave propagation is Transverse Electro-Magnetic (TEM) and the electromagnetic field inside the plasma chamber is affected by the plasma electrode. The difference in the electromagnetic field pattern with respect to the theoretical one referring to a pure cylindrical shape of the plasma chamber is clear. The analysis mentioned refers to a plasma chamber filled by a medium with an

electric permittivity equal to one.[69]

We have also analyzed the variation of the excitation frequency and of the plunger position. In figure 3.11 the results of the simulations concerning the electric field inside the CAPRICE ECRIS for three different frequencies, 14.49, 14.5 and 14.51 GHz are shown. The frequencies were chosen very close to the operation frequency (14.5 GHz) in order to point out that a variation of a few MHz is enough to tune the microwave coupling and then the ECRIS performances, as experimentally confirmed in [70] and [71]. The electric field amplitude is shown for the  $yz$  plane and similar results can be analyzed by plotting the other planes. The variation of the frequency affects the electromagnetic field distribution inside the whole structure (injection box, first stage and plasma chamber). Different maxima points are shown in particular inside the plasma chamber. This will affect, as largely described in the previous section, the EEDF, the electron heating and the ion confinement. Around the coaxial plug the electric field is inhomogeneous but we recognized that, since the pipe dimensions are small compared to the wavelength (the outer diameter is 6 mm) a higher meshing refinement of the structure is required to obtain more precise results. This requires higher calculation resources and more powerful workstations in order to obtain converging simulations in a reasonable calculation time.

The effect of the tuning of the matching plunger position is shown in figure 3.12 where the simulation of the electric field amplitude is shown for two settings of the plunger: 25.05 mm of distance with respect to the plasma chamber axis (top figure), which is the same setting also used in figures 3.10 and 3.11, and 20.05 mm (almost a variation of a quarter wavelength calculated at 14.5 GHz) with respect to the plasma chamber axis (bottom figure). We have used the first setting for the experimental investigation carried out to validate the dependance of the ECRIS performances from the plunger position described in the next section 3.7. The electric field amplitude, at 14.5 GHz, is shown for the  $yz$  and  $zx$  planes, respectively. It is clear that the piston tuning produces the similar effect on the electric field of the variation of the microwave frequency. Different positions of the maximum electric field are visible.

With these results the determination of the mode excited or the relationship with the ion source performances when the frequency is changed or when the geometry is modified, cannot be analyzed. For this purpose we carried out dedicated experiments and the interesting results are presented in the next sections.

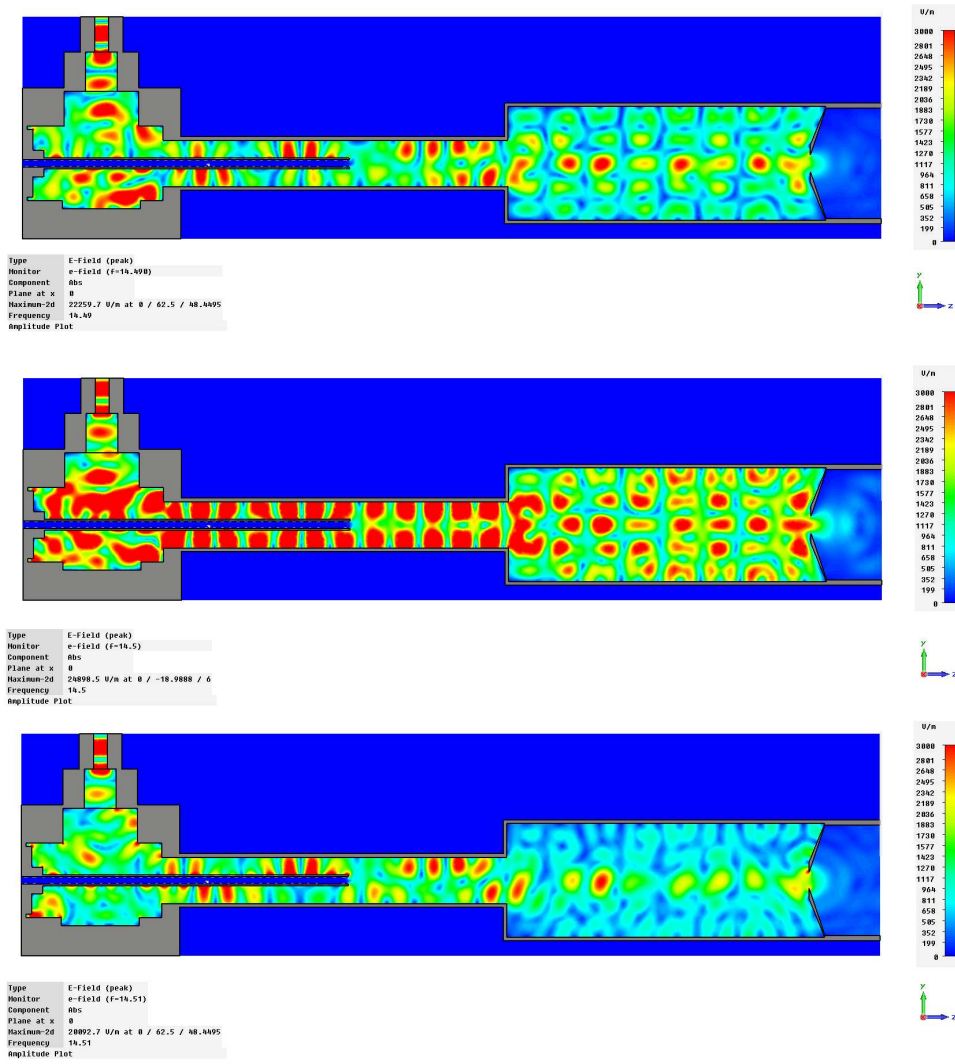


Figure 3.11: CAPRICE ECRIS Electric field amplitude in the yz plane (at  $x = 0$ ) at three different frequencies: 14.49, 14.5, 14.51 GHz.

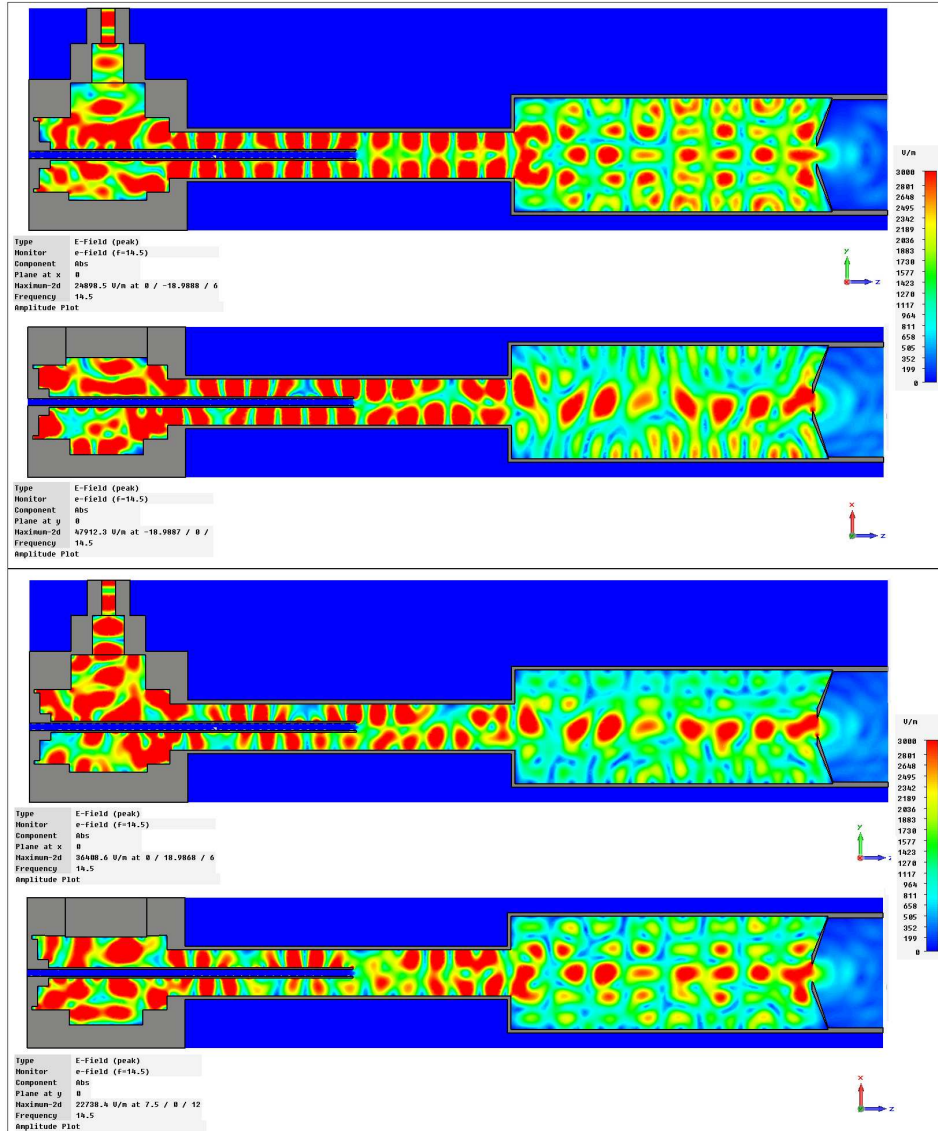


Figure 3.12: CAPRICE ECRIS Electric field amplitude in the plane  $yz$  (at  $x = 0$ ) and in the  $zx$  plane (at  $y = 0$ ) at 14.5 GHz for two settings of the matching plunger: 25.05 mm (top) and 20.05 mm (bottom) of distance with respect to the plasma chamber axis.

### 3.4 Plasma filled resonant cavity

As discussed in section 1.5.2 a magnetized plasma can be described as an electrically anisotropic medium. According to the propagation's direction and of the polarization and of the frequency of the electromagnetic wave propagating inside a plasma, the refraction index assumes the expression indicated in table 1.1. The dependence on the plasma oscillations and then on the electron density affects these values. An ECR plasma, due to the confinement magnetic field distribution, contained in a plasma chamber is not uniform: several electron energies and electron densities are present. In fact this plasma can be separated into a high density plasma inside the

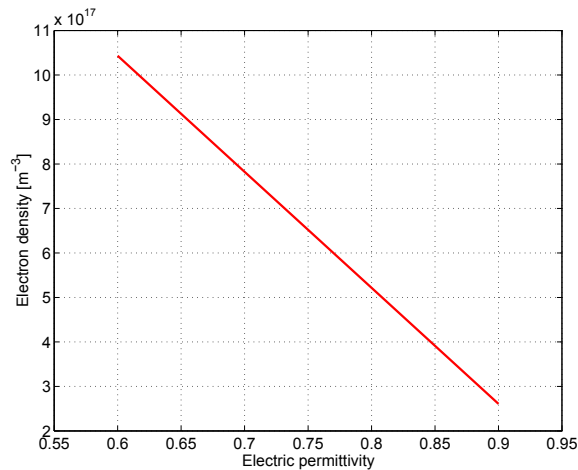


Figure 3.13: *Electron density as a function of the electric permittivity for a not magnetized plasma.*

resonance volume and a lower density plasma in the outer region of the resonance volume. For this reason the definition of a model to calculate the electromagnetic field inside an ECRIS when the plasma is present is complex. However, it was possible to simulate the CAPRICE ECRIS electromagnetic field when the plasma chamber is filled with a medium with an electric permittivity lower than 1. This assumption takes into account the definition of electric permittivity of a non magnetized plasma indicated in (1.41). If the electric permittivity is in the range 0.6–1 the corresponding electron density is indicated in figure 3.13. These values are in agreement with the values of the electron densities expected inside an ECR plasma. By including in the model reported in the figure 3.10 a medium filling the plasma chamber with such electric permittivity it is possible to analyze the electromagnetic



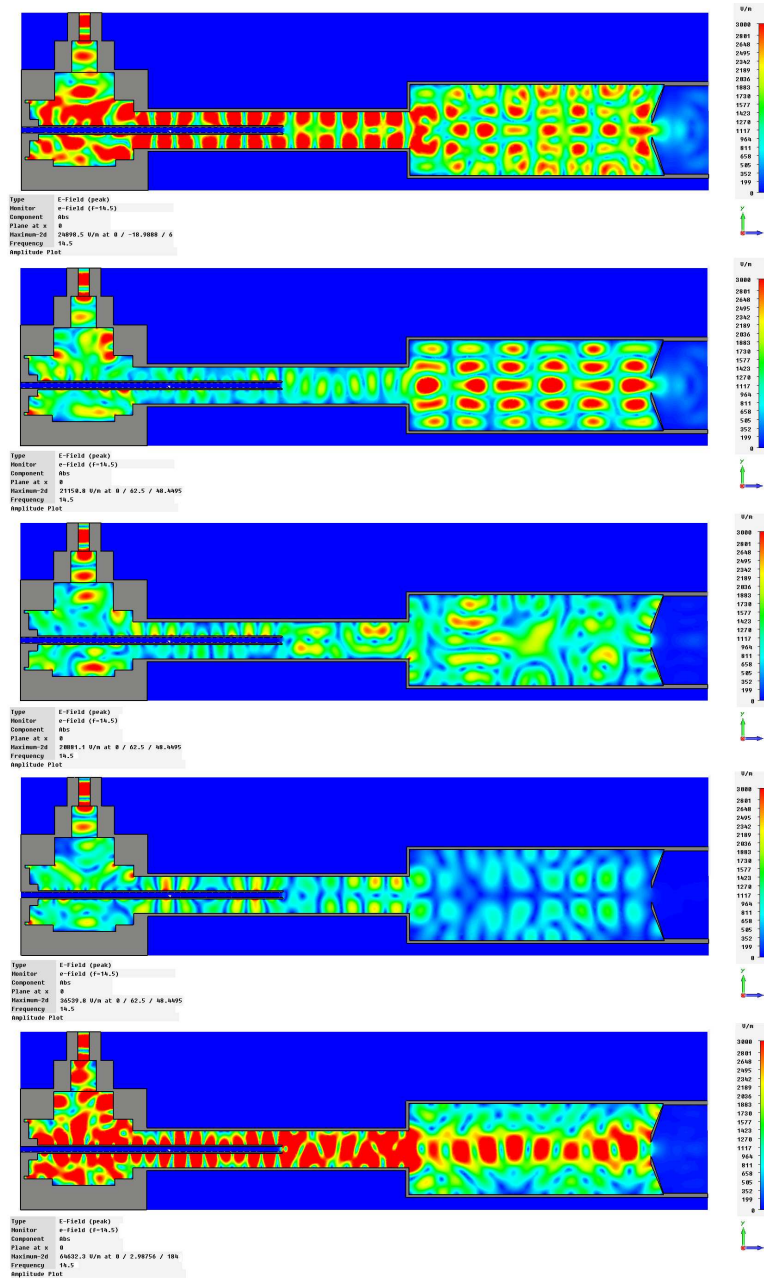


Figure 3.14: Electric field amplitude at 14.5 GHz in the  $yz$  plane (at  $x = 0$ ) when the medium filling the plasma chamber has an electric permittivity in the range  $(1 - 0.6)$ .



field which can be excited inside the CAPRICE ECRIS. In figure 3.14 the electric field of this ECRIS is shown at 14.5 GHz and 1 W power when the electric permittivity of the medium filling the plasma chamber varies from 1 (top figure) to 0.6 (bottom figure) in steps of 0.1. The differences on the electromagnetic field patterns are clear. A more detailed analysis should be possible if the electric permittivity featuring the plasma was defined according to the proper electron density. Future investigations in this field are planned.

### 3.5 Microwave coupling to the plasma filled chamber

In order to investigate the presence of standing waves in plasmas we carried out several experiments at INFN-LNS with a plasma reactor. The device, shown in figure 3.15, is used for environmental applications and it is based on the same physics principles of the Microwave Discharge Ion Sources, generally used for industrial applications or as proton sources in nuclear physics.[72],[73] The plasma chamber is a stainless steel cylinder 268.2 mm long, with a radius of 68.5 mm. Three NdFeB permanent magnets rings generate an off-resonance magnetic field along the plasma chamber axis. In the

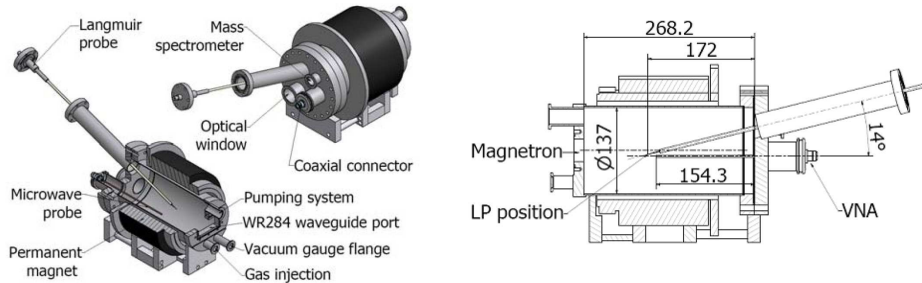


Figure 3.15: *Plasma reactor (left) and experimental set-up (right).*

injection flange the gas inlet is located together with a  $WR284$  rectangular waveguide, placed on the cavity axis, operating in the  $TE_{10}$  dominant mode, connected to a Magnetron (operating at 2.45 GHz and providing up to 300 W CW power). In the opposite flange are connected the plasma diagnostics devices like the microwave probe and the Langmuir probe (inserted inside the plasma chamber off axis with a slope of  $14^\circ$  with the probe tip positioned at  $z = 17.2$  cm inside the cavity). We used this testbench to investigate the

standing wave formation inside the resonant cavity in presence of plasma. A Vector Network Analyzer (VNA) has been used to measure the reflection coefficient with and without plasma. The microwave frequency feeding the plasma was provided by the Magnetron at 2.45 GHz and we analyzed the plasma properties in terms of the reflection coefficient with the VNA in the 1 – 3 GHz frequency range. The VNA was connected to the coaxial connector (a series of attenuators were used to reduce the coupled power) and the plasma effect on the resonating modes existing inside the resonating cavity was characterized. We measured the resonant modes of the cavity in vacuum at the microwave probe and from the WR284 waveguide. Figure 3.16 shows the results of this measurement. The numerical calculation, with the

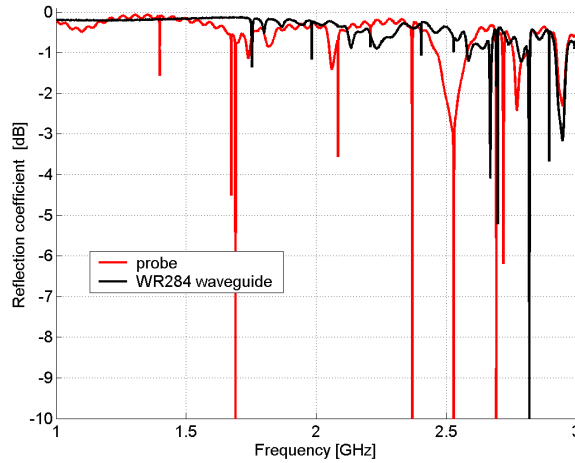


Figure 3.16: *Reflection coefficient measured at the two microwave inputs.*

equation (3.13), of the resonant modes in the 1 – 3 GHz frequency range is reported in table 3.3 where the resonating frequencies measured with the VNA are also included: since many of the calculated modes are excited and only minor differences exist with the measured frequencies, a good agreement is found. The Langmuir probe insertion at  $z = 17.2$  cm, introduced the perturbations on the reflection coefficient already described in section 3.1.2 and visible in figure 3.4. Some of the measured modes have resonant frequencies close to calculated ones. However the introduced perturbations by the Langmuir probe forbid the determination of the TE or TM modes. The plasma is created by switching on the Magnetron generator and different operating conditions of gas pressure and microwave power (gas pressure

Table 3.3: Resonant modes inside the plasma reactor in the 1 – 3 GHz frequency range.

	Mode	Calculated resonance frequency [GHz]	Measured resonance frequency probe [GHz]	Measured resonance frequency WR284 [GHz]
1	$TE_{1,1,1}$	1.39896	1.3978	
2	$TM_{0,1,0}$	1.67507	1.6731	
3	$TE_{1,1,2}$	1.70123	1.6897	
4	$TM_{0,1,1}$	1.76585		1.7534
5	$TM_{0,1,3}$	2.01378		1.9822
6	$TE_{1,1,3}$	2.11092	2.0838	
7	$TE_{2,1,1}$	2.19960	2.2091	2.2089
8	$TM_{0,1,3}$	2.37005	2.3687	
9	$TE_{2,1,2}$	2.40320		2.4033
10	$TE_{1,1,4}$	2.57732	2.5288	2.5287
11	$TM_{1,1,0}$	2.66896	2.6925	2.6975
12	$TE_{2,1,3}$	2.70872	2.6975	2.6975
13	$TE_{0,1,1}$	2.72685	2.7198	
14	$TM_{1,1,1}$	2.72685	2.7198	
15	$TM_{0,1,4}$	2.79352	2.8191	2.8191
16	$TE_{0,1,2}$	2.89358	2.8956	2.8956
17	$TM_{1,1,2}$	2.89358	2.8956	2.8956

in the range of 0.1-0.9 mbar and microwave power in the range of 40-70 W) were analyzed with good reproducibility. It must be once more remarked that this analysis cannot determine which modes are really excited inside the plasma chamber, but only that an electromagnetic modal structure is preserved even in presence of plasma. This is clear by looking at the figure 3.17. The microwave power is 70 W and the gas pressure is 0.7 mbar. By making a comparison with the vacuum condition some modes are shifted in frequency by the plasma, some others disappear and a few modes appear only in presence of the plasma. Therefore, the plasma formation modifies the  $S_{11}$  structure due to the different coupling between electromagnetic waves and plasma, however a resonating structure is still preserved as a sign of the presence of standing waves also when the plasma is created inside the chamber.

In order to define which modes existing in vacuum and listed in the table 3.3 shifted to higher frequency, we used the measurement of the electron density with the Langmuir probe. If the chamber is supposed to be filled by a homogeneous and non magnetized plasma the corresponding electrical

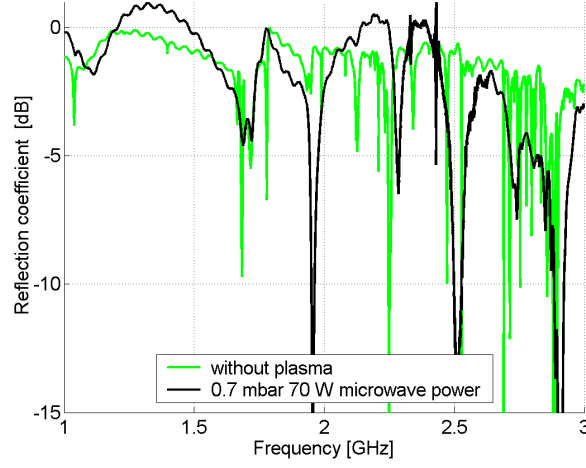


Figure 3.17: *Effect of the plasma creation on the reflection coefficient measured at the probe port.*

permittivity is given by the equation (1.36) where the pulsation related to the collisions can be neglected:

$$\epsilon_{plasma} = \epsilon_0 \left( 1 - \frac{\omega_p^2}{\omega^2} \right) \quad (3.22)$$

Where  $\omega = 2\pi \cdot 2.45 \cdot 10^9 \text{ rad/sec}$  and the plasma pulsation  $\omega_p$  is a function of the electron density according to the equation (1.6). Therefore, the change in the electrical permittivity from  $\epsilon_r = 1$  to  $\epsilon_r = \epsilon_{plasma}$  determines a variation of the resonant frequencies, because of the change of the  $\epsilon = \epsilon_0 \epsilon_r$  in the equation 3.13.

A frequency shift was observed in the reflection coefficient with the RF power and with the gas pressure and it has been correlated with the electron density measured by means of a Langmuir probe. At 70 W of microwave power and 0.7 mbar of gas pressure an electron density value of  $6 \cdot 10^{15} \text{ m}^{-3}$  was measured with the Langmuir probe inserted at  $z = 17.2 \text{ cm}$ . By inserting this electron density value into the equations (1.6) and (3.22) it is possible to reconstruct the mode frequency in the vacuum condition for the modes measured at 2.28 GHz and 2.913 GHz. In particular for the first mode the frequency in vacuum is around 2.2091 GHz (a mode is present also before the LP insertion around this frequency). By using the same value of permittivity for the mode at 2.913 GHz the resonant frequency in vacuum

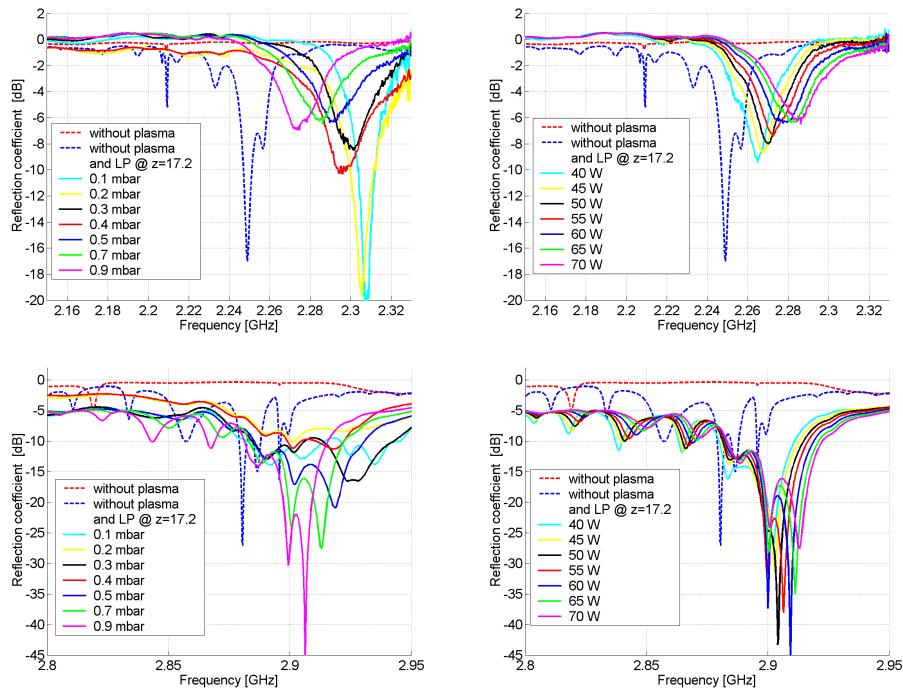


Figure 3.18: Reflection coefficient without plasma and with plasma vs frequency around the  $TE_{2,1,1}$  mode (top figures) and the  $TM_{0,1,4}$  mode (bottom figures) at different gas pressures and 70 W power (left) and at different microwave powers and 0.7 mbar pressure (right).

should be around 2.8 GHz. It is assumed that the shifting mode is the closer one with frequency of 2.8191 GHz. According to the resonance frequency calculation (see table 3.3), the above frequencies can be the two resonant frequencies related to the modes:  $TE_{2,1,1}$  and  $TM_{0,1,4}$ .

The procedure to use the measured electron density in order to determine the mode shift when the plasma is created can be inverted.

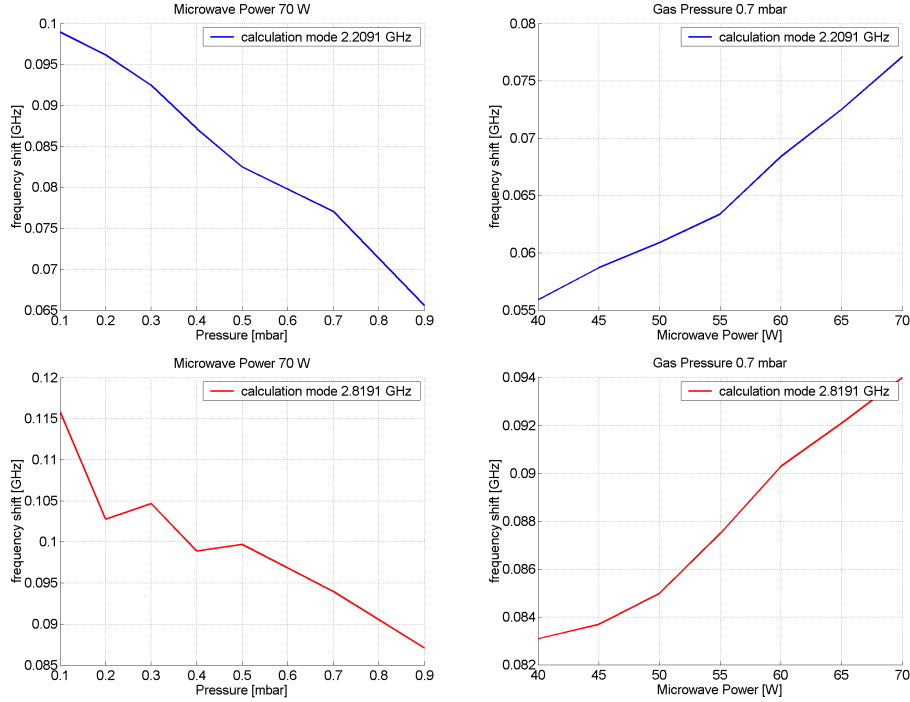


Figure 3.19: Peak variation with respect to the calculated resonance frequencies 2.2091 GHz and 2.8191 GHz with the gas pressure for fixed microwave power (left) and with the power for fixed gas pressure (right).

In fact if there is a shift of the resonant frequencies due to a change of the plasma reactor parameters (gas pressure or microwave power) this is due to a variation of the plasma conditions in terms of the electron density, which can be calculated proper from this frequency shift. Figure 3.18 describes the variation of the reflection coefficient in terms of a resonance frequency shift with the gas pressure (left figures) and with the microwave powers (right figures). In fact the resonances existing inside the plasma chamber in vacuum shift to higher frequencies by decreasing the gas pressure or by increasing the microwave power. This observed effect is due to the change

of plasma density for the different operating conditions. The effect of the plasma on the reflection coefficient is a resonance frequency shift shown in figure 3.19 due to a decreasing value of the electrical permittivity in equation (3.13).

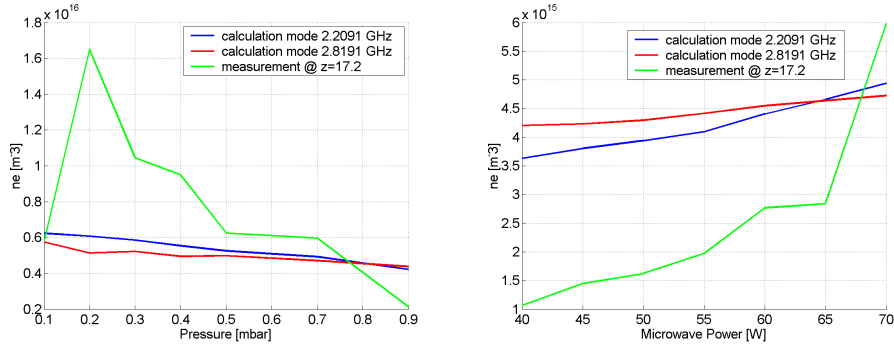


Figure 3.20: *Electron density variation with the gas pressure for fixed microwave power (left) and with the microwave power for fixed gas pressure (right).*

The frequency shift can be also used to determine the electron density once the mode in vacuum is identified as described above. By applying the hypothesis that the modes shifting to higher frequency are the ones above reported, two electron densities curves can be obtained. The figure 3.20 shows the calculated electron density with the equation (1.6) (where  $\omega_p$  is function of the electric permittivity calculated from the frequency shift). A comparison with the measurement of the electron density with the Langmuir Probe is reported and we found a good agreement between the measurement results and the calculation.

### 3.6 Microwave coupling to the CAPRICE ECRIS plasma

The experiment described in the previous section was carried out on a test bench where a microwave discharge plasma reactor was operating. Even if we obtained interesting results concerning the microwave propagation and the standing wave formation inside a plasma, such a system is not an ECR ion source. The magnetic field is almost off resonance for the whole plasma chamber, thus determining no charged particle confinement and low energy of the electrons. Furthermore no correlation between the electromagnetic field and the ionization efficiency or the beam parameters can be observed.

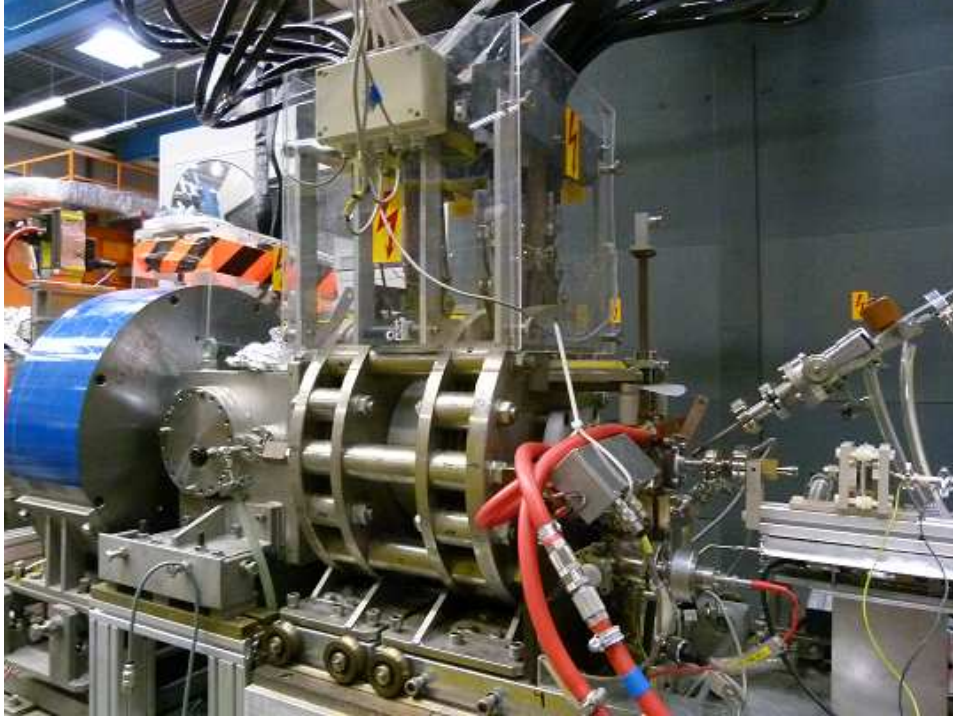


Figure 3.21: *CAPRICE ECRIS and experimental setup to measure the standing wave formation.*

Then we carried out experiments to validate and to measure the standing wave presence in an ECR plasma with the CAPRICE ECRIS installed on the ECR Injector Setup (EIS) testbench of GSI and shown in the picture in figure 3.21. The ion source main features are largely described in the section 4.2.1.

Here it is important to point out which additional components were included in the experimental set-up. In order to measure the reflection coefficient with and without the plasma a coaxial probe was guided into the oven housing up to the end of the first stage (the first section of the plasma chamber visible in figure 3.10) of the plasma chamber where a tip long 11 mm with 3 mm diameter was inserted (figure 3.22). The choice of the length was due to avoid the maximum power transfer (occurring when the probe length into the plasma chamber is  $\lambda/2$ ) to the probe in the range 13.5 – 15 GHz which corresponds to the wavelength range 22.2 – 19.99 mm. The mantel and the internal pin were guided into a bellow (in order to adjust



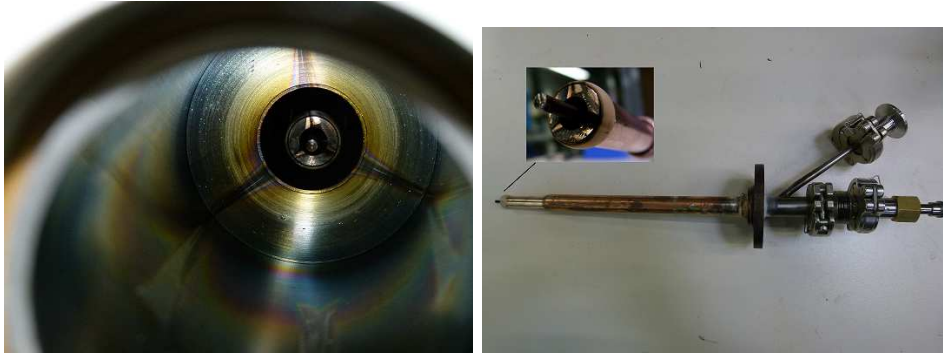


Figure 3.22: Coaxial probe inserted into the oven housing (right) and view of the internal tip inside the plasma chamber (left).

the pin position inside the plasma chamber from 11 mm to 16 mm) out of the oven housing. In order to avoid that the power feeding the plasma can be coupled into the housing a sliding contact was mounted at the end of the oven housing and dielectric (alumina) rings were mounted in the mantel of the coaxial connector to maintain a diameter continuity along the first stage. The mantel was also drilled and alumina pins of 0.6 mm diameter were inserted into the mantel to block the internal probe thus avoiding any bending of the pin for the heating due to the plasma. The mantel and the pin were connected to a hermetically sealed N connector like shown in figure 3.22 (right). In order to shield the measurements device from the high voltage applied to the source, a dielectric foil was inserted into two coaxial to WR62 waveguide adapters (see figure 3.21). Then a cable 15 m long (attenuating around 10 dB) was used to connect a Network Analyzer placed inside the control room to the connector. Argon and Helium gas were injected into the source at pressures around  $10^{-5}$  mbar through remotely controlled valve connected to the pipe soldered in the oven housing. A Traveling Wave Amplifier driven by a synthesizer was used to create the plasma and the reflection coefficient measured at the waveguide inputs was measured by recording the forward and the reflected power at two directional coupler mounted along the injection waveguide line.

The use of a synthesizer allowed us to adjust the microwave frequency feeding the plasma from 14.5 GHz which is the usual operation frequency to a value where the microwave coupling was improved. It was found a stable behavior of the ECRIS with an improved extracted beam intensity at 14.6 GHz. This result is described in figure 3.23 where the drain current, the  $Ar^{8+}$  current, the reflection coefficient measured at the waveguide input and

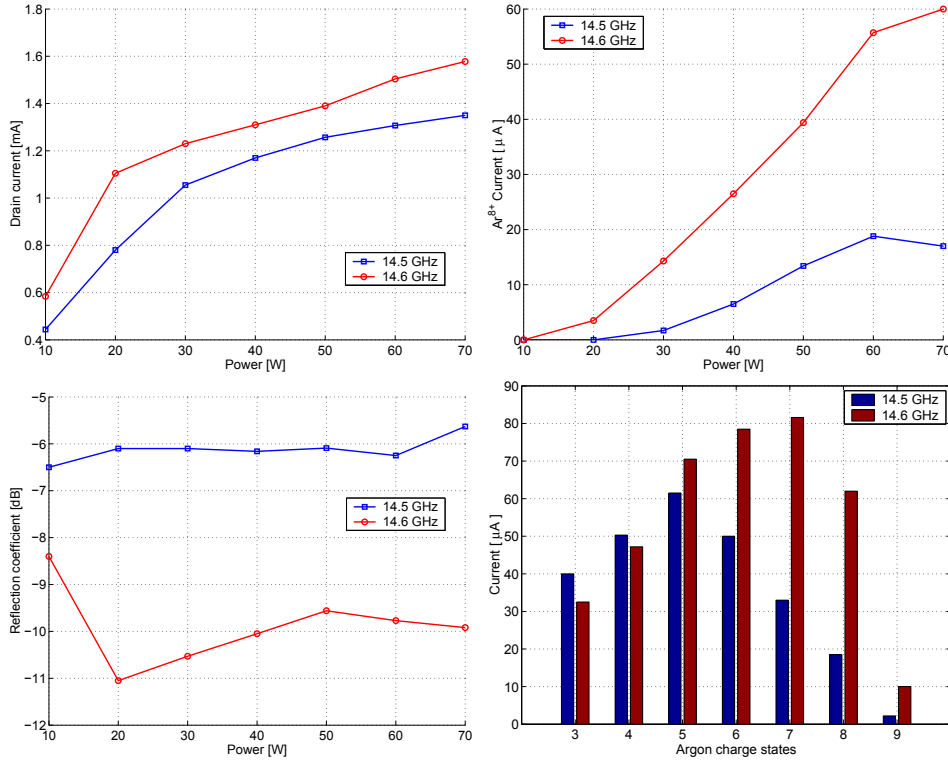


Figure 3.23: Drain current,  $\text{Ar}^{8+}$  current and reflection coefficient variation with the microwave power for two settings of the microwave frequency. The bottom right figure is the charge state distribution at 70 W power for the two frequencies.

the charge states distribution are shown. Due to the improved microwave coupling (visible in the reflection coefficient plot) an increased drain current and an enhanced production of higher charge states was measured. In the next chapter a detailed analysis of the effect of the variation of the microwave frequency on the CAPRICE performances is reported. For the experiment here illustrated the microwave frequency, for the reasons above described, was set to 14.6 GHz. Then a plasma was created from the microwave input with a power increasing up to 70 W at steps of 10 W and simultaneously the reflection coefficient was measured in the 13.5–15 GHz frequency range with the Network Analyzer connected to the coaxial probe. The results of this measurements are shown in figure 3.24. The frequency feeding the plasma is clearly coupled to the coaxial probe. The resonances measured in vacuum conditions shift toward higher values with the microwave power. This result

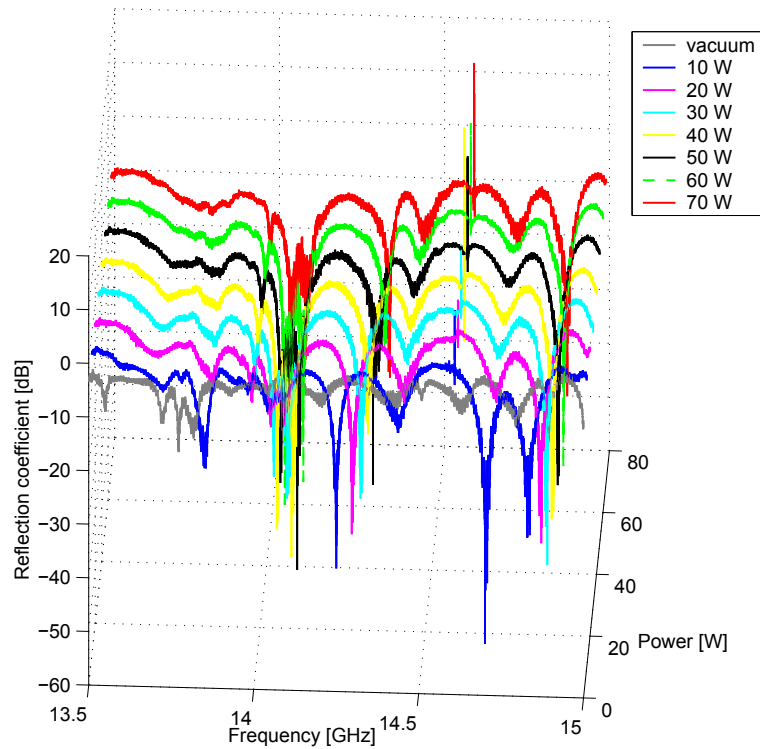


Figure 3.24: Reflection coefficient measured at the coaxial probe when the plasma is created at the waveguide input for different microwave powers.

can be better visualized in figure 3.25 where the ranges 14.1 – 14.4 GHz and 14.65 – 14.95 GHz are shown.

According to the method described in section 3.5 the resonance shift was used to calculate the electron density in the CAPRICE ECRIS at different power level. Figure 3.26 shows the results of this calculation when the resonances shift, shown in figures 3.25, with the microwave power increase. A value around  $10^{16} \text{ m}^{-3}$  is obtained for both cases. This value is lower than the expected value. It has to be remarked that the method used to calculate the electron density assumes the electric permittivity on a non magnetized plasma and furthermore in an ECR plasma the electron density is mostly concentrated inside the ECR volume.

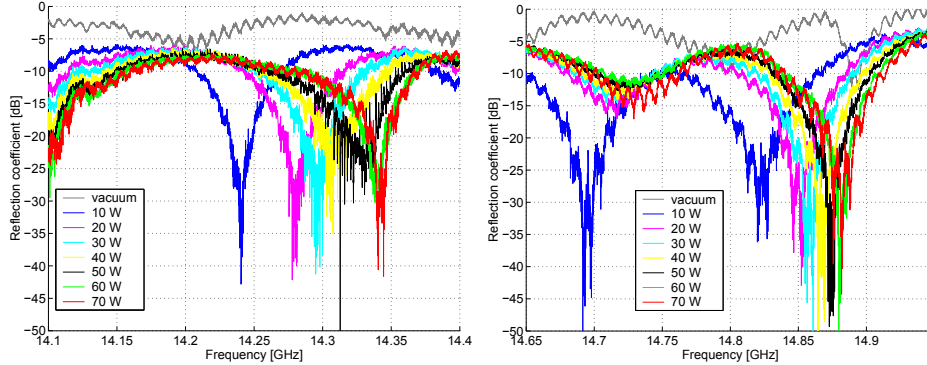


Figure 3.25: Detailed view of the plot in figure 3.24 in the ranges 14.1 – 14.4 GHz (left) and 14.65 – 14.95 GHz (right).

### 3.7 Plunger tuning on the CAPRICE ECRIS

An interesting investigated effect is connected with the tuning of a plunger to enhance the microwave coupling to the plasma. We analyzed experimentally the effect of the matching impedance variation due to the plunger adjustment with the CAPRICE ECRIS. The CAPRICE ion source injection system consists of a cubic copper matching box where the WR62 waveguide line, connecting the microwave supply to the ion source, is mounted. The gas feeding system or the oven housing constitute a coaxial line, inside the first stage, where the electromagnetic wave is transmitted into the plasma chamber. Inside the copper box a cylindrical movable plunger (the diameter is 46 mm) is used to optimize the impedance matching between the electromagnetic wave and the plasma filled chamber. However, this structure movement determines a volume modification which affects the electromagnetic field inside the matching cube and inside the plasma chamber. We previously simulated this effect with CST Microwave Studio and the results are shown in section 3.3. We already analyzed the effect of a small movement (1 mm) on the  $Ar^{5+}$  beam current and on the beam shape at GSI in 2009.[74] The analysis of the charge states distribution shown that its maximum shifted from the  $Ar^{8+}$  to the  $Ar^{5+}$  and the beam current of  $Ar^{5+}$  increased by 7.4% without changing the forward power (around 60 W). The  $Ar^{5+}$  beam shapes recorded on the viewing target presented small variations. We investigated the effect of the variation of this plunger over the complete range of movement (around 16 mm).[69] It has been set to a distance of 25.05 mm from the plasma chamber axis for the optimization

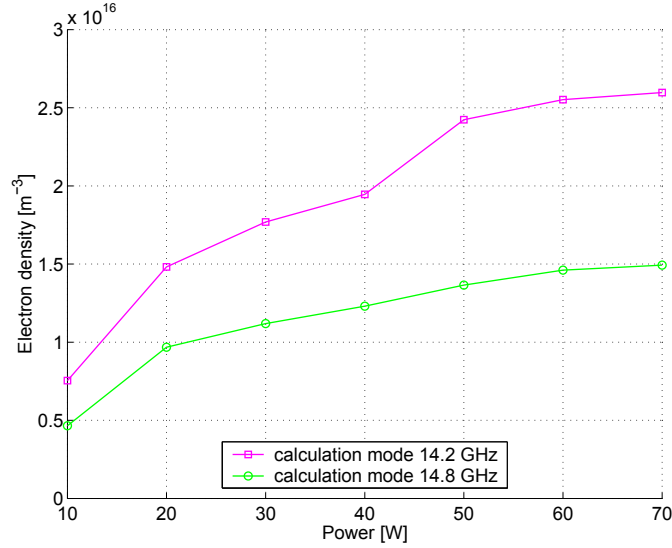


Figure 3.26: *Electron density variation with the microwave power calculated by measuring the resonances shifts at 14.2 GHz and 14.8 GHz.*

of the source parameters to obtain a charge state distribution with a maximum on the  $Ar^{8+}$  with a microwave power of 100 W at 14.5 GHz. Then we varied the position from the inner position to the outer position while the  $Ar^{8+}$  and the drain current were measured. Figure 3.27 shows the effect of this variation (the horizontal scale indicates the distance in millimeters with respect to the central axis) on the drain current (left) and on the  $Ar^{8+}$  current (right). In these figures the transmission coefficient (referred to the right scales), calculated according to the equation (3.23), is also included and the currents evolution during the movement are compared.

$$Transmission\ coefficient = 1 - \frac{Reflected\ power}{Forward\ power} \quad (3.23)$$

In the equation (3.23) the forward power is the microwave power sent to the ion source and the reflected power is the one reflected by the ion source. A fine impedance matching can be obtained by changing the physical dimensions of the system composed of the injection box, of the coaxial line and of the plasma loaded cavity. There is a difference in the transmission coefficients of the two figures; this is due to the hysteresis of positioning during the movement because of the lack of a control loop.

Figure 3.27 points out that the drain current and the  $Ar^{8+}$  current can

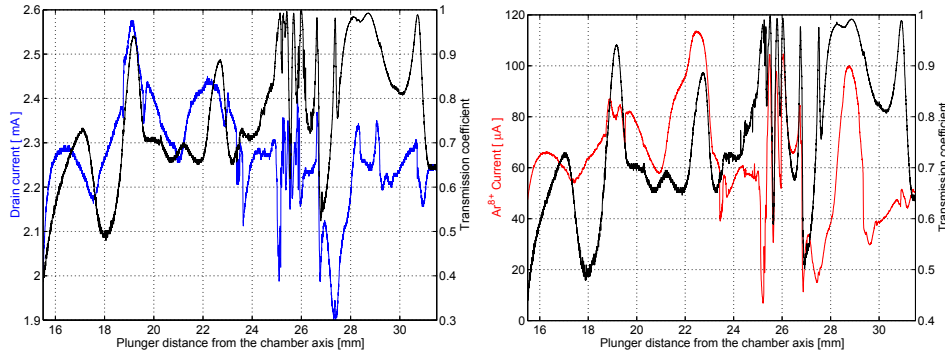


Figure 3.27: Effect of the plunger variation on the drain current (left) and on the  $Ar^{8+}$  current (right) and on the transmission coefficient (right scales).

be enhanced by adjusting the plunger position. It was then possible to optimize the  $Ar^{8+}$  current production by setting the plunger position to a distance of 22.5 mm from the central axis. At this point the current of  $Ar^{8+}$  attained its maximum of  $115 \mu A$ . At this plunger position it was interesting to measure the Argon charge state distribution and compare it with the one measured when the piston was set at a distance of 25.05 mm from the plasma chamber axis. Figure 3.28 (left) shows the measured charge states distributions for the two piston settings. It is evident that the optimization

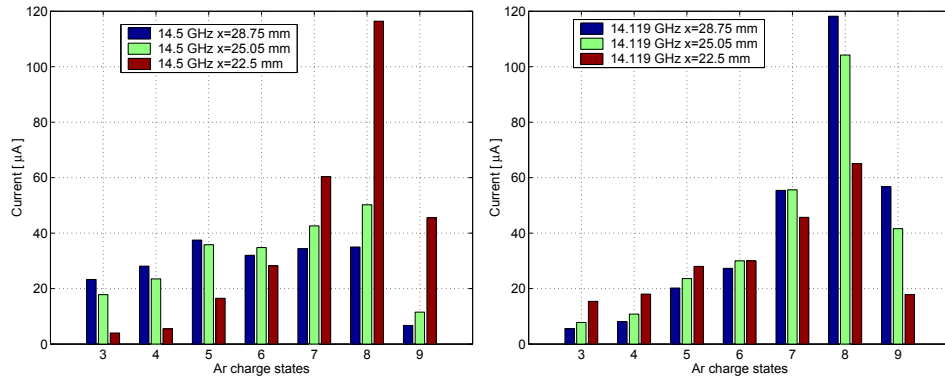


Figure 3.28: Effect of the plunger tuning on the Argon charge states distribution for three settings of the plunger at 14.5 GHz (left) and at 14.119 GHz (right).

of the coupling of the electromagnetic wave with the plasma filled chamber is useful to optimize the production of the highly charged ions. It is then possible to change the equivalent plasma impedance experienced by the mi-

crowave generator by using movable plungers because of the variation of the electromagnetic field in the ionization chamber due to change the physical dimensions of the resonator constituted by the plasma chamber and of the injection box as it was simulated and described in section 3.3. This phenomenon depends on the coupling of the electromagnetic wave to the plasma loaded cavity where an intrinsic mode distribution is present. This variation of coupling determines the amount of power entering into the cavity according to the excited mode. This significantly affects the heating rapidity and other plasma parameters like the EEDF.[75] It is possible to change the equivalent plasma impedance experienced by the microwave generator by using movable plungers or else by changing the microwave frequency feeding the plasma. This effect, called *frequency tuning* will be described in the following chapter. By changing the microwave frequency it will be demonstrated that the ionization efficiency increases with a consequent enhancement of the production of highly charged ions. For the same setting of the source a frequency where this enhancement occurred was 14.119 GHz (see section 4.2.3). For this frequency the charge state distribution was measured for different positions of the plunger. The result is shown in the left bar plot in figure 3.28 (right). The plunger positions indicated in the legend as a distance from the plasma chamber axis are: 25.05 mm was the initial position; 22.05 mm was the position where a maximum of the  $Ar^{8+}$  was measured in the case of the frequency excitation of 14.5 GHz (for this setting of the frequency the highest charge state current decreased) and 28.75 is the position where the maximum of the  $Ar^{8+}$  production was measured for an excitation at 14.119 GHz. Then the two effects can be combined together to increase the high charge state ions current. This optimization process could proceed in a different sequence by changing frequency and position of the plunger, respectively. However, if the power is not increased or if the other parameters of the ion source remain unchanged a saturation of the ion currents in higher charge states is expected. This results will be discussed in the section 4.5 where the effect of the piston tuning and of the frequency tuning will be compared.

By increasing the power it was also possible to analyze the piston tuning on the higher charge state Argon ions like the  $Ar^{11+}$ . The measurement results shown in figure 3.29 are obtained by measuring the  $Ar^{8+}$ ,  $Ar^{9+}$  and  $Ar^{11+}$  (which was multiplied by ten in this figure in order to make a comparison) current when a microwave power of 450 W at 14.5 GHz was sent to the source and the piston position set to 24.98 mm of distance from the plasma chamber axis. The noisy measurement is an indication of the high plasma

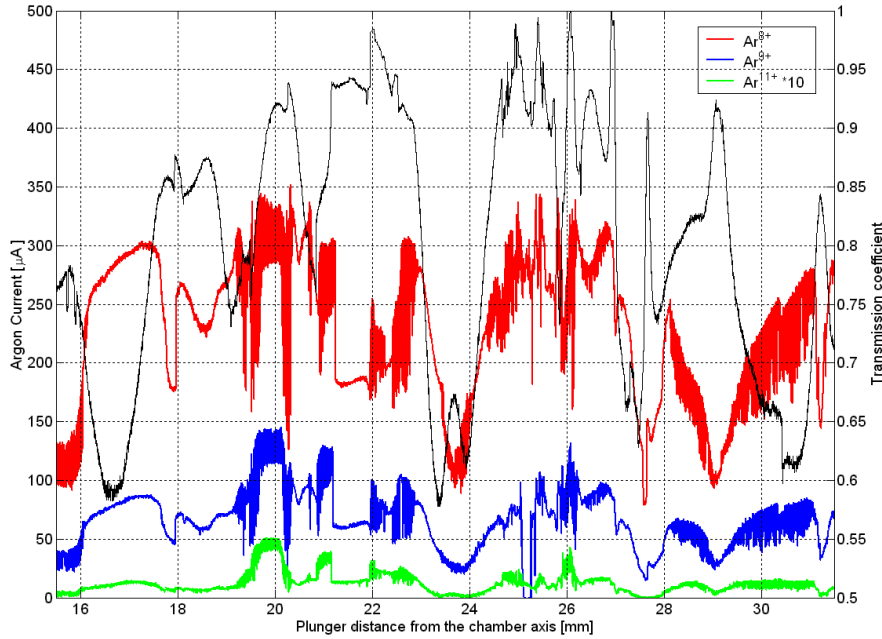


Figure 3.29: *Effect of the plunger tuning on the Argon beam currents and on the transmission coefficient (black line referred to the right scale).*

instability due to the strong variation of microwave coupling. In fact during this experiment the power levels feeding the plasma filled chamber ramped from a few tens of watt (at frequencies where the reflection coefficient had a maximum) up to 450 W (at frequencies where a condition of optimum matching was fulfilled) and vice versa. This change of power coupled to the source may have caused this noisy signal dynamic. When setting the piston position to a distance of 19.88 mm from the plasma chamber axis the  $Ar^{11+}$  current can be increased from  $1 \mu A$  to  $4 \mu A$ . It is possible to conclude that the ECRISs equipped with a matching plunger have the advantage that it is possible to optimize the high charge state ion production by simply adjusting the microwave coupling to the plasma.



## Chapter 4

# The frequency tuning and the double frequency heating

The development of better performing ECRIS providing higher intensity beams of high charge state ions is requested at present accelerator facilities. Together with the projects of ECRISs working at higher microwave frequency with confining magnetic fields up to 4.5 T on axis there has been a spreading interest in developing techniques to improve the performances of the existing ECRIS or of those under development. The variation of microwave frequency is a promising aspect for suchlike improvement. Several experiments confirming this assumption have been carried out in the last years and interesting interpretations of the results of this "so called" *frequency tuning effect* have been proposed. Another technique successfully used to enhance the ion beam current is called *double frequency heating* and consists in the multiple injection of two electromagnetic waves at different frequencies into the ion source. This chapter illustrates the experimental investigations we carried out on the efficient applicability of these techniques for the production of intense beams of highly charged ions.

### 4.1 Application of the frequency tuning on the ECRIS

The choice of the operating frequency of the electromagnetic wave igniting the confined plasma of an ECRIS is fundamental for the ion beam production. In fact, it was proven that the variation of the ECRIS operating frequency affects the ion source performance, according to the so called

”frequency tuning effect” [70], [76]. The results of this technique were confirmed by several experiments at different laboratories as for the full permanent magnet ECRIS Supernanogan developed by Pantechnik [77] where this method has been used to enhance the performance of the produced beam [78]. The origin of these performance improvements has to be researched in the variation of the excited resonant modes which determines a change of the parameters and conditions of the plasma when the frequency is changed. Some explanations of the relationship between the choice of the frequency and the plasma conditions have been formulated [67] and simulation results indicating how to select the microwave frequency have been provided as well [79]. These studies are based on the assumption that the plasma chamber is a resonating cavity and by varying the microwave frequency different resonant modes can be excited and this affects the plasma properties. Within this section the experimental measurements to prove these assumptions will be described and commented.

#### 4.1.1 Experimental evidences and observations on the performance variation

The electromagnetic field excited inside the plasma chamber of the ECR ion sources plays an important role, by affecting the EEDF, the electron heating and the ionization efficiency as we theoretically investigated (see section 3.2). Several measurements have been carried out to prove the previous statements and the firsts date back to the end of '90s [80]. In fact, in 1996 G. D. Alton proposed new techniques based on the use of high power, variable frequency, multiple discrete frequency or broadband microwave radiation, to enhance the performances of the existing ECRIS. The explanation of the effect produced by these techniques was the creation of a large ECR plasma volume thus permitting the coupling of more power into the plasma. This translates into the heating of a much larger electron population to higher energies and then into the enhanced production of higher charge state ions with higher intensity.[81] One year later he was able to demonstrate that the frequency domain technique can be used to enhance the performance of a traditional B-minimum ECR ion source. He studied at the Oak Ridge National Laboratory the performances in terms of high charge state ion production capability of a Caprice ECRIS, when excited with high-power, single-frequency, or multiple-discrete-frequency microwave radiation. Figure 4.1 confirmed that the frequency dependence is determined by the modal structure of the plasma chamber in combination with a TEM injector.[80]

The enhancement of the ECRIS performances with the use of a frequency

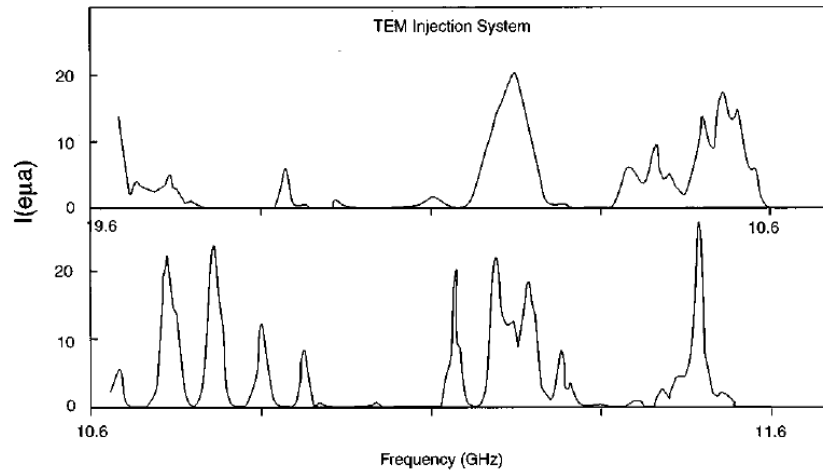


Figure 4.1: *Current intensity of  $Ar^{8+}$  versus microwave frequency measured at low RF injection power levels for the integrated TEM injection system.*

tunable generator was then confirmed in 2002 by S. Gammino *et al.*. In fact, they observed a different behavior of the CAESAR and of the SERSE ECRIS installed at INFN-LNS, when they were operated by means of a travelling-wave-tube-based generator with respect to the standard operation by means of a klystron-based generator. In figure 4.2 an increase for the highly charged ion, when the ion sources were set with the same parameters except for the type of generator, is clearly visible. [82]

Several explanation of these results and measurements were carried out but, since the only one difference between the two generators, was the different frequencies of operation (the TWT was driven by a DRO set to a frequency different of a few hundreds MHz with respect to the one of the Klystron) this opened the way to the next experiments carried out by the INFN-LNS team to support the effect of the variation of the microwave frequency on the ECRIS performances. Recently, this technique has been investigated and a breakthrough experiment, described in the next section, has been performed at GSI a few years ago [70]. The investigation of the effect of the variation of the frequency on the beam quality and on the beam emittance was carried out at JYFL [83] where a set of measurements was performed. These experiments pointed out that the frequency tuning can have a remarkable effect on ion beam intensity and quality. Figure 4.3 shows that the beam structure varies strongly with the microwave frequency

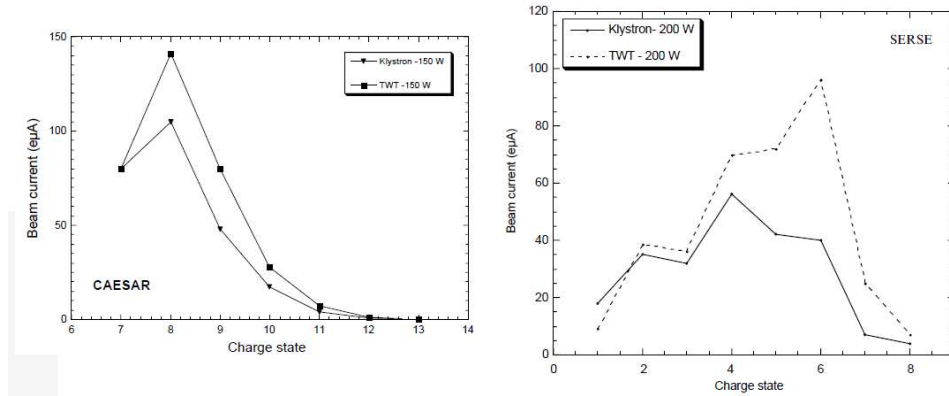


Figure 4.2: Measured current for the highest charge states of Argon obtained with the CAESAR ion source at 150 W (left) and of Oxygen obtained with the SERSE ion source at 200 W (right).

as an indication of the plasma-wave coupling variation during the frequency change. In recent times experiments were carried out also at CNAO, Pavia and with the Caesar ECRIS installed at LNS-INFN [75] where the X-Ray spectra for several frequencies have been measured without a remarkable effect.

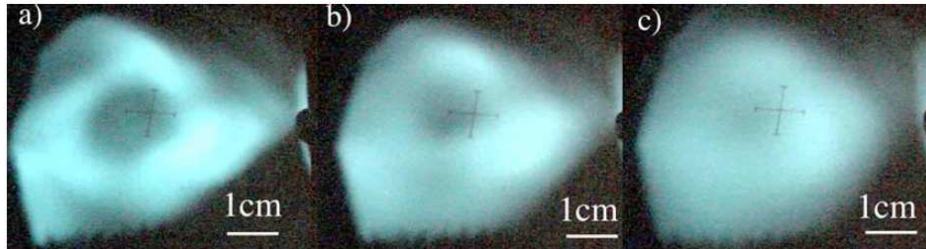


Figure 4.3: Structure of the  $Ar^{9+}$  ion beam at different plasma heating frequencies: a) 14.050 GHz, b) 14.090 GHz, and c) 14.108 GHz.

Besides the experiments reported, some theoretical model have been proposed to explain the origin of these variations and the influence on the plasma particles motion. Single particle and particle-in-cell (PIC) simulations are particularly useful for the electron dynamics calculation: the effect of magneto-static and electromagnetic fields can be evaluated. A model proposed by D. Mascali *et al.* explained the variation in the performances in terms of charge states and extracted current by taking into account the

different patterns of the electromagnetic fields on the resonance surface.[67] They were able to demonstrate that the shape of the plasma present inside the ECR surface, which in turn depends on the excited electromagnetic mode, influences the ion motion up to the extraction region, where the ion beam is formed. With this model they explained the different shapes of the extracted beam experimentally observed in [70] obtained at two different microwave frequencies (see picture 4.4).

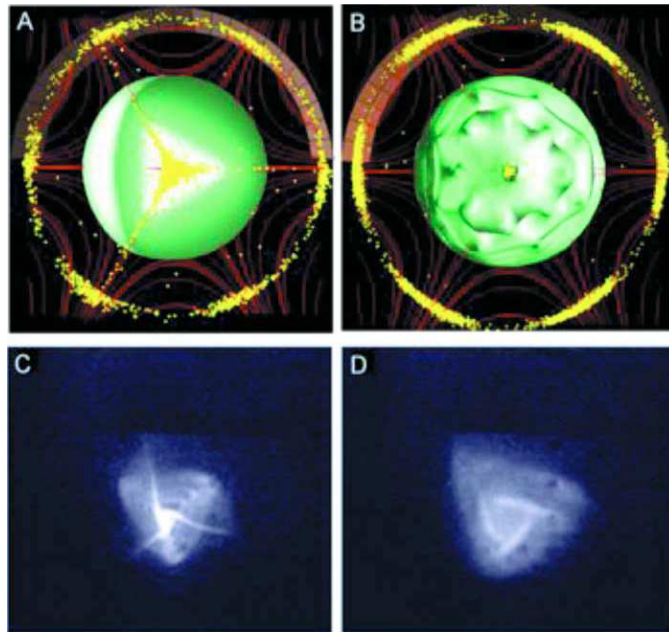


Figure 4.4: (a) and (b) Front view of the ions positions after  $100 \mu\text{s}$ ; (c) and (d) Extracted beam shape experimentally observed at two different microwave frequencies in the case of the CAPRICE ion source as described in [70].

## 4.2 Operation of the CAPRICE ECRIS with applying the frequency tuning

We performed with the CAPRICE-type ECRIS installed at GSI an interesting investigation on how the frequency tuning can affect the ion source performances in terms of beam current, production of higher charge states and beam quality. In 2008 we operated this ECRIS with a klystron generator driven by an analog oscillator sweeping in the  $14.46 - 14.54 \text{ GHz}$  frequency

range and the current and shape of helium ion beams were measured. Figure 4.5 shows the results of the frequency tuning effect on the extracted current. Here the total beam current is divided by three to compare its evolution with the  $He^+$  and  $He^{2+}$  evolution with the frequency. In figure 4.5 the reflection coefficient (dashed line referred to the right scale) is included and a clear relationship between the reflection coefficient and the beam current is visible.

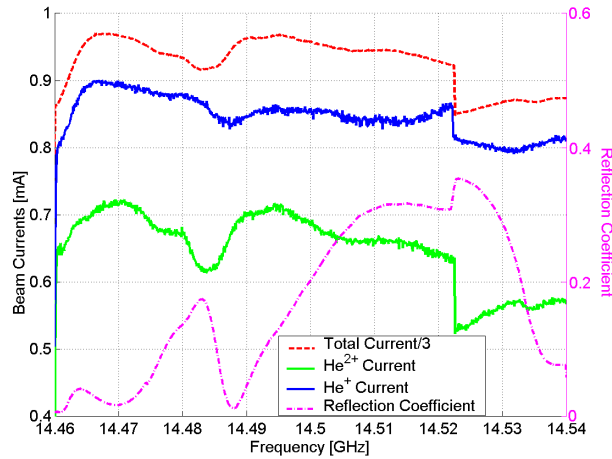


Figure 4.5: Frequency tuning effect on the beam current extracted by a CAPRICE-Type ECRIS.

In 2010 we replaced this generator with a Traveling Wave Tube Amplifier (TWTA) driven by a synthesizer sweeping in the 12.5 – 16.5 GHz frequency range and the measurements of the ion beam current and shape were extended to a larger frequency range. This experiment was carried out by operating the source with a maximum power of 150 W because the TWTA was not able to handle high levels of reflected power. For this reason, in 2011 we performed an experiment including a waveguide isolator able to accept up to 650 W and the effect on the high charge state ion production of the frequency tuning was then analyzed. Recently we operated once more the CAPRICE ECRIS with the frequency tuning technique in order to investigate the effect on the production of metal ion beams.

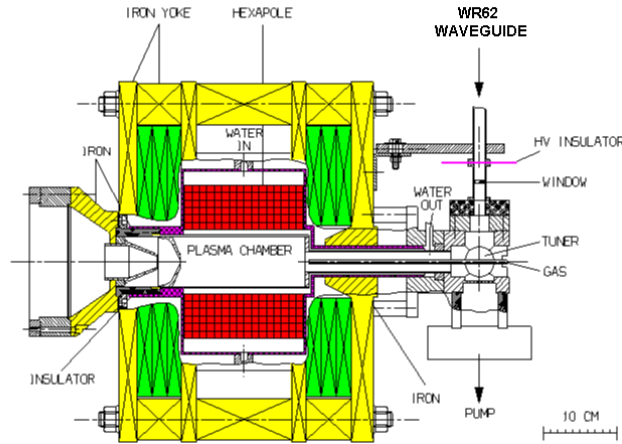


Figure 4.6: Cross section of the CAPRICE ECRIS.

#### 4.2.1 The CAPRICE ECR ion source description

The CAPRICE ECRIS is a compact ion source thanks to the iron yoke and to the small dimensions of the plasma chamber (long around 160 – 180 mm length with a 64 mm diameter). The detailed description of the main features of the ion source can be found in [84]. In figure 4.6 the cross section of the CAPRICE source installed at GSI in the EIS testbench are shown. The magnetic confining field is generated by two solenoid coils (1.2-1.3 T is the maximum longitudinal magnetic field at the injection and at the extraction) indicated in green in the picture in figure 4.6. A NdFeB permanent magnet sextupole combine to the longitudinal field a radial confinement (there are several version of the CAPRICE sources equipped with 1.0 T or 1.2 T magnetic field at the plasma chamber wall). The microwave injection system is composed by a waveguide to coaxial transition inside a copper cube where the WR62 rectangular waveguide is connected. Inside the copper cube the gas inlet (or the oven housing for the metal ion production) is mounted. The extraction system is composed by a plasma electrode (biased together with the plasma chamber at 12 – 15 kV), a ground electrode and a screening electrode negatively biased (usually at  $-2$  kV).

#### 4.2.2 The experimental set-up

In order to measure the effect of the frequency tuning on the CAPRICE performances, the microwave injection of the ion source was modified. In

fact some components, for instance the waveguide vacuum window, were changed and some passive devices like the high directivity directional couplers were inserted in the waveguide injection line. Furthermore the microwave generator has to be equipped with a variable oscillator or else a wideband microwave amplifier driven by a sweep generator must be used. Some components of the beamline of the testbench have been used to measure the effect of the frequency tuning on the ion source performances. The layout of the EIS testbench, where the ions source is installed, is shown in the figure 4.7 and it is described in [85].

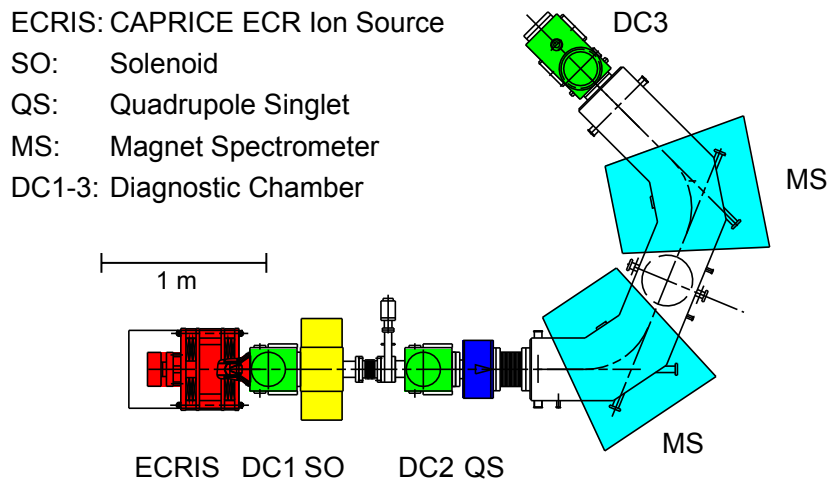


Figure 4.7: *Layout of the EIS testbench.*

The main elements of the beamline are: a diagnostic chamber DC1 (where Faraday Cups, emittance measurements or viewing targets devices can be mounted) a focusing solenoid, a second diagnostic chamber DC2, a quadrupole singulet, a dipole for the mass over charge ratio separation, a third diagnostic chamber DC3. The Faraday Cups inside the diagnostic chambers DC2 and DC3 can measure the beam intensity. The variation of the beam current with the frequency was measured with the Faraday Cup at the DC3 position and by recording the drain current at the high voltage power supply for the total current. In order to measure the effect of the variation of the microwave frequency on the beam quality, viewing targets mounted on feedthroughs remotely controlled are inserted inside the diagnostic chamber along the beam line. We have chosen all the diagnostic



chambers indicated in figure 4.7 to monitor the beam shape: before and after the extracted beam focusing solenoid (*DC1* and *DC2*, respectively) and in the diagnostic box *DC3* after the magnet spectrometer. During the frequency sweeps the forward power and the reflected power were measured simultaneously with the beam current or with the beam shape.

### 4.2.3 The effect of the frequency tuning on the ion extracted current

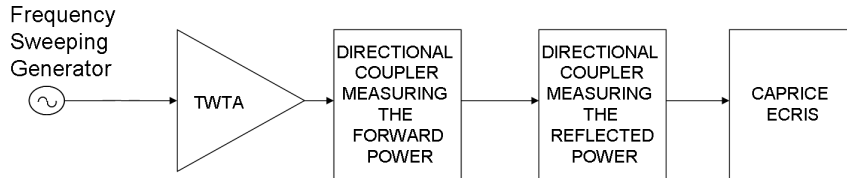


Figure 4.8: Block diagram describing the main components of the microwave injection system used for the frequency tuning measurements.

A signal generator produces the electromagnetic wave, which power is amplified by a TWTA, feeding the plasma. Figure 4.8 shows the block diagram describing the microwave injection. The used TWTA covers the 8 – 18 GHz frequency range and it is able to provide an output power up to 650 W. The maximum manageable power reflected to the amplifier was restricted to 80 W, then the microwave power feeding the plasma was kept lower than 150 W. The automatic level control of the output power of the amplifier was always active. For frequencies higher than 16.5 GHz high reflected power was measured and the TWTA was not able to handle it over a long time. This may be due to the confining magnetic field which is no longer adequate for these high frequencies. A digital signal generator working in the range from 1 to 20 GHz was used. Since the calculated minimum distance between two resonant frequencies of the CAPRICE vacuum filled plasma chamber, when assumed as a cylindrical resonating cavity, in the specified frequency range is around 500 kHz, steps of 200 kHz were chosen. A dwell time of 20 ms for each step has been set. Then one measurement ranging from 12.5 GHz to 16.5 GHz had a duration of about 400 seconds. We analyzed the plasma

properties by measuring, for different ion source conditions, the reflection coefficient with the two directional couplers of high directivity inserted in the waveguide line. The forward power and the reflected power were measured with two probes. Argon as a main gas and Helium as a support gas at gas pressures around  $4 \cdot 10^{-6}$  mbar were used. We measured the ion currents of the charge states  $Ar^{7+}$ ,  $Ar^{8+}$  and  $Ar^{9+}$  with a Faraday cup inserted in the DC3 diagnostic chamber; the drain current of the high voltage power supply of the extraction has been recorded simultaneously.

During the current measurements, while the frequency swept, the ion source parameters were kept constant. First the ion source parameters were set to optimize the  $Ar^{8+}$  production at 14.5 GHz. This is the operating frequency of the CAPRICE ECRIS provided by the klystron oscillator which is the device used for the normal operation of the ion source. During the preliminary frequency sweeps there were values where we experienced a mismatch condition and then the forward power at the output of the TWTA was decreased to 100 W for all the next experiments: the maximum  $Ar^{8+}$  current for this setting of the source was around  $75 \mu A$  with a drain current of 2.36 mA. With these ion source conditions the frequency sweep was ramped from 12.5 GHz up to 16.5 GHz. During the frequency sweep the reflection coefficient, the analyzed ion currents and the drain current were recorded simultaneously and the measurements results are shown in figure 4.9. The reflection coefficient indicated in the upper figures 4.9 has been calculated with the formula:

$$Reflection\ coefficient = 10 \cdot \log_{10} \left( \frac{Reflected\ power}{Forward\ power} \right) \quad (4.1)$$

In the equation (4.1) the forward power is the microwave power sent to the ion source and measured with a power probe connected to one of the two WR62 directional couplers, while the reflected power is the one reflected by the ion source and measured at the power probe connected to the second directional coupler. By analyzing the reflection coefficient shown in the upper figures 4.9, it is clear that the plasma chamber has a resonating behavior. This result was already found in 2008 [70]. We observed a correlation between the peaks of the reflection coefficient and of the current amplitude in particular where the impedance matching condition is fulfilled (when there is no reflected power). The Argon drain current and the charge states currents are affected by the choice of the operating frequency; for instance the  $Ar^{8+}$  current ranges from a few  $\mu A$  up to  $200 \mu A$  and the evolution is similar to the  $Ar^{7+}$ . However at the frequencies where both currents present a peak,

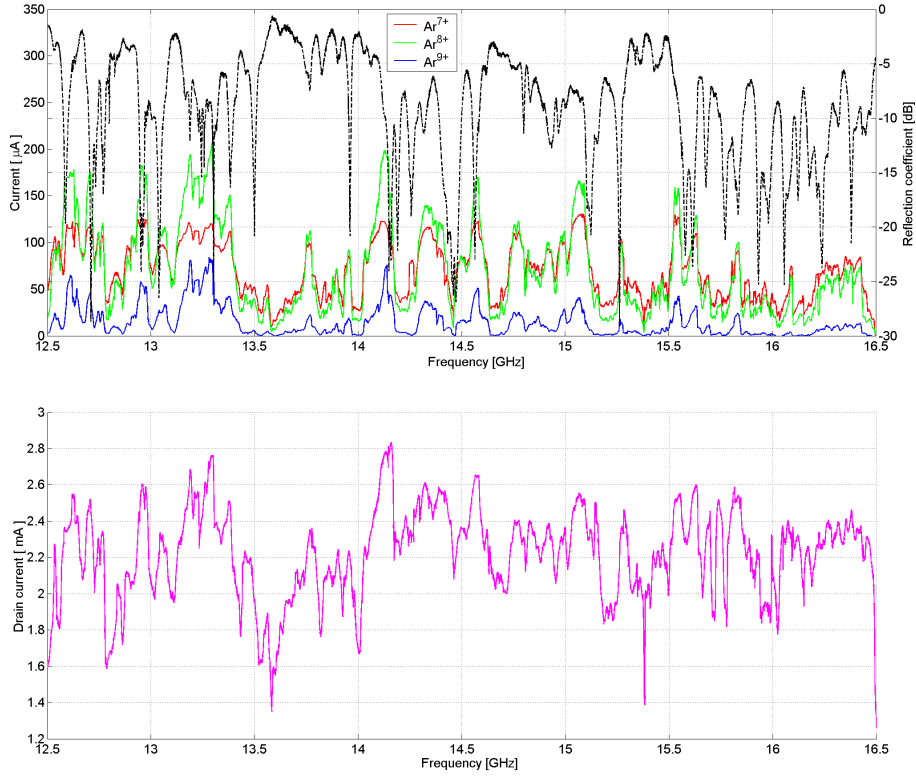


Figure 4.9: (Top) Ion current for 3 different Argon charge states, reflection coefficient (dashed line referred to the right scale) and total ion current (bottom) for the Argon beam as a function of the microwave frequency.

the  $Ar^{8+}$  is quite higher than the current of  $Ar^{7+}$  (for instance at 14.119 GHz the difference between the two currents is a factor two). An opposite behavior is visible for the minima of the current amplitudes where the  $Ar^{7+}$  current is higher than the  $Ar^{8+}$  current. The  $Ar^{9+}$  beam current rise up to  $80\mu A$  within the considered frequency range and starting from 15.64 GHz tends to lower values even if the reflected power is less than 10%. This results seems to be correlated with the confining magnetic field restricting the ion source operation to lower frequencies. The total beam current is indicated in the bottom figures 4.9 and it is varying with the frequency with the same evolution of the charge states current. We checked the obtained results for several runs by repeating the measurements during the frequency sweeps and no remarkable variations were recorded on the beam currents

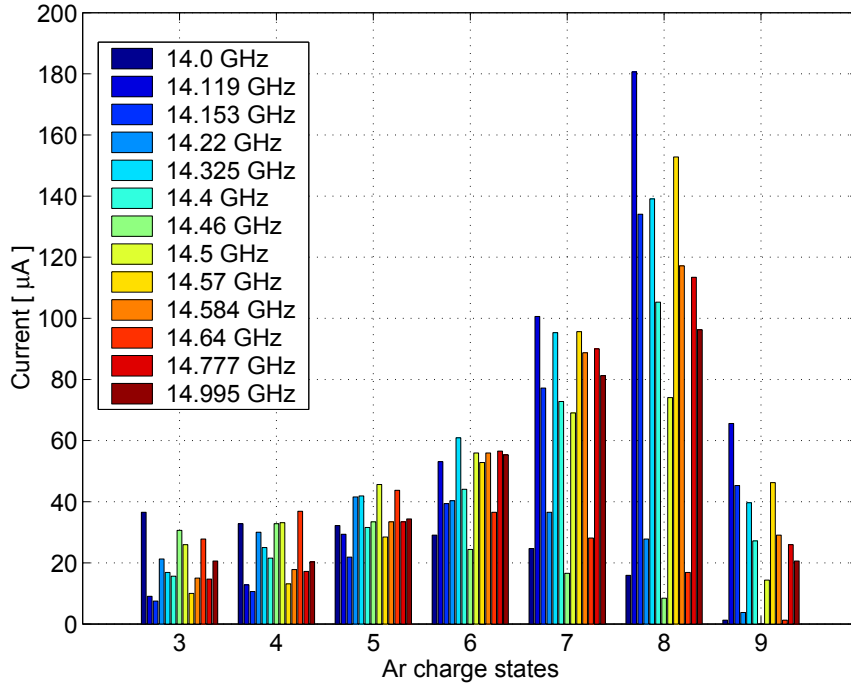


Figure 4.10: Argon charge states distributions for thirteen different frequencies in the 14 – 15 GHz frequency range.

and on the reflection coefficients. Then a good reliability of the measurements results is expected.

The frequency tuning effect was also analyzed on the other Argon charge states by comparing the charge state distributions for different frequencies. The analysis was restricted to the 14 – 15 GHz range and, within this range, the most interesting frequencies (i.e. where the  $Ar^{8+}$  current was minimum and maximum) the charge state distributions were chosen from the frequency sweeps. In figure 4.10 the Argon charge state distributions are shown for thirteen frequencies. It is useful to restrict our analysis to the most significant ones and figure 4.11 shows six of them. The inset of this plot indicates the reflection coefficient. The highest  $Ar^{8+}$  current was measured at 14.119 GHz and at this frequency the lowest current of the lower charge states was measured (measured at 14.57 GHz as well). The  $Ar^{8+}$  is more than doubled, with respect to the standard operation frequency of 14.5 GHz. It is also important to mention that at 14.119 GHz and at 14.995 GHz the power feeding the plasma was the same (almost the same

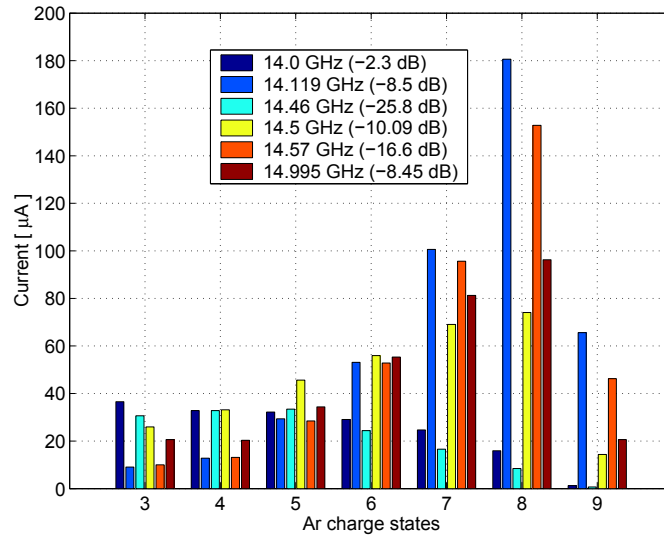


Figure 4.11: Argon charge states distributions for six different frequencies in the 14 – 15 GHz frequency range.

measured reflection coefficients) but the enhancement of the higher charge states is quite different. Different reflection coefficients can be related to similar charge state distributions like at 14.0 GHz and 14.46 GHz where the current of the higher charge state is quite low.

The microwave coupling varies, while the frequency sweeps and for this reason the reflection coefficient presents a strong variation. This is related to the fact that the coupling of the electromagnetic waves to the plasma changes by changing the microwave frequency. The amount of power feeding the plasma varies during the sweep and if higher charge states are requested the microwave power has to be increased.[5]

At high power the frequency tuning can be more effective for the high charge state production. In order to validate this assumption it is interesting to show in figure 4.12 the  $Ar^{7+}$  and  $Ar^{8+}$  beam current evolutions for two different power levels, 50 W and 100 W. All the other ion source parameters remained unchanged. The beam currents are restricted in the frequency range from 14 to 15 GHz. At 50 W the curves of  $Ar^{7+}$  and  $Ar^{8+}$  current are very similar but at 100 W higher values of current are obtained, a pronounced difference between the two curves appears and the frequencies at which the current peaks occur are shifting by a few MHz.[69]

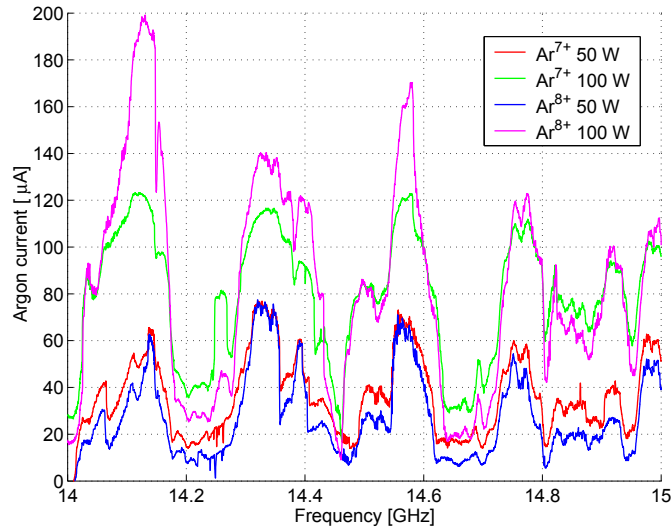


Figure 4.12: Argon beam currents course with the frequency for different microwave powers.

#### 4.2.4 Enhancement of the current of highly charged ions

In order to analyze the frequency tuning effect on the high charge state ion production the power provided to the source had to be enhanced and for this reason we included a waveguide isolator in the waveguide injection line. The block diagram shown in figure 4.13 describes the modified set-up. The water-cooled waveguide isolator included in the WR62 waveguide line is characterized by a low insertion loss and a high insulation (around 20 dB) among the covered frequency range of 12.5–18 GHz. The CAPRICE source parameters were set in order to maximize the production of the  $Ar^{11+}$  ion current at 14.5 GHz and 450 W microwave power and then a frequency sweep was run in the 12.5–16.5 GHz frequency range. During the frequency sweeps the  $Ar^{8+}$ ,  $Ar^{9+}$  and  $Ar^{11+}$  ion currents were measured. The evolution of these ion currents with the frequency is shown in figure 4.14.

In this figure the  $Ar^{11+}$  values are multiplied by a factor 10 in order to better visualize the comparison with the other charge states. With respect to the measurement reported in the previous section, the currents were more noisy and less stable during the sweep. This behavior, already observed in [83] can be explained by analyzing the reflection coefficient measured with the set-up described in figure 4.13 and shown in the dashed line of figure 4.14. During this experiment the power levels coupled to the plasma ramped

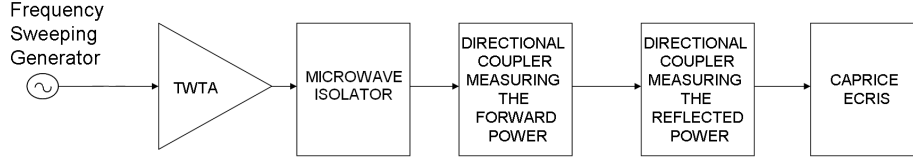


Figure 4.13: Block diagram describing the main components of the microwave injection system used for the frequency tuning measurements at high power.

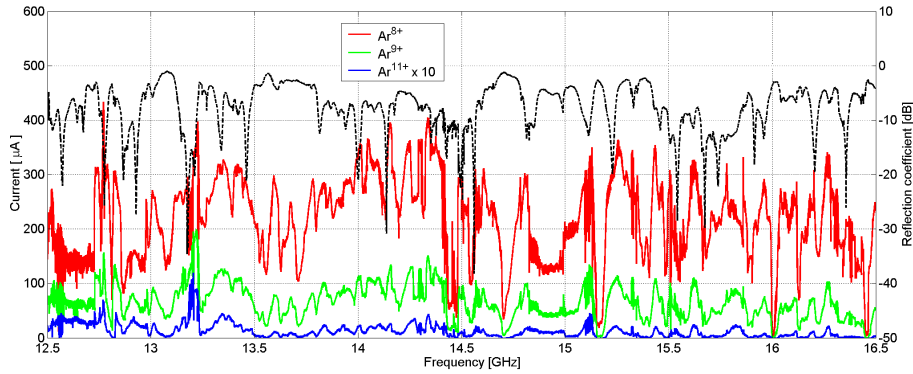


Figure 4.14: Argon beam currents and reflection coefficient (dashed line referred to the right scale) during the high power frequency sweeps.

from a few tens of watt (at frequencies where the reflection coefficient had a maximum) up to 450 W (at frequencies where a condition of optimum matching was fulfilled) and vice versa. This change of coupled power may have caused this noisy signal dynamic.

Figure 4.14 clearly shows that it is possible to enhance the current of the highly charged ions, i.e.  $Ar^{9+}$  and  $Ar^{11+}$ , by changing the microwave frequencies with respect to the 14.5 GHz default setting. In particular one frequency where this enhancement occurs is 13.221 GHz. It has to be mentioned that during the experiment described in the previous section one optimized frequency was 14.119 GHz. However, the frequency where the highest  $Ar^{8+}$  and  $Ar^{9+}$  current peak was measured was around 13.29 GHz (see figure 4.9). Since some source parameters, like the plunger position, the balance of gases and the position of the plasma electrode, are not the same

as in the previous experiment, the two optimized frequencies are different and a direct comparison cannot be done.

By keeping the source parameters in the condition corresponding to figure 4.14 the beam currents were measured at different microwave powers for two microwave frequencies: 13.221 GHz which is the optimized one and 14.5 GHz.

Table 4.1: Currents of Argon beams expressed in  $\mu A$  for different power levels at two microwave frequencies.

	MICROWAVE POWER [W]													
	250		300		350		400		450		500		550	
	14.5 GHz	13.221 GHz	14.5 GHz	13.221 GHz	14.5 GHz	13.221 GHz	14.5 GHz	13.221 GHz	14.5 GHz	13.221 GHz	14.5 GHz	13.221 GHz	14.5 GHz	13.221 GHz
Ar <sup>3+</sup>	34.5	56.4	30.9	56.8	29.2	46.3	27.9	53.9	26.5	39.2	25.7	35.7	26.6	36.5
Ar <sup>4+</sup>	65.2	71.7	60.7	64.5	58.9	66.7	57.2	71.3	55.1	68	54.3	66.4	54.7	64.7
Ar <sup>5+</sup>	116.2	99.4	112.1	87.8	110.3	98	111.2	109.5	105.9	105.9	109.3	103.5	106.8	103.9
Ar <sup>6+</sup>	180.4	144.5	186.2	101.2	185	160.8	184.2	173.5	185.4	182.8	187.9	174.7	180.9	166
Ar <sup>7+</sup>	219.3	175.9	232	147.8	244.3	230.1	252.4	259.6	259.5	297.3	262.3	280.8	265.3	267.6
Ar <sup>8+</sup>	226.9	283.7	270.2	267.4	290.5	361.6	295.9	377.2	310.5	449	327.1	445	310.9	421
Ar <sup>9+</sup>	60.6	127.1	72.9	140.5	85.3	162.5	92.3	175.4	96.4	204.6	104.2	202.1	104.1	207.8
Ar <sup>11+</sup>	0.78	4	1	5.85	1.3	6	1.5	6.4	1.8	7.7	2.0	8.5	2.2	9.6
Ar <sup>12+</sup>	0.04	0.21	0.06	0.28	0.08	0.9	0.1	0.85	0.13	1	0.13	1.1	0.14	1.2

The charge state distributions were measured at these two frequencies for microwave powers ramping from 250 W to 550 W in steps of 50 W. The results of these measurements are reported in the Table 4.1. During these measurements the other source settings were not varied. The measured current values reveal how the increase of power can be effective only for the higher charge states (i.e. above the charge state 8+). For the production of lower charge states it is clear that the power levels must be kept low in order not to provide higher energies for the electron heating [5].

In order to visualize the enhancement of current for the higher charge states (above 8+) when the frequency is changed from 14.5 GHz to 13.221 GHz it is useful to plot the values contained within this table. Figure 4.15 shows the ratio of the two current values for the last four rows of table 1. The Ar<sup>12+</sup> can be increased from 5 times to almost 9 times by increasing the power and by choosing an optimized feeding frequency. The result contained



in this figure demonstrates how effective is the choice of the frequency for the high charge state ion production. It is also confirmed that the choice of the microwave frequency can improve the ionization efficiency. In fact the ion currents for the lower charge states are higher if the ion source is operating at a frequency which is not *optimized* for the production of high charge states.

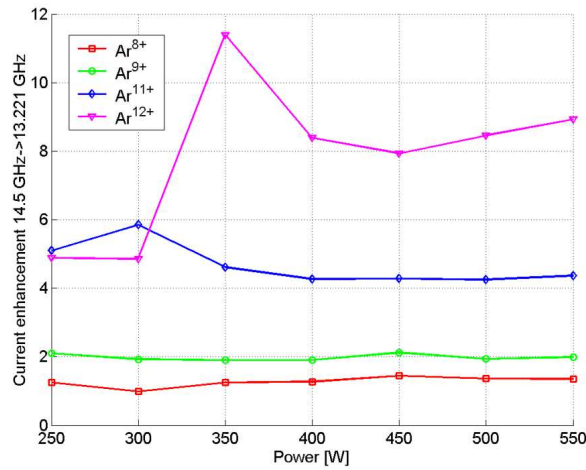


Figure 4.15: *Current enhancement of Argon high charge states ions for different microwave powers.*

One important observation is that if the power increases a shift of the resonant modes towards the higher frequencies is also expected, as confirmed by the experimental evidences reported in section 4.1.1. For this reason for each power level the optimized frequency could not be the one measured at 450 W and indicated for the comparison of the current levels in table 4.1.[86]

#### 4.2.5 The effect on the beam shape

Beam inhomogeneities and aberrations can be observed by monitoring the beam shape and, for this purpose, the viewing targets revealed to be a powerful diagnostic tool.[56] The viewing target technique to measure the ion beam properties in terms of quality and shape has been described in section 2.5.2 where the viewing targets have been introduced.

We made use of this beam diagnostic tool to measure the variation of the beam properties when the frequency tuning is applied to the CAPRICE ECRIS. In 2008 we analyzed the beam quality at GSI with the beam viewers

on a helium beam when the microwave frequency was swept from 14.46 GHz to 14.54 GHz. In figure 4.16 the  $He^{2+}$  and the drain current evolutions with the frequency (left) and the beam shape (right) right after the extraction (at the diagnostic chamber  $DC1$  indicated in figure 4.7) are shown. Figure 4.16 shows that the beam intensity distribution is inhomogeneous and that this distribution changes with the microwave frequency, while keeping all the other parameters constants.[70]

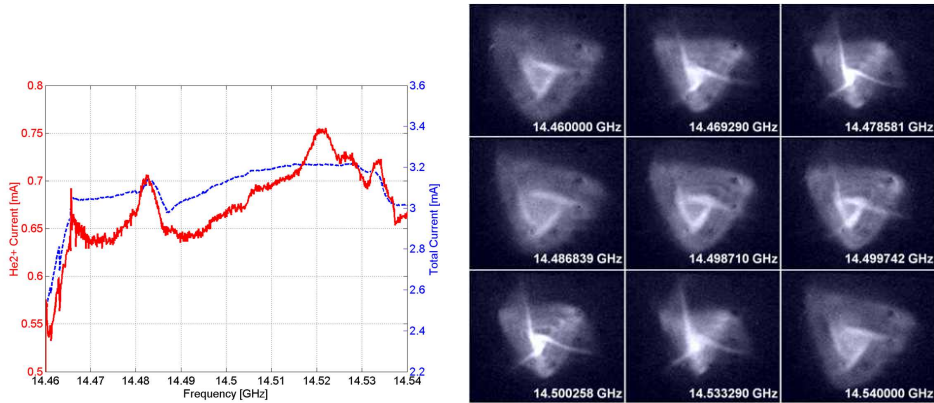


Figure 4.16: Evolution of the  $He^{2+}$ , of the drain current (left) and of the beam shape (right) with the frequency.

The experiment was repeated in 2010 at GSI with the experimental setup indicated in the section 4.2.2. Along the beamline shown in figure 4.7 the viewing targets have been mounted on feedthroughs in order to analyze the effect of the frequency tuning by recording the shape of the ion beam with a camera during the frequency sweep. The variation of the ion beam shape was measured in the diagnostic chamber  $DC2$  and  $DC3$ . The beam shape during the sweep was analyzed for different settings of the ion source. First the ion source was optimized for  $Ar^{8+}$  (see figure 4.9) and then the Faraday Cup was taken out from the  $DC3$  and a viewing target was inserted along the beam line and, while the microwave frequency swept, we recorded the  $Ar^{7+}$ ,  $Ar^{8+}$  and  $Ar^{9+}$  beam shapes. A selection of images extracted from the videos are reported in figure 4.17. In this figure the corresponding frames taken from the measurement of the focused beam shape at the  $DC2$  plasma chamber are included in the first column. These images are recorded when the focusing solenoid was set to optimize the transmission of the  $Ar^{8+}$  beam current and the visible rings are the unfocused charge states. The

reported frames are corresponding to the first four frequencies indicated in figure 4.11: 14.0 GHz and 14.46 GHz (minimum  $Ar^{8+}$  intensity), 14.119 GHz (maximum  $Ar^{8+}$  intensity) and 14.5 GHz is the usual operation frequency of the CAPRICE ion source when the klystron provides the microwaves feeding the plasma. For the frequencies where the minimum of  $Ar^{8+}$  current

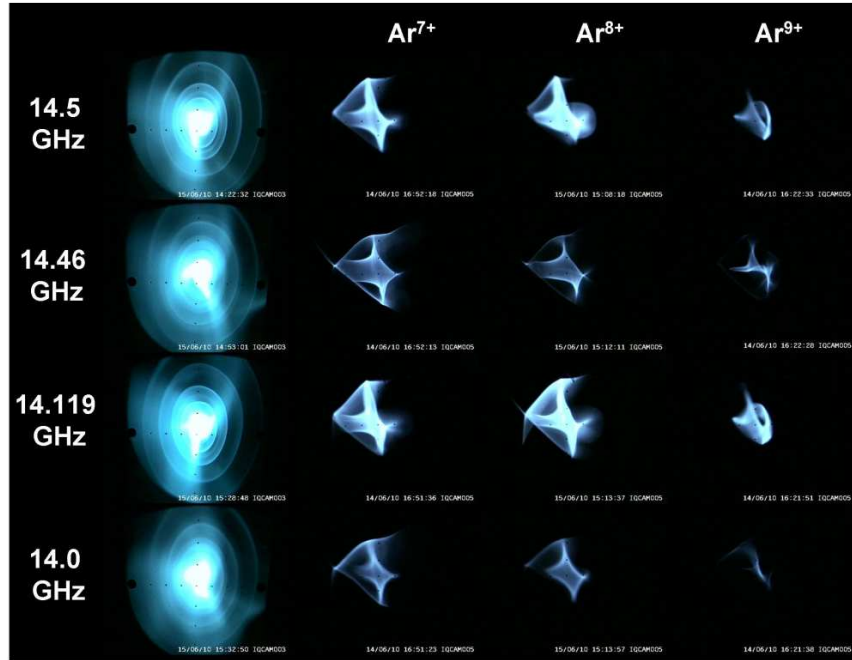


Figure 4.17: Argon beam, at different microwave frequencies, on the targets located behind the focusing solenoid (first column) and behind the dipole for  $Ar^{7+}$ ,  $Ar^{8+}$  and  $Ar^{9+}$ , respectively.

is measured, 14.0 and 14.46 GHz, the focused beam shape seems to remain unchanged concerning the orientation of the arms. At 14.0 GHz the image is brighter and this can be related to the higher intensity measured at the Faraday cup with respect to 14.46 GHz. It is worth noting that at 14.46 GHz the reflection coefficient is at the minimum (see caption of figure 4.11) between the analyzed frequencies. The beam recorded in the *DC3* remains similar but for the  $Ar^{9+}$  some differences between the two frequencies are present. This is a further confirmation that a fundamental role is played by the electromagnetic field pattern which influences the heating rapidity, and the ion confinement time [75].

The beam shapes at 14.119 GHz (optimum performance for the highly

charged ion production) and the usual 14.5 GHz operation can be compared. Concerning the focused beams, recorded on the *DC2*, at 14.119 GHz is bigger and brighter than the one at 14.5 GHz and the orientation of the arms is turned clockwise by more than  $40^\circ$  with respect to the beam shapes at 14.0 – 14.46 GHz. The brightness of the images at *DC3* is higher at 14.119. The beam shapes measured at *DC3* remain unchanged with the exception of the shape of the  $Ar^{8+}$  ion beam which presents some minor changes. The similar shape of all the charge states on this position for all the analyzed frequencies can lead to the following observation: even if the focusing solenoid and the magnetic quadrupole singlet located in front of the analyzing dipole magnet were set differently for the three charge states, and for different current intensities, the "hyperbolic shape" of the beam is preserved.[69] Then it is possible to observe that while the beam intensity is very sensitive on the effect of the frequency tuning the beam shape is affected by the magnetic structure of the beam line and a variation of the frequency affects the brightness of the image as an indication of the variation of the beam intensity.

#### 4.2.6 Application of the frequency tuning for the production of metal ions

We carried out an interesting experiment in order to achieve higher charge state ion current for a Titanium beam produced at GSI for the future nuclear physics projects. The element used for this experiment was natural Titanium ( $^{48}Ti$ ), while the requested beam to be injected into the accelerator will be the enriched material  $^{50}Ti$ . Concerning the metal vapor production no differences involving the oven construction have been observed when using the natural or the enriched material. Since the melting point of the Titanium is higher than  $1600^\circ$ , the High temperature Oven described in section 2.4.4 has been used for this purpose and around 200 mg of  $^{48}Ti$  have been introduced in the crucible. The goal of this experiment was to produce, by applying the frequency tuning technique, a stable beam with sufficiently intensity of a beam of ions with charge state higher than 8+ ( $Ti^{8+}$ ,  $Ti^{9+}$ ,  $Ti^{10+}$ ..). The normal operation of the source for this purpose make use of a Klystron microwave generator working at 14.5057 GHz providing a power up to 350 W to the ion source. We replaced this generator with a Traveling Wave Tube Amplifier driven by a synthesizer (initially set at 14.507 GHz) providing a power around 250 W for the whole duration of the experiment. Additional Helium gas was used to stabilize the plasma. The heating of the oven usually takes half a day of operation while the applied voltage is slowly

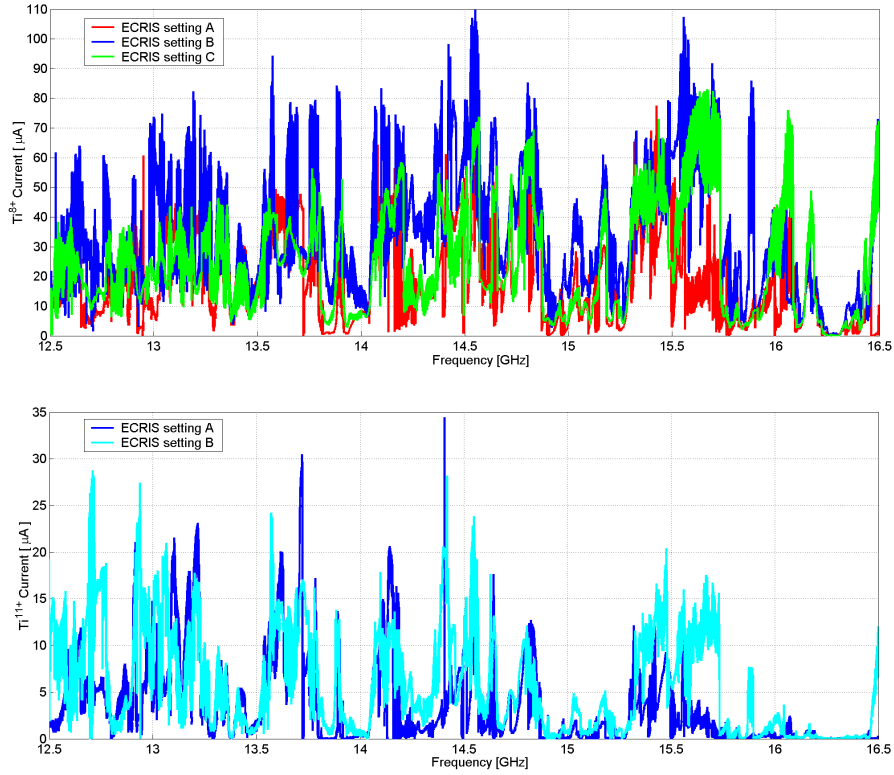


Figure 4.18:  $Ti^{8+}$  (top) and  $Ti^{11+}$  (bottom) evolution varying the microwave frequency.

ramped until a sufficient power (in this case a power of 200 W was enough but this value is sensitive on the type of oven and of the material inserted) was reached in order to obtain a few tens of  $Ti^{7+}$  and the spectrum was free of Oxygen charge states, indicating that the outgassing phase of the oven is finished. When the source parameters were set to obtain the condition "A" indicated in table 4.2 a frequency sweep was carried out to measure the variation of the beam intensity for the  $Ti^{8+}$  and for the  $Ti^{11+}$  with the frequency. The results of this current evolution is shown in figures 4.18.

We observed a different behavior of the  $Ti^{8+}$  with respect to the  $Ti^{11+}$  during the frequency sweeps. First a noisy  $Ti^{8+}$  current was measured with respect to  $Ti^{11+}$  current. Then while at 14.5057 GHz the  $I_{Ti^{8+}} = 49 \mu A$  and no enhancement was gained by changing the microwave frequency, the

Table 4.2: CAPRICE ECRIS settings for the  $^{48}\text{Ti}$  ion production.

Setting	Oven power	Inj coil current	Ext coil current	Gas pressure
<i>A</i>	234 W	1228 A	1078 A	$4.8 \cdot 10^{-6}$ mbar
<i>B</i>	262 W	1237 A	1099 A	$7.8 \cdot 10^{-6}$ mbar
<i>C</i>	269 W	1163 A	1094 A	$8.8 \cdot 10^{-6}$ mbar

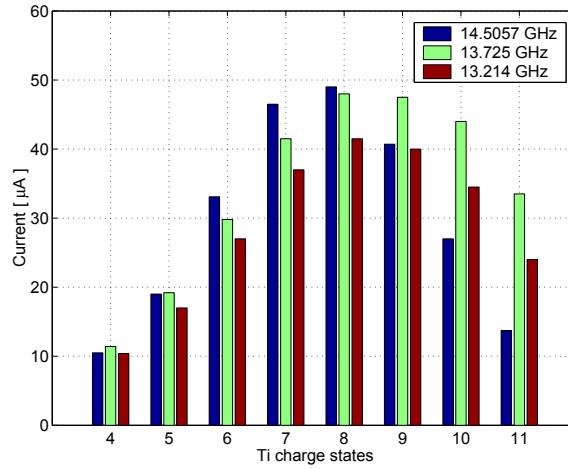


Figure 4.19: Titanium charge state distribution for three microwave frequencies (same source settings: the condition "A" in table 4.2).

$I_{Ti^{11+}} = 13 \mu\text{A}$  can be enhanced up to  $34 \mu\text{A}$  if the frequency is changed to 13.725 GHz, for instance, which is one value where an increase of the intensity was measured.

After this sweep it was then possible to identify some frequencies where the  $Ti^{11+}$  had a maximum like at 13.725 GHz and 13.214 GHz and, for these frequencies, the charge state distributions, shown in figure 4.19, revealed the current gain when the frequency tuning is applied for the production of metal ion beams in particular for the higher charge states like the  $Ti^{11+}$ . Since it was previously observed that the electromagnetic field distribution is sensitive on the plasma parameters, if the electric power provided to the oven is increased (and consequently the gas pressure inside the plasma chamber) also the frequencies, where the maximum of the currents was measured,

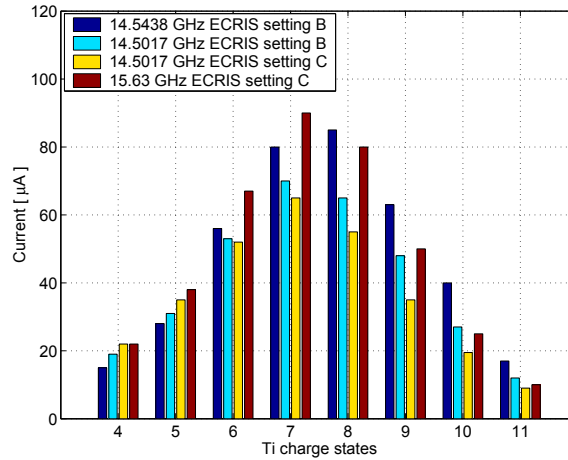


Figure 4.20: Titanium charge state distribution for three microwave frequencies and different settings of the ion source (see table 4.2).

can vary. For this reason in figures 4.18 it is shown the effect of varying the source setting (mainly by increasing the oven voltage) into the "B" (for the  $Ti^{11+}$ ) and "C" (for the  $Ti^{8+}$  and  $Ti^{11+}$ ) conditions described in the table 4.2. Once more it is possible to identify some frequencies where the current of the  $Ti^{8+}$  is enhanced with respect to the 14.5017 GHz frequency (a more stable beam was obtained by slightly change the operating frequency with respect to the 14.5057 GHz previously used). Due to the higher gas pressure it was expected a decrease of the current of the highest analyzed charge states. For this reason a change of the frequency is not longer effective for the enhancement of the  $Ti^{11+}$  current. All these results are summarized in figure 4.20. After almost 48 hours of operation the beam was stable and the ion source worked continuously without any adjustment of the parameters with the exception of the oven power which was increased for compensating the consumed material leading to a slow decrease of the current over the time. Like the gaseous plasmas also the plasmas obtained from a ionized vapor of a metallic element is sensitive on the variation of the frequency and this is visible in figure 4.21 (left) where the drain current is plotted over the frequency for the three source setting above mentioned. During the frequency sweeps, like described in the previous paragraph, the directional couplers and the power probes for measuring the forward and reflected power where used. Then it was possible to measure the reflection coefficient during the frequency sweeps. This is shown in figure 4.21 (right). A resonant be-

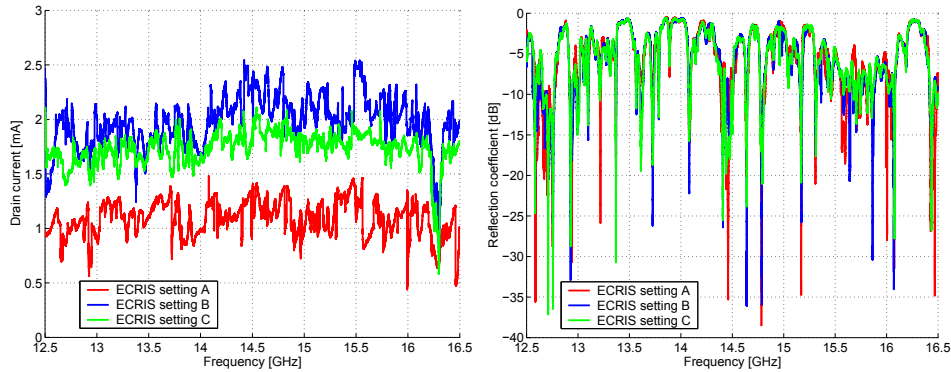


Figure 4.21: Titanium drain current (left) and reflection coefficient (right) evolution by varying the microwave frequency.

havior of the source is preserved but it is interesting that the distribution of the resonances is almost constant, when the source parameters are changed, with respect to the measurement carried out with a gaseous plasma.

### 4.3 The double frequency heating

The trend to increase the operating frequency together with the confining magnetic field permits to achieve higher plasma densities which are necessary to increase the ion current for higher charge states [5]. As shown in the second chapter, the state of the art ECRISs are mainly using operation frequencies above 24 GHz with magnetic field values up to 4.5 T for confinement, i.e., SECRAL ion source at IMP (Lanzhou) working at 24 GHz [36], SC-ECRIS at RIKEN [33] (Japan), VENUS ion source at LBNL [87] and the European MS-ECRIS, designed to work at 28 GHz [40]. In order to reach the desired current intensity of high charge states most of these ion sources are using feeding systems with two electromagnetic waves at different frequencies [88],[89]. This technique, so called "double frequency heating", or "multiple frequency heating" when more than two frequencies feed the plasma, is revealed to enhance the ion current intensity. Since 1994, this technique has been used to improve the production of highly charged ions. In [80] G.D. Alton *et al* used a multi discrete injection system to feed a CAPRICE-type ECRIS with up to three electromagnetic waves thus demonstrating that the charge-state populations for Argon and Xenon ions move toward higher values when excited with two and three discrete-frequencies.



In 2005 the 10.5 GHz ECRIS at Argonne National Laboratory was operated with a 10.5 GHz klystron and an 11 – 13 GHz TWTA.[90] A factor 2 enhancement of the beam intensities for the higher charge states was obtained from the source with two-frequency heating over single-frequency heating. Some possible explanations of this increase of current have been provided in the past and some guidelines for the choice of the two frequencies have been given [91], [64]. However, in most of the cases this choice is made according to the available microwave generators without a possibility for fine tuning of the provided frequency which, as we have largely shown in the previous section, is mandatory to maximize the effectiveness of this technique. The next section reports the results of the experimental measurements of the performances of a CAPRICE-type ECRIS when the double frequency heating is applied **after that** the application of the frequency tuning technique allowed to select the operation frequencies.

#### 4.4 Operation of the CAPRICE ECRIS with the double frequency heating

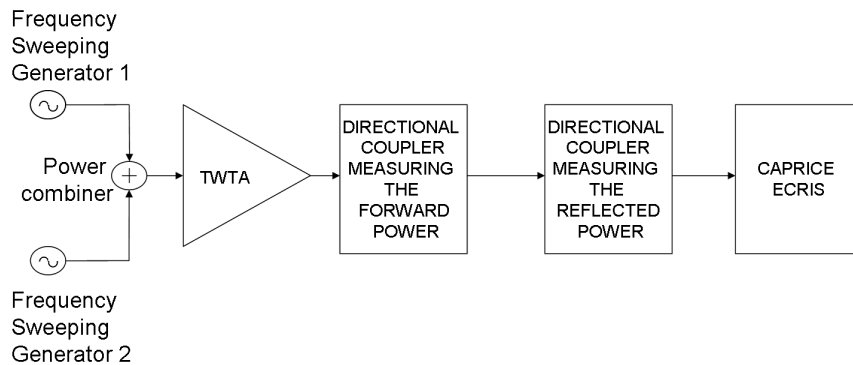


Figure 4.22: Block diagram describing the main components of the microwave injection system used for the double frequency heating measurements.

We used the CAPRICE ECRIS installed at GSI to carry out experiments to investigate the effect of the double frequency heating on the production of high charge state ion beams. In section 4.2.3 the variation of the ion current intensities of  $Ar^{7+}$ ,  $Ar^{8+}$  and  $Ar^{9+}$  in the range 12.5 – 16.5 GHz has been described. The Argon charge state distributions were analyzed for different frequencies and we found that for some of them an enhanced intensity of the

higher charge states occurred. For instance, at 14.119 GHz the current, with respect to the standard operating frequency (14.5 GHz), enhances from 75 to 180  $\mu A$  for the  $Ar^{8+}$  and from 14  $\mu A$  to 65  $\mu A$  for the  $Ar^{9+}$  at 100 W (see figure 4.11). The frequencies 14.119 and 14.5 GHz were selected to analyze the CAPRICE performances in terms of higher current and production of higher charge states when the double frequency heating is applied. Figure 4.22 shows the block diagram describing the experimental set-up. A power combiner was used to send to the TWTA two electromagnetic waves with different frequency provided by two sweeping generators. With this experimental set-up it was possible to explore the double frequency heating when one frequency is fixed (to 14.5 GHz in one case and to 14.119 GHz in another case) and the second one sweeps in the 12.5–16.5 GHz range. First, we kept at 100 W (the output power of each generator was balanced) the amount of power feeding the plasma in order to compare the results of the double frequency heating with the measurements of single frequency sweeping. We

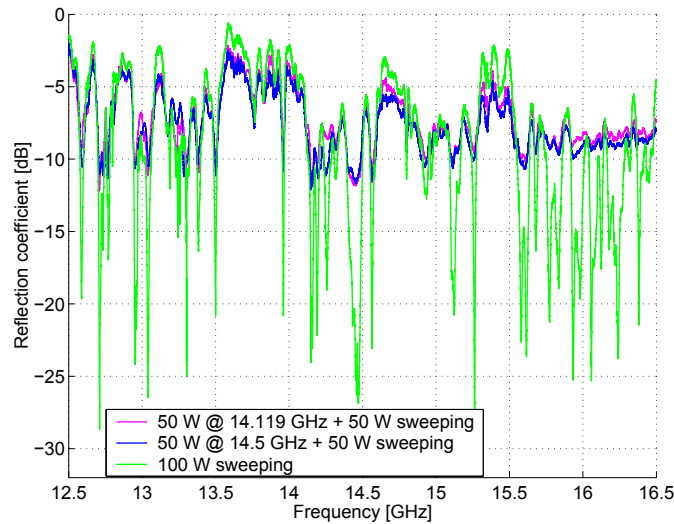


Figure 4.23: *Effect on the reflection coefficient of the double frequency heating for two settings of the fixed frequency and comparison with the single frequency tuning.*

set the ECRIS parameters including the magnetic field, the gas pressure, the extraction voltage, etc, to the same values as used for single frequency sweep analysis with the charge state distribution optimized for the  $Ar^{8+}$  intensity and they have been kept constant during this experiment. We analyzed the double frequency heating by measuring the  $Ar^{7+}$ ,  $Ar^{8+}$  and  $Ar^{9+}$  currents and the drain current. Concerning the forward power and

the reflected power they have been measured simultaneously but, with the double frequency heating the power probes cannot distinguish the respective measured values of forward/reflected related to each of the two waves. The forward power and the reflected power indicated in equation (4.1) are each the sum of the respective power value related to the fixed frequency and the one related to the sweeping frequency. The reflection coefficients calculated with the formula (4.1) are shown in figure 4.23 where the one related to the single frequency sweep, already shown in the upper figure 4.9, is also included. Figure 4.23 allows to make a comparison between the two techniques concerning the behavior of the ion source. As expected, in the case of the two frequencies the minima of the reflection coefficient are higher because of the higher level of reflected power due to the superposition of the two waves. It is interesting to observe that these minima occurs at almost the same frequencies for both techniques. Since the frequencies when a min-

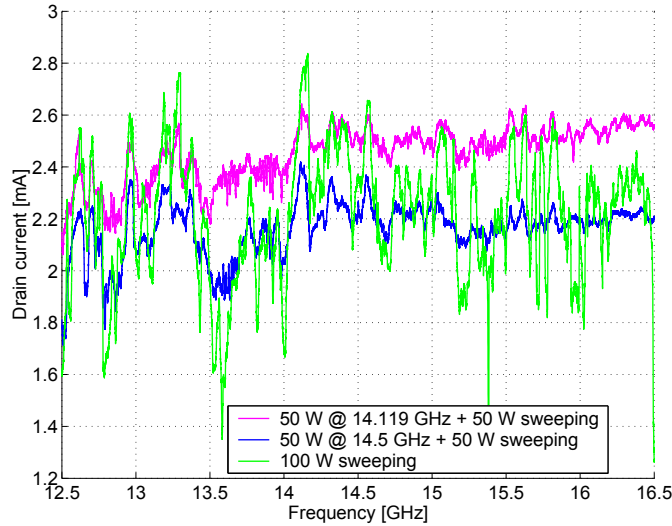


Figure 4.24: *Effect on the drain current of the high voltage power supply of the double frequency heating for two settings of the fixed frequency and comparison with the single frequency tuning.*

imum of the reflection coefficient occurs does not vary it can be expected that the peaks of the ion current are located at the same frequencies for the two heating methods. This assumption can be confirmed by analyzing the figure 4.24 where for the drain current of the high voltage power supply is shown for the two techniques. During the single frequency sweeping the drain current varies from around 1.4 mA to 2.8 mA while with the double

frequency heating the range of variation is 0.6 mA with a reduced dynamic. The drain current is more stable with the frequency when the second frequency sweeps instead of the single frequency tuning. In the first case 50 W are provided at one fixed frequency and the effect of the sweeping of a second frequency with a power of 50 W produces a different course of the current with respect to the single sweeping frequency (and the same power). This is also visible in figures 4.25-4.27). The more stable behavior of the ion current with the frequency is also observed in the evolution of the  $Ar^{7+}$  current shown in figure 4.25. A possible interpretation of this result can be found in

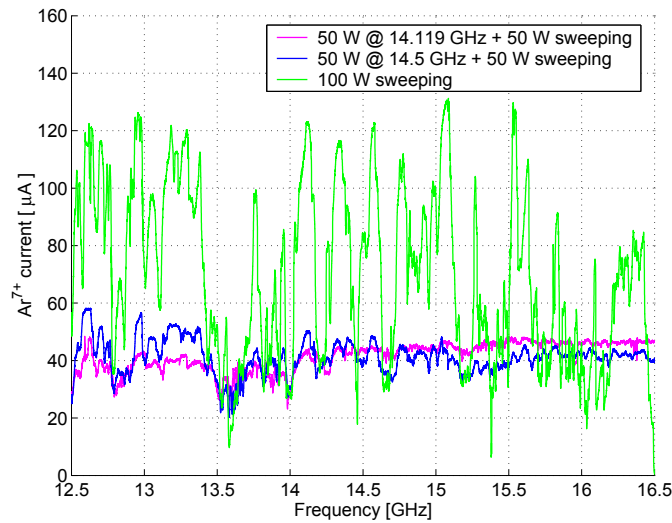


Figure 4.25: Effect on the  $Ar^{7+}$  current of the double frequency heating for two settings of the fixed frequency and comparison with the single frequency tuning.

the power provided by the two methods. In the case of the single frequency tuning 100 W are provided to the source and during the frequency sweep when the impedance matching is not fulfilled the sent power is completely reflected (see figure 4.23). In the case of the double frequency heating just 50 W of the total forward power of 100 W are associated to a sweeping frequency and at the frequencies where the power is not coupled to the plasma, one half of the total power are provided at a fixed frequency which is well coupled to the source (14.5 GHz or better when the fixed frequency is an optimized one). The behavior of the  $Ar^{8+}$  and  $Ar^{9+}$  in the range 12.5 – 16.5 GHz is also more stable in the case of the double frequency heating and this is confirmed by analyzing the figures 4.26 and 4.27. Here the average level of the ion current is higher with respect to the case of the single frequency

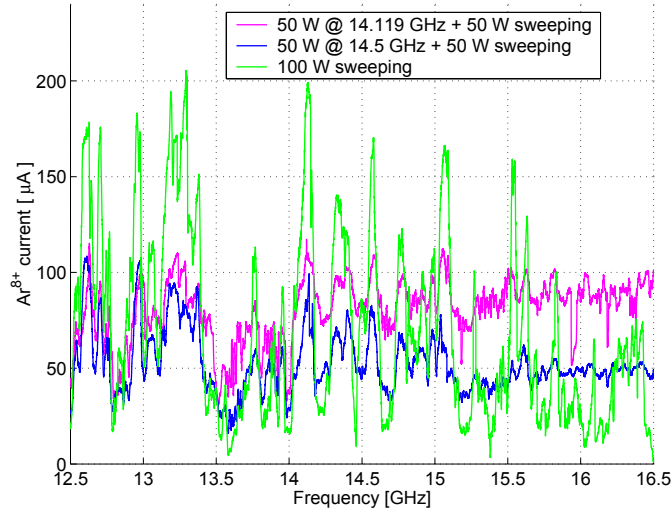


Figure 4.26: Effect on the  $Ar^{8+}$  current of the double frequency heating for two settings of the fixed frequency and comparison with the single frequency tuning.

tuning but for the frequencies when a current peak occurs the level is higher in the case of the single frequency tuning. The comparison is carried out between the single frequency tuning and the double frequency heating when one of the two frequencies is set to 14.5 GHz.

Another important results of this experimental analysis is connected to the choice of the fixed frequency. This choice in fact allows to enhance the ion currents of the higher charge states as already observed in [90]. A comparison concerning the double frequency heating for the two values of fixed frequencies, 14.5 GHz and 14.119 GHz, can be carried out. The drain current is 0.2 – 0.4 mA higher (see figure 4.24) when the fixed frequency is changed from 14.5 GHz to 14.119 GHz. A very important results concerns the high charge state production: with respect to the 14.5 GHz fixed frequency, with the choice of 14.119 GHz the higher charge states tend to higher ion currents when increasing the frequency (See figures 4.26 and 4.27).

There is a strong difference when the operating frequency is optimized according to a frequency tuning. In fact when operating in the double frequency heating and when optimizing one of the two frequencies (14.119 GHz for the considered setting of the ion source) the current increases linearly with the second frequency (with respect to the 14.5 GHz fixed frequency). This is, for instance, the case of the  $Ar^{9+}$  current which enhances up to 30  $\mu A$  (see figure 4.27).

It is possible to summarize the found results and make a comparison between the single frequency and the double frequency sweeps: the evolution of the ion currents and of the reflection coefficient remains almost the same with the frequency between the two techniques. The ECRIS performances can be further optimized when the double frequency heating technique is used. In fact the single frequency tuning can be used to find optimized frequencies to be used for operating in the multiple heating mode. In order to investigate

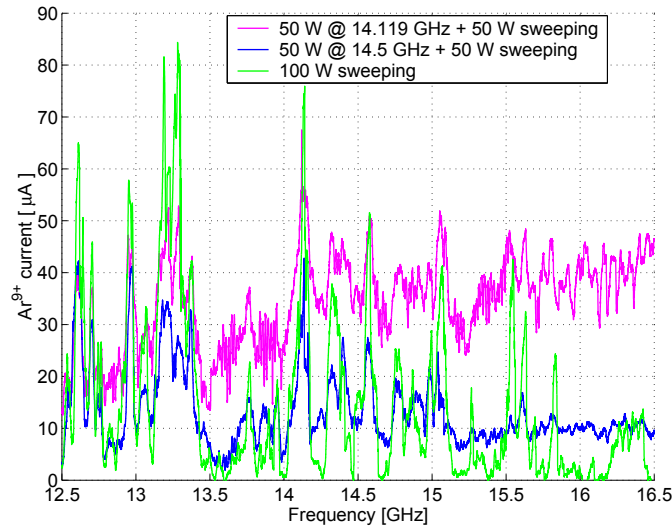


Figure 4.27: Effect on the  $Ar^{9+}$  current of the double frequency heating for two settings of the fixed frequency and comparison with the single frequency tuning.

the effect on the Argon ion beams of the choice of the power between the fixed frequency and the sweeping one we changed the power distribution between them by doubling the power of the fixed one in one case and the power of the sweeping one in the second case. In both cases two fixed frequencies were chosen and even in this case the possibility to set the fixed frequency to an optimized one, obtained with the fine tuning of the frequency, made possible to increase the beam intensity. This is shown in figure 4.28 where the evolution of the  $Ar^{9+}$  current is reported when 150 W of total power are distributed between two waves in different fractions, one of fixed frequency and a second frequency sweeping from 12.5 GHz to 16.5 GHz. Once more the single frequency sweeping carried out at 100 W is included in the figure for comparison. We noted small differences on the  $Ar^{9+}$  ion current when the frequency is not optimized, like 14.5 GHz and the power is differently distributed. For the optimized frequency, 14.119 GHz, up to a factor 2.5 of

enhancement is recorded when the power of the fixed frequency is doubled with respect to the sweeping one. Then, when one of the two frequencies is optimized, the average level of the extracted current remains high with respect to a not optimized frequency (like 14.5 GHz) and it is increasing with the second frequency (quite evident above 15 GHz). It came out from this measurement that it is more effective to increase the power at the fixed frequency. By observing this figure it comes out once more that the choice of the optimized frequency obtained in a previous experiment applying the frequency tuning, hence is very important for using the double frequency heating at higher power.[69]

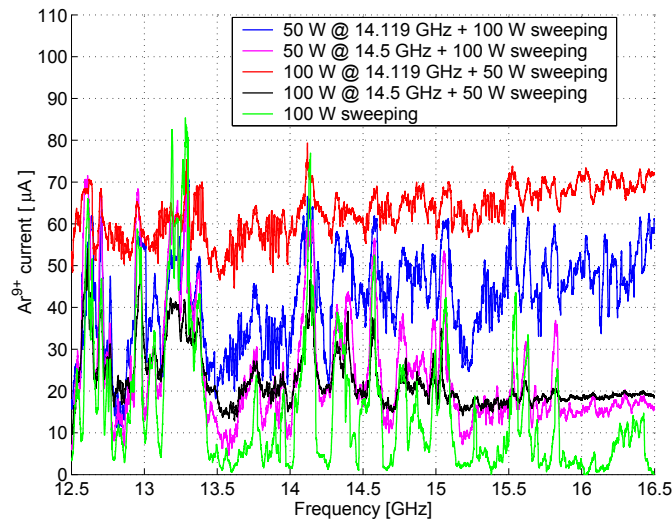


Figure 4.28:  $Ar^{9+}$  current - Different power distributions between the two waves.

#### 4.4.1 Effect of the double frequency heating on the current of highly charged ions

In the previous section we pointed out that it is possible to enhance the production of high charge state ions, with the double frequency heating with the increase of the power of the fixed *optimized* frequency and the decrease the second one carried by the sweeping frequency. In order to confirm this result also for the higher charge states ions, the microwave power has to be increased. For this reason we modified the experimental set-up by including the waveguide isolator described in section 4.2.4 and shown in figure 4.29. With this arrangement we were able to send up to 550 W, distributed by

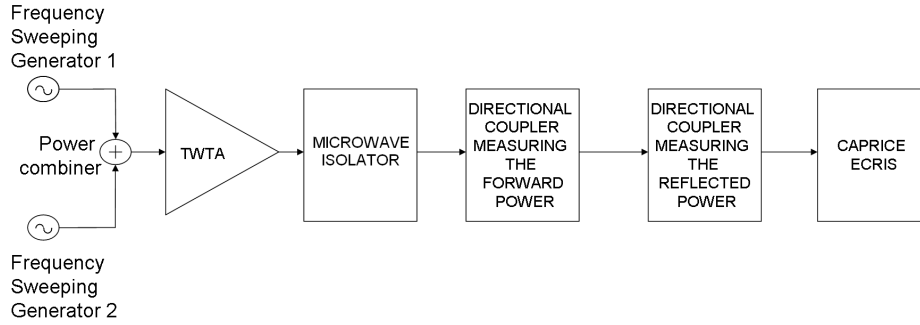


Figure 4.29: Block diagram describing the main components of the microwave injection system used for the double frequency heating at high power.

two waves at different frequency, to the CAPRICE ECRIS. In section 4.2.4 we demonstrated that the microwave frequency can be used as an optimizing parameter and this can strongly modify the charge state distribution thus increasing the ion current of the higher charge states. The results of the high power experiment revealed that for the frequency 13.221 GHz an enhancement of the high charge state production was measured. Then we analyzed, for this frequency, the high charge state production in combination with the double frequency heating technique and the results are compared with the ones obtained when the fixed frequency is 14.5 GHz. Figures 4.30 show the results of measurements of the  $Ar^{9+}$  and the  $Ar^{11+}$  beam currents when two frequencies are provided to the source: a fixed one (13.221 GHz or 14.5 GHz, respectively) and a second frequency sweeping in the range of 12.5 ÷ 16.5 GHz. The power provided to the amplifier by the two waves is the same so that a total power of 450 W is injected into the ion source for comparison with the single frequency sweeping operation. As observed for lower power the choice of the fixed frequency determined an enhancement of the intensity mainly at the frequencies where a current peak occurs.

Then we analyzed the  $Ar^{9+}$  and the  $Ar^{11+}$  beam currents when one frequency (13.221 GHz) is fixed and a second frequency sweeps in the 12.5–16.5 GHz frequency range with different settings of the power levels. The results of this measurement for the  $Ar^{9+}$  and the  $Ar^{11+}$  beam current, respectively, are shown in figures 4.31 and it is clear that the increment of a few tens of Watt is enough to increase the ion current. The confirmation that the optimized frequency chosen as one of the two frequencies allows to increase the highly charged ion production is clear by observing the  $Ar^{11+}$  current in the middle figure 4.31. In fact once the optimized frequency is chosen with a



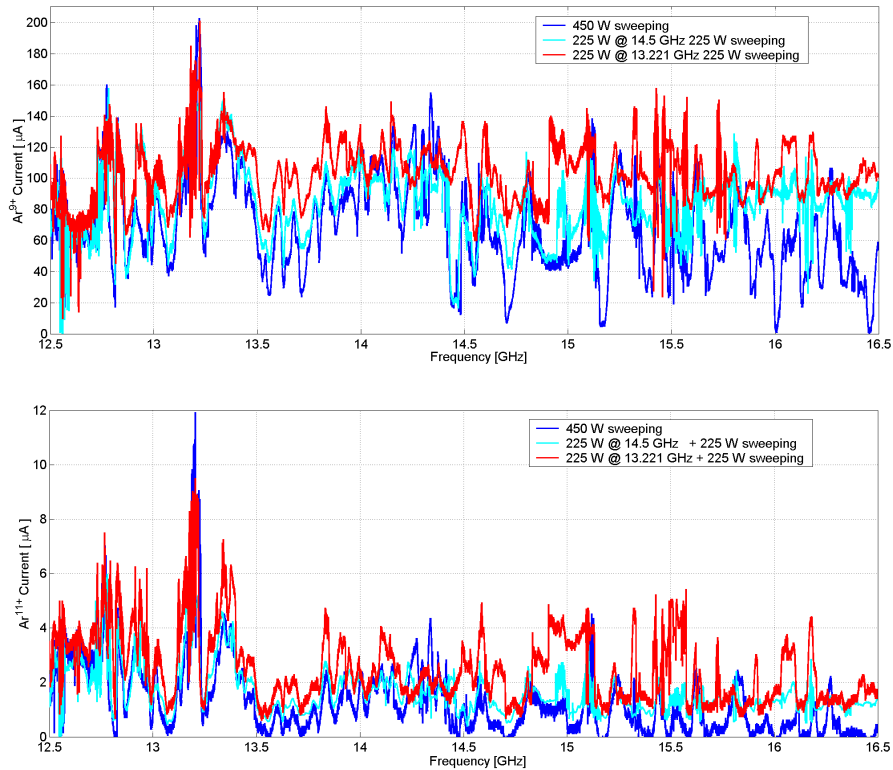


Figure 4.30: *Effect on the  $Ar^{9+}$  (top) and  $Ar^{11+}$  (bottom) current of the double frequency heating for two settings of the fixed frequency and comparison with the single frequency tuning.*

frequency tuning experiment, the addition of a second wave with low power (just 50 W) can enhance the high charge state ion current by optimizing the microwave coupling as shown in the bottom figure 4.31. This result is very important for the future projects making use of ECR ion sources fed by Gyrotron oscillators to operate with the double frequency heating. In fact it would be expected that in such a case it is possible to provide a few hundreds of watts by a TWTA in addition to the power provided by the Gyrotrons in order to get the advantages of a tunable double frequency heating for the enhancement of the production of highly charged ions.[86]

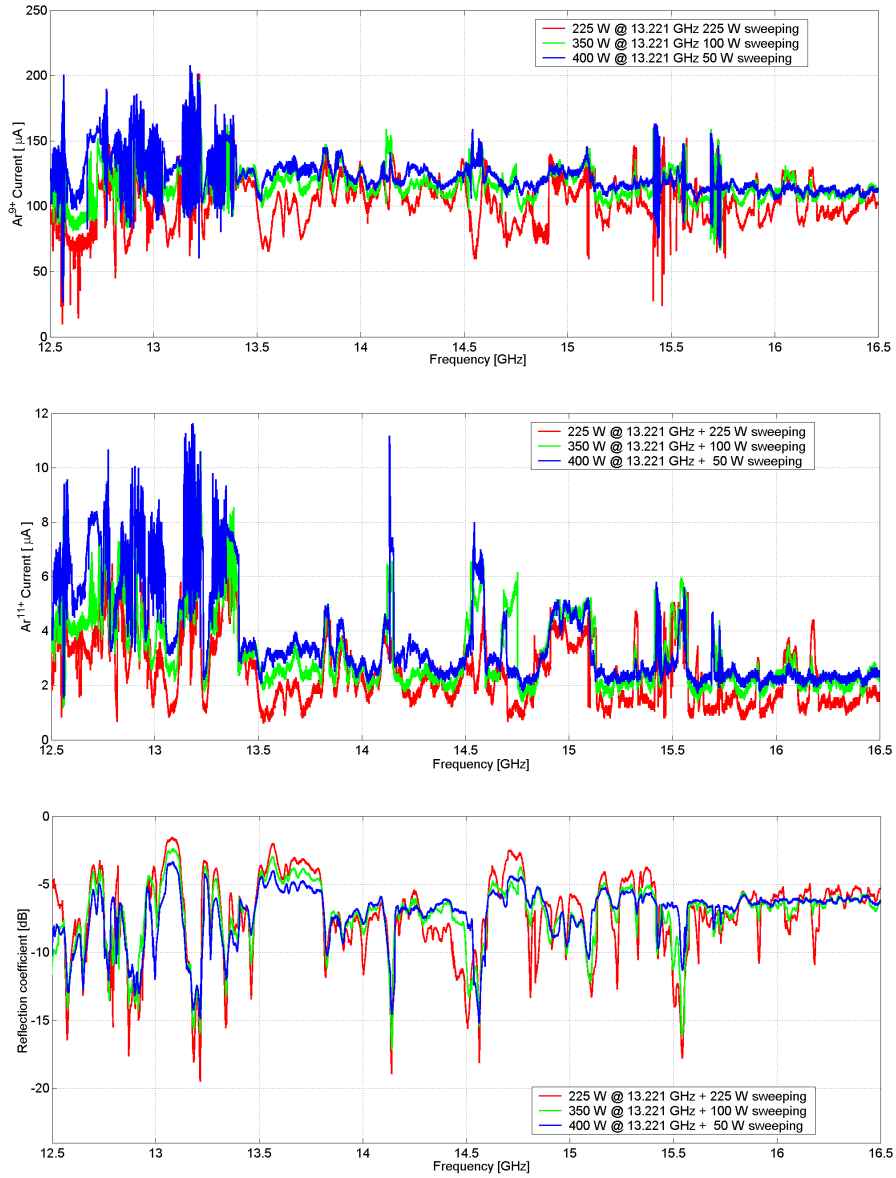


Figure 4.31:  $Ar^{9+}$  (top) and  $Ar^{11+}$  (middle) beam currents and reflection coefficients (bottom) when the double frequency heating is applied with different settings of power levels.

## 4.5 Comparative analysis of the frequency tuning and of the plunger tuning

In section 3.7 we described the technique of the plunger tuning for the matching impedance optimization. The variation of the physical dimensions of the system composed of the injection box, of the coaxial line and of the plasma loaded cavity can produce a variation on the beam current like observed in this chapter with the frequency tuning. In both cases, in fact a fine impedance match can be obtained. The existing modes inside the plasma chamber can be excited by changing the microwave frequency or by changing the volume at fixed frequency. During the frequency tuning experiment described in section 4.2.3 the plunger was set at a distance of 25.05 mm from the central axis during all measurements. Then we moved the plunger inside the injection box to 22.5 mm of distance from the central axis where the current of  $Ar^{8+}$  attained its maximum of  $115 \mu A$  as described in section 3.7. For this setting of the ion source the microwave frequency has been swept in the frequency range mentioned above. The results concerning the  $Ar^{8+}$  current are shown in figure 4.32. As expected at 14.5 GHz now a maximum

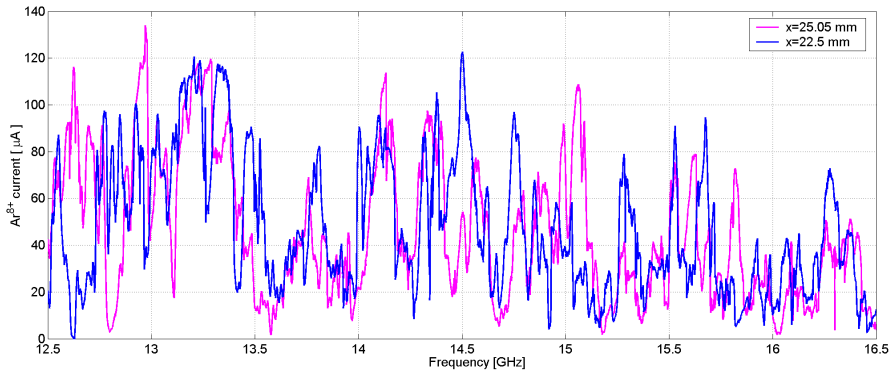


Figure 4.32: Frequency tuning effect on the  $Ar^{8+}$  current for two plunger positions.

of the  $Ar^{8+}$  current is present. Almost all peaks are shifted in frequency and amplitude. The value of 14.119 GHz does no longer correspond to a maximum of the  $Ar^{8+}$  current in the frequency range between 14 GHz and 15 GHz. The reason of this variation of the peaks has to be researched in the different modes distribution, now present inside the plasma chamber, as noted in figure 4.33 showing the reflection coefficient versus the frequency for the two plunger positions. A similar dependence can be expected when any

kind of perturbing structure, like biased discs, Langmuir probes, or ovens for the metallic ion beam production, is inserted into the plasma chamber as already reported in [62].

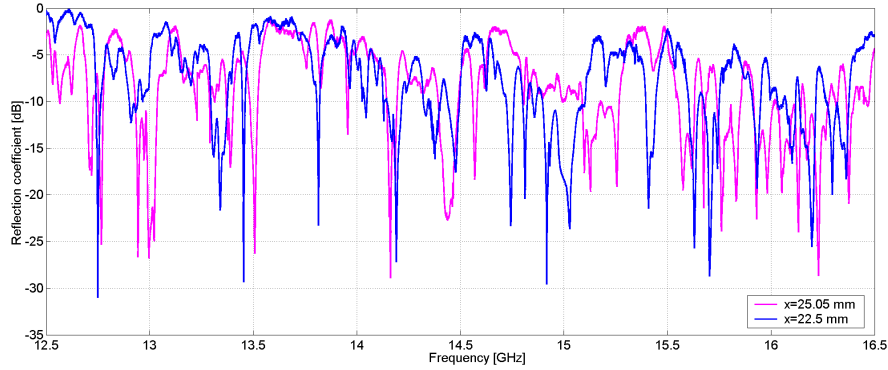


Figure 4.33: *Frequency tuning effect on the reflection coefficient for two plunger positions.*

According to the different current amplitudes, shown in figure 4.32, figure 4.34 shows the charge state distribution measured for these two different positions of the plunger. In this figure we included a comparison with the charge state distribution related to the optimized case of 14.119 GHz frequency. It is clear that the plunger tuning plays the same role as the frequency tuning. The two methods to optimize the impedance matching can be used simultaneously (see blue bar in figure 4.34). In this case, since the frequency was changed to the optimized one the tuner was set to the position where the  $Ar^{8+}$  current was the highest. This optimization process could proceed in a different sequence by changing frequency and position of the plunger, respectively. However, if the power is not increased or if the other parameters of the ion source remain unchanged a saturation of the ion current of the higher charge states is expected.

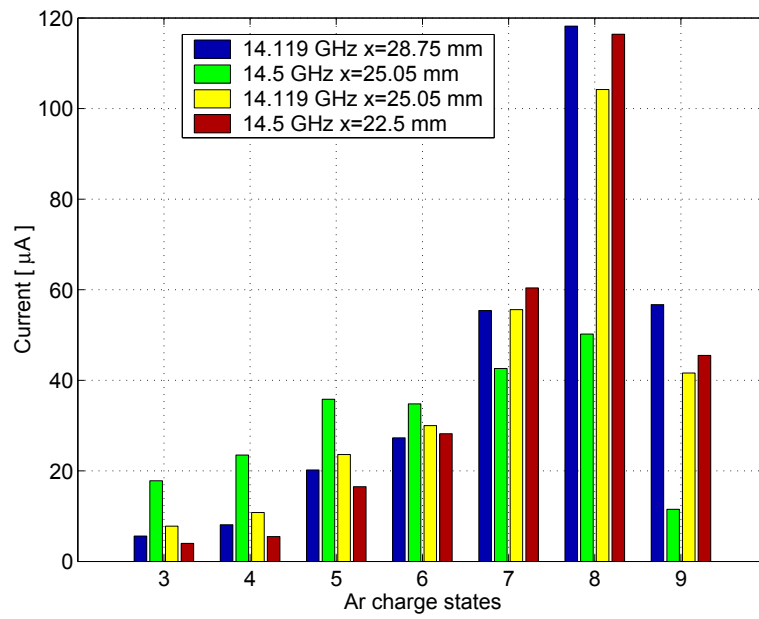


Figure 4.34: Argon charge states distributions for four different conditions of frequency and plunger positions.

# Conclusions and future perspectives

The theoretical and experimental investigations presented within this research work provided useful explanations on the performance enhancement of the Electron Cyclotron Resonance Ion Sources, in terms of production of more intense beams of highly charged ions, when techniques based on the tuning of the microwave coupling to the plasma filling the chamber of such ion sources are applied.

The obtained experimental results showed that the current, the charge states and even the beam shape change by varying the microwave coupling to the plasma, by tuning the microwave frequency (according to the so called frequency tuning effect) or by modifying the volume where the plasma is contained. The theoretical explanation of the variation of these ion beam properties has been related to the difference in the electromagnetic field pattern over the resonance surface, i.e. that region where the electrons resonantly interact with the incoming wave, when the microwave frequency provided to the source, or the physical dimensions of the system, are changed. This explanation is in agreement with the assumption that the plasma chamber is a resonating cavity for the electromagnetic wave feeding the plasma. We demonstrated that the electromagnetic field distribution inside the cavity of an electron cyclotron resonance ion source can be changed significantly by means of frequency variations thus having a huge effect both on the spatial distribution of minima and maxima and on the amount of energy coupled from the feeding waveguide to the cavity. The resonant modes have completely different patterns and some of them are more effective on the acceleration of the confined electrons and on the rate of ionization and, therefore, on the plasma formation. The confirmation of this assumption was provided by means of a series of measurements performed with a network analyzer connected to a plasma reactor operating at 2.45 GHz, according to the prin-

ciples of the Microwave Discharge Ion Sources (MDIS). We obtained an electromagnetic characterization of the plasma chamber in terms of possible excited resonant modes with and without plasma and we observed that the plasma dynamics strongly depends on the structure of the standing waves that are generated. We observed a shift of the resonant frequencies when the gas pressure or the microwave power were varied. By linking the shift to the decrease of the electric permittivity due to the variation of the electron density, this latter parameter was calculated. We compared the measurements of the plasma electron density with a Langmuir probe to the calculated values and a good agreement was found.

We also investigated the microwave coupling on a CAPRICE-type ECRIS, installed at the GSI Helmholtzzentrum für Schwerionenforschung GmbH, by featuring the existence of standing waves inside the plasma chamber for different conditions of the plasma. The microwave coupling variation by using a matching plunger was also investigated and the effects on the beam current extracted by this ion source were measured. The plunger tuning provided comparable results on the intensity variation as the frequency tuning. We demonstrated that these techniques can be used simultaneously for the enhancement of the high charge state production. The use of a matching plunger on an ECRIS provides interesting advantages concerning the normal operation and the performance optimization. However, the determination of the electromagnetic field patterns is complicated for the complex geometry which this system introduces. Then, only electromagnetic simulators can calculate the electromagnetic field inside these geometries and in this research work we used CST Microwave Studio and interesting results were found. The geometry of the CAPRICE ECRIS was reproduced and the effects of the plunger tuning and of the frequency tuning were analyzed for different parameters like the microwave frequency or the plunger position. The presence of a non magnetized plasma was considered in the model by including a medium with an electric permittivity lower than one. Future investigations on the different distributions of this medium inside the plasma chamber are planned. Furthermore the model of a magnetized plasma, which will reproduce the plasma contained inside the plasma chamber of the ECRIS, is considered to be included and evaluated. This will improve the consistence of the simulation results and the effect introduced by the presence of the ECR plasma will be investigated more precisely. The simulated model showed that a different electromagnetic field pattern, with respect to a first order approximation of the chamber as purely cylindrical, exists inside the plasma chamber when all the ECRIS components, i.e. like

the plasma electrode or the matching plunger, are taken into account. The introduction into the plasma chamber of any perturbing object, like probes or biased discs, has proven to perturb this electromagnetic field pattern, thus affecting the ECRIS performances. This assumption has been confirmed by the experimental results reported within this work. The reported measurements hereinafter resulted to be relevant for the ECRIS knowledge and operation, because they confirmed the validity of the theoretical model describing the frequency tuning and the double frequency heating.

The experiments largely described in the fourth chapter provided interesting and important results concerning the operation of the ECRIS when making use of the microwave frequency tuning and of the superposition of different microwave sources feeding the plasma. The effect of the frequency tuning is more pronounced for higher charge states. A variation of the intensity and the shape of the extracted ion beams with the frequency is the main effect. We measured the variation of the microwave coupling by changing the frequency and, by analyzing the reflection coefficient, a resonant behavior was observed. We also observed a clear relationship between the resonances of the reflection coefficient and the current intensity and an enhancement of the current for the highly charged ions was measured. Some frequencies were identified where the current of the higher charge states was more than doubled and this effect was more effective for the higher charge states. This result was confirmed by operating the CAPRICE ion source with higher microwave power. The measurements of the charge state distributions revealed how the frequency tuning is more effective on the higher charge states and how important is the choice of the microwave frequency for the normal operation of the ECRIS and for the optimization of the beam properties. The performance improvement when applying this technique is confirmed for ions obtained by elements both gaseous and metallic.

In conclusion, it is possible to state that the electromagnetic field pattern inside the chamber plays an important role to determine the current density distribution of the extracted ion beam and its total intensity. In particular, we demonstrated that the frequency tuning can be a powerful method which permits, just by changing the operating frequency, the optimization of the coupling between the electromagnetic wave and the plasma filled chamber. However, since the ECRIS performances depend on the plasma characteristics which are also function of the gas pressure in the cavity, and on the magnetic field used for its confinement, the relationship between the performance enhancements and the different plasma conditions have still to be investigated. The interest of the scientific community in the use of the fre-



quency as a "knob" to tune the ion source performances pushes toward new developments and better understanding of this technique. Emittance measurements and investigations on the X-ray production when this technique is applied are also planned. The knowledge of the ion trajectories and of the energy transferred to the electrons can provide additional information to the comprehension of the frequency tuning.

Another investigated technique within this research work is the double frequency heating. It is based on the plasma feeding by different frequencies and, by applying this technique, the performances of the ECRIS in terms of the beam current intensity, particularly of the higher charge states, can be enhanced. This has been clearly demonstrated. We pointed out that when operating with double frequency heating the choice of the frequencies allows a further enhancement of the intensity of the higher charge states. The efficient application of this technique cannot be separated by the frequency tuning for the choice of the operation frequency. We observed that the higher charge states tend to higher currents when the second frequency is increased. We also demonstrated that the power distribution between the two waves is also important. By feeding the ECRIS plasma with two frequencies, the power of one of them can be a small percentage of the other and this setting was sufficient to obtain a remarkable increase of the ion current and of the high charge state ion production. This results turned out to be important for the future developments of the next generation ECRISs making use of higher magnetic fields and operating with Gyrotron generators providing microwave frequencies higher than 24 GHz at power levels in the 10 – 15 kW range. Future investigations will make use of these ECRIS to validate the advantage of the double frequency heating by combining, as a microwave injector, a system composed by a Traveling Tube Amplifier (providing a few hundreds of Watt at a variable frequency) and a Gyrotron Generator (providing a power of several kW at a fixed frequency). The availability of the MS-ECRIS ion source to be assembled at GSI will allow to carry out these promising investigations.

# Acknowledgements

First I would like to thank my tutor, the Professor Francesco Musumeci. He gave me the opportunity to develop all my research activities in the field of the Electron Cyclotron Resonance Ion Sources. All of his suggestions were fundamentals to prepare and to carry out my PhD studies.

I would like to acknowledge the PhD coordinator, the Professor Gaetano Giaquinta. He was always available and friendly in providing me his academic support.

I am grateful to the Professor Sebastiano Barbarino. He transmitted me his passion for the electromagnetism and for the plasma physics. He always encouraged me and he had faith in me during the dissertation process. He was and he will remain a mentor to me.

I would like to give a special thank to the colleagues of the ion sources Department I had the pleasure to find at GSI. In particular I am warmly grateful to the colleagues of the ECR Ion Sources team: Dr. Klaus Tinschert and Peter Spädtke, which offered me the opportunity to work with them and Jon Roßbach, Jan Mäder and Ralf Lang. They shared with me all of their knowledge of the ECRIS. From the beginning they made me feel as a part of this valuable team. I am grateful to them for the working experience I gained by working with them. Part of the research work was carried out at GSI in the framework of the EU under the ENSAR project (FP7 under the Grant agreement n° 262010). This support is also acknowledged.

I also want to acknowledge the ECR Ion Sources group of INFN-LNS and in particular: Luigi Celona, Giovanni Ciavola and Santo Gammino. They introduced me in the field of the ECRISs and during the dissertation process

they were motivating and encouraging. I would like to give special thanks to Luigi Celona. He was a colleague and a sincere friend. He transmitted me his experience on the Microwave coupling to the ECRISs. I really enjoyed working with them and with the other colleagues of INFN-LNS.

I will be forever grateful to my mother and my sister for the invaluable love they have to me and for the support they always gave me.

I reserve the last, but very important, acknowledgment for a person always believing in me and which decided to share her life with me: my wife Alessia.

# Bibliography

- [1] F. Chen, *Introduction to the Plasma Physics and Controlled Fusion: Plasma Physics*, London Press, second edition, 1986.
- [2] B. Wolf *Handbook of Ion Sources*, CRC Press, 1995.
- [3] T.A. Carlson, C.W. Nestor Jr., N. Wasserman, and J. D. McDowell, *At. Data*, 2, 63, 1970.
- [4] I. Brown, *The Physics and Technology of Ion Sources*, Wiley-WCH, 2004.
- [5] R. Geller, *Electron Cyclotron Resonance Ion Sources and ECR Plasmas* IOP, Bristol, 1996.
- [6] K. S. Golovanivsky, *Plasma Sources Sci. Technol.* 2, 240, 1993.
- [7] S. Barbarino, *Appunti di Campi elettromagnetici*, 2011, [http://www.diit.unict.it/users/campi/appunti\\_campi\\_indice.htm](http://www.diit.unict.it/users/campi/appunti_campi_indice.htm).
- [8] C.D. Child, *Phys. Rev. (Ser. 1)*, 32, 492, 1911.
- [9] I. Langmuir and K.T. Compton, *Rev. Mod. Phys.* 3, 251, 1931.
- [10] A. Septier, *Applied charged particle Optics*, 1980.
- [11] A.T. Forrester, *Large ion Beams*, Wiley Interscience, 1988.
- [12] P. Spädtke, A. Adonin, B. Gutermuth, F. Heymach, R. Hollinger, R. Lang, J. Mäder, F. Maimone, K. Ochs, J. Roßbach, P. Schäffer, S. Schäffer, M. Stork, K. Tinschert, C. Vierheller, S. Zulauf, *Ion source development and operation*, GSI Scientific Report 2010, Darmstadt, p 436-437.

- 
- [13] R.W. Schmieder, Physics of EBIS and first ions, in *Proc. NATO Workshop Physics of Highly Ionized Atoms*, Cargese, Corsica, 1988.
- [14] E.D. Donets, The Status of Electron Beam Ion Sources, Proc. HCI-92, Manhattan, edited by P. Richard, M. Stoeckli, C. L. Cocke, and C. D. Lin, AIP Conf. Proc. 274, 663, 1993.
- [15] S. Gammino and G. Ciavola, Plasma Source Sci. Technol. 5, 19-27, May 1996.
- [16] R. Geller *et al*, Proc. of the 2<sup>nd</sup> Int. Conf. Ion Sources, Vienna, 632, 1971.
- [17] P. Briand *et al*, Nucl. Instrum. Methods, 131, 407, 1975.
- [18] V. Bechtold *et al*, Nucl. Instrum. Methods, 178, 305, 1980.
- [19] F. Bourg, R. Geller, B. Jaquot and M. Pontonnier, Proc. of the 4<sup>th</sup> International Workshop on ECR Ion Sources and related topics, Grenoble, edited by M. C. Boraso, CEN-Grenoble Press, 1982.
- [20] R. Geller, Proc. of the 11<sup>th</sup> International Workshop on Cyclotrons and their Applications (Ionics Publishing Co., Tokyo, 1986).
- [21] C.M. Lyneis *et al*, Proc. of the 10<sup>th</sup> Int. Workshop on ECR Ion Sources, Knoxville, 1990.
- [22] Z.Q. Xie, Rev. Sci. Instrum. 75, 1389, 2004.
- [23] M. Schlapp *et al*, Rev. Sci. Instrum. 69, 631, 1998.
- [24] H. Koivisto *et al*, Nuclear Instrum. Methods B, 174, 379, 2001.
- [25] M.P. Bourgarel *et al*, Rev. Sci. Instrum., 63, 2854, 1992.
- [26] A. Antaya, *et al* Proc. of the 6<sup>th</sup> Int. Workshop on ECR Ion Sources, Berkeley, 1985.
- [27] P. Sortais *et al*, Proc. of the Int. Workshop on ECR Ion Sources, East Lansing, 1987.
- [28] P. Sortais *et al*, Proc 11<sup>th</sup> Int. Workshop on ECR Ion Sources, Groningen, 1993.
- [29] H.P. Winter *et al*, Rev. Sci. Instrum., 65, 1091, 1994.

- 
- [30] P. Ludwig, F. Bourg, P. Briand, A. Girard, G. Melin, D. Guillaume, P. Seyfert, A. La Grassa, G. Ciavola, S. Gammino, M. Castro, F. Chines, and S. Marletta, *Rev. Sci. Instrum.* 69, 4082, 1998.
- [31] S. Gammino and G. Ciavola, *Rev. Sci. Instrum.* 71, 631, 2000.
- [32] S. Gammino, G. Ciavola, L. Celona, M. Castro, F. Chines, and S. Marletta, *Rev. Sci. Instrum.* 70, 3577, 1999.
- [33] T. Nakagawa, Y. Higurashi, J. Ohnishi, T. Aihara, M. Tamura, A. Uchiyama, H. Okuno, K. Kusaka, M. Kidera, E. Ikezawa, M. Fujimaki, Y. Sato, Y. Watanabe, M. Komiyama, M. Kase, A. Goto, O. Kamigaito and Y. Yano, *Rev. Sci. Instrum.* 81, 02A320, 2010.
- [34] P. A. Zavodszky, B. Arend, D. Cole, and J. Dekamp, *Rev. Sci. Instrum.* 77, 03A334, 2006.
- [35] D. Kanjilal *et al*, Proceedings of Indian Particle Accelerator Conference, Indore, India, 3 – 6 February 2003, p 144 (unpublished).
- [36] H. W. Zhao, L. T. Sun, W. Lu, X. Z. Zhang, X. H. Guo, Y. Cao, H. Y. Zhao, Y. C. Feng, J. Y. Li, H. Y. Ma, Y. Shang, B. H. Ma, H. Wang, X. X. Li and D. Z. Xie, *Rev. Sci. Instrum.* 81, 02A202, 2010.
- [37] H. W. Zhao, L. T. Sun, X. Z. Zhang, and Z. M. Zhang, *Rev. Sci. Instrum.* 77, 03A333, 2006.
- [38] S. Gammino, G. Ciavola, L. Celona, D. Hitz, A. Girard, and G. Melin, *Rev. Sci. Instrum.* 72, 11, 2001.
- [39] D. Leitner, M. L. Galloway, T. J. Loew, and C. M. Lyneis, *Rev. Sci. Instrum.* 79, 02C710, 2008.
- [40] G. Ciavola, S. Gammino, S. Barbarino, L. Celona, F. Consoli, G. Gallo, F. Maimone, D. Mascali, S. Passarello, A. Galatà, K. Tinschert, P. Spädtke, R. Lang, J. Mäder, J. Roßbach, H. Koivisto, M. Savonen, T. Koponen, P. Suominen, T. Ropponen, C. Barùè, M. Lechartier, J. P. M. Beijers, S. Brandenburg, H. R. Kremers, D. Vanrooyen, D. Kuchler, R. Scrivens, L. Schachter, S. Dobrescu, and K. Stiebing, *Rev. Sci. Instrum.* 79, 02A326, (2008).
- [41] D. Leitner, C.M. Lyneis, M. Leitner, A. Hodgkinson, T. Loew, P. Ferracin, G.L. Sabbi, G. Machicoane, E. Pozdeyev, Proc. of the 19<sup>th</sup> Int. Workshop on ECRIS Grenoble, 23 – 26 August 2010.

- 
- [42] K.Tinschert *et al*, Proc. of the ICIS Conference, 11-16 September 2011, Catania, Italy.
- [43] R. Lang *et al*, Rev. Sci. Instrum. 71, number 2, 2000.
- [44] F. Bourg, R. Geller, and B. Jacquot, Nucl Instrum Methods A 254, 13, 1987.
- [45] R.C. Vondrasek, R. Scott, and R.C. Pardo, Rev. Sci. Instrum. 75, 1532, 2004.
- [46] D.P. May, Rev. Sci. Instrum. 69,688, 1998
- [47] H. Koivisto, J. Arje, and M. Nurmia, Rev. Sci. Instrum. 69, 785, 1998.
- [48] S.R. Gunn, Radiometric calorimetry: a review, Nuclear Instrum. Methods 29, 1, 1964.
- [49] L. Panitzsch, M. Stalder, R.F. Wimmer-Schweingruber, Proc. of the 19<sup>th</sup> Int. Workshop on ECRIS Grenoble, 23 – 26 August 2010.
- [50] J. W. Stetson, NSCL, THCO-A03, ECRIS08, Chicago, IL USA, 2008.
- [51] Private communications between P. Spaedtke and T. Winkelmann, 2007.
- [52] P. Spädtkke, R. Lang, J. Mäder, J. Roßbach, K. Tinschert, J. Stetson, High energy physics and nukl. physics, Vol.31(I), page 192, 2007.
- [53] J. Mäder, J. Roßbach, R. Lang, F. Maimone, P. Spädtkke, K. Tinschert, L.T. Sun, Y. Cao, H.W. Zhao, GSI Report 2009-03.
- [54] H.R. Kremers, J.P.M. Beijers, S. Brandenburg, Proc. of DIPAC 2007, Venice, Italy, p. 195 – 197.
- [55] H. R. Kremers, J.P.M. Beijers, S. Brandenburg, S. Saminathan, V. Mironov, T. Thuillier, Proc. of Workshop of ECRIS 2008, Chicago, USA.
- [56] J. Mäder J. Roßbach, F. Maimone, P. Spädtkke, K. Tinschert, R. Lang, L. Sun, Y. Cao, and H. Zhao, Rev. Sci. Instrum. 81, 02B720, 2010.
- [57] Hiden ESPion-Advanced Langmuir Probe for Plasma Diagnostics, <http://www.hidenanalytical.com/>, accessed in September 2010.

- [58] J.D. Swift, M.J.R. Schurar, *Electrical Probe for Plasma Diagnostic*, Iliffe, London, 1970.
- [59] S. Barbarino, *Appunti di Microonde*, 2011,  
[http://www.diit.unict.it/users/campi/appunti\\_microonde\\_indice.htm](http://www.diit.unict.it/users/campi/appunti_microonde_indice.htm).
- [60] F. Consoli et al, Rev. Sci. Instrum. 79, 02A308, 2008.
- [61] F. Consoli, L. Celona, G. Ciavola, S. Gammino, F. Maimone, S. Barbarino, R. S. Catalano, and D. Mascali, Rev. Sci. Instrum. 79, 02A308, 2008.
- [62] L. Celona, S. Gammino, F. Maimone, D. Mascali, N. Gambino, R. Miracoli and G. Ciavola, Eur. Phys. J. D 61 1, 107 – 115, 2011
- [63] F. Maimone, D. Mascali, F. Consoli, S. Barbarino, L. Celona, G. Ciavola, S. Gammino, INFN-LNS Report, 27 February 2006
- [64] S. Gammino, G. Ciavola, L. Celona, D. Mascali, and F. Maimone, IEEE Trans. Plasma Sci. 36, 1552 2008.
- [65] D. Mascali, S. Gammino, S. Barbarino, F. Consoli, L. Celona, G. Ciavola, INFN report INFN/05/10, 2005.
- [66] S. Gammino, D. Mascali, L. Celona, F. Maimone, G. Ciavola, Plasma Sources Sci. Technol. 18, 045016, 2009.
- [67] D. Mascali, L. Neri, S. Gammino, L. Celona, G. Ciavola, N. Gambino, R. Miracoli, S. Chikin, Rev. Sci. Instrum. 81, 02A334, 2010.
- [68] See the software description at  
<http://www.cst.com/Content/Products/MWS/Overview.aspx>
- [69] F. Maimone, L. Celona, R. Lang, J. Mäder, J. Roßbach, P. Spädtke K. Tinschert, "Influence of frequency tuning and double-frequency heating on ions extracted from an ECR ion source", accepted for publication in Rev. Sci Instrum.
- [70] L. Celona, G. Ciavola, F. Consoli, S. Gammino, F. Maimone, D. Mascali, P. Spädtke, K. Tinschert, R. Lang, J. Mäder, J. Roßbach, S. Barbarino, and R. S. Catalano, Rev. Sci. Instrum. 79, 023305, (2008).
- [71] F. Maimone, K. Tinschert, P. Spädtke, J. Mäder, J. Roßbach, R. Lang, L. Celona, Proc. of the 19<sup>th</sup> Int. Workshop on ECRIS Grenoble, 23 – 26 August 2010 (edited by T. Tuillier, Grenoble, June 2011 p. 143 – 145).



- 
- [72] D. Mascali, N. Gambino, R. Miracoli, S. Barbarino, S. Gammino, L. Torrissi, F. Maimone, L. Tumino, *Radiation Effects e Defects in Solids*, Vol. 163, Nos. 4 – 6, April-June 2008, 471.
- [73] S. Gammino, L. Celona, G. Ciavola, N. Gambino, F. Maimone, D. Mascali, R. Miracoli, *Proceedings of the 35<sup>th</sup> EPS Plasma Physics Conference*, 9-13 June 2008, Hersonissos, Crete, Greece.
- [74] F. Maimone, R. Lang, J. Mäder, J. Roßbach, P. Spädtke, K. Tinschert, *GSI annual report*, 2009.
- [75] D. Mascali, G. Gammino, L. Celona, G. Ciavola, L. Neri, R. Miracoli, N. Gambino, G. Castro, F. Maimone, *Proceedings of the 19<sup>th</sup> International Workshop on ECRIS*, Grenoble, 23 – 26 August 2010, edited by T. Tuillier, Grenoble, June 2011 p. 165 – 167.
- [76] C. Lyneis, J. Benitez, D. Leitner, J. Noland, M. Strohmeier, H. Koivisto, O. Tarvainien, *Proceedings of the 19<sup>th</sup> International Workshop on ECRIS*, Grenoble, 23 – 26 August 2010, edited by T. Tuillier, Grenoble, June 2011 p. 162 – 164.
- [77] PANTECHNIK S.A., Rue de la Resistance 13, 14400 Bayeux, France.
- [78] T. Winkelmann, R. Cee, T. Haberer, B. Naas, and A. Peters, *Rev. Sci. Instrum.* 81, 02A311, 2010.
- [79] L. Maunoury, J.Y. Pacquet, M. Dubois, P. Delahaye, P. Jardin, P. Leherissier and M. Michel, C. Pierret, X. Donzel, G. Gaubert, R. Leroy, A.C.C. Villari, S. Biri, *Proceedings of the 19<sup>th</sup> International Workshop on ECRIS*, Grenoble, 23 – 26 August 2010, edited by T. Tuillier, Grenoble, June 2011 p.37 – 39.
- [80] G. D. Alton, F. W. Meyer, Y. Liu, J. R. Beene, and D. Tucker, *Rev. Sci. Instrum.* 69, 2305, 1998.
- [81] D. Alton, *NIMA*, 382, 276-282, 1996.
- [82] G. Gammino, G. Ciavola, L. Celona, *NIMA*, 491, 342-345, 2002.
- [83] V. Toivanen, H. Koivisto, O. Steczkiewicz, L. Celona, O. Tarvainen, T. Ropponen, S. Gammino, D. Mascali, and G. Ciavola, *Rev. Sci. Instrum.* 81, 02A319, 2010.

- 
- [84] H. Schulte, K. Tinschert, J. Bossler, B. H. Wolf, J. Klabunde, L. Dahl, Th. Schwab, and J.P. Klein, *Rev. Sci. Instrum.* 63, 2883, 1992.
- [85] K. Tinschert, J. Bossler, S. Schennach, and H. Schulte, *Rev. Sci. Instrum.* 69, 709, 1998.
- [86] F. Maimone, K. Tinschert, L. Celona, R. Lang, J. Mäder, J. Roßbach, P. Spädtke, "Operation of the CAPRICE electron cyclotron resonance ion source applying frequency tuning and double frequency heating", Accepted for publication in *Rev. Sci. Instrum.* as a Proceeding of ICIS2011.
- [87] C. Lyneis, D. Leitner, M. Leitner, C. Taylor, and S. Abbott, *Rev. Sci. Instrum.* 81, 02A201, 2010.
- [88] D. Leitner, M. L. Galloway, T. J. Loew, C. M. Lyneis, I. Castro Rodriguez, and D. S. Todd, *Rev. Sci. Instrum.* 79, 02C710, 2008.
- [89] A. Kitagawa, Proc. of the 19<sup>th</sup> Int. Workshop on ECRIS Grenoble, 23–26 August 2010.
- [90] R. C. Vondrasek, R. Scott, R. C. Pardo, *Rev. Sci. Instrum.* 77, 03A337, 2006.
- [91] Z. Q. Xie and C. M. Lyneis, *Rev. Sci. Instrum.* 66, 4218, 1995.